

# Biochemical analysis of *Arabidopsis thaliana* IQ67-Domain Protein 1 and related proteins

Dissertation  
wissenschaftliche Arbeit  
zur Erlangung des akademischen Grades Dr. rer. nat.  
eingereicht an der Naturwissenschaftlichen Fakultät I  
Martin-Luther-Universität Halle-Wittenberg

Dipl. Biochem. Friedrich Paul Pflug

Geb. am 06.01.1986 in Dresden

1. Gutachter: Prof. Dr. Stefan Abel, Martin Luther Universität Halle-Wittenberg
2. Gutachter: Prof. Dr. Ingo Heilmann, Martin Luther Universität Halle-Wittenberg
3. Gutachterin: Prof. Dr. Petra Dietrich, Friedrich-Alexander-Universität Erlangen-Nürnberg

Die Verteidigung dieser Arbeit erfolgte am 11.12.2019



## Abstract

Within the cellular signaling machinery, calcium ions ( $\text{Ca}^{2+}$ ) act as secondary messenger and are involved in transducing environmental and developmental cues. Stimulus specific changes of cytosolic  $\text{Ca}^{2+}$  concentrations are perceived by  $\text{Ca}^{2+}$  sensors like Calmodulins (CaM). Binding of  $\text{Ca}^{2+}$  by Apo-CaM changes the conformation of CaM ( $\text{Ca}^{2+}$ -CaM) which alters the affinity regarding a broad array of protein targets and by this modulates the molecular function of the targets. One family of CaM targets are the plant specific IQ67-domain proteins (IQD) comprising of 33 members in *Arabidopsis thaliana*. The IQ67-domain composes a repetitive arrangement of CaM binding motifs and has been shown to be the CaM binding site. Beside the most likely helical structure of the IQ67 domain IQD proteins are predicted to contain mostly intrinsically disorderer regions. Most IQD proteins are associated with microtubules (MT) and localize to the nucleus or subnuclear structures. Besides the interaction with CaM, some IQD proteins also interact with Kinesin Light Chain-Related (KLCR) proteins. The KLCR binding site is adjacent to the IQ67-domain, suggesting mutual effects. Reverse genetic analysis revealed that IQDs most likely are involved in regulating cell shape and therefore influence organ morphology. Although studied in many organisms little is known about their biological role or molecular function.

This study shows that IQD1 and IQD proteins in general interact with  $\text{Ca}^{2+}$ - and Apo-CaM. We further provide evidence that IQD proteins directly interact with KLCR proteins as well as with MTs *in vitro* and can recruit KLCRs and CaM to the MTs simultaneously *in planta*. We found that KLCR proteins are  $\text{Ca}^{2+}$ -CaM binding proteins and are recruited to Apo-CaM in an IQD dependent fashion. *In vitro* and *in planta* experiments reveal that IQD and KLCR proteins are targets of Mitogen Activated Protein Kinases (MPK) and that the localization of IQD1 might be regulated by MPK derived phosphorylation.

Collectively this study supports the hypothesis that IQD proteins act as scaffolding proteins mediating CaM dependent  $\text{Ca}^{2+}$  signaling at specific sites at the cell the ensure a fast and local response.

## Zusammenfassung

Als Teil der zellulären Signalverarbeitungsmechanismen spielen die Kalzium-Ionen ( $\text{Ca}^{2+}$ ) als sekundäre Botenstoffe eine wichtige Rolle bei der Vermittlung Umwelt- und entwicklungsspezifischer Stimuli. Diese Reize führen zu einem Anstieg der zytosolischen Kalziumkonzentration, welche von  $\text{Ca}^{2+}$ -Sensorproteinen wie den Calmodulinen (CaM) perzipiert wird. Die Bindung von  $\text{Ca}^{2+}$  durch Apo-CaM ändert die Faltung von CaM ( $\text{Ca}^{2+}$ -CaM) und damit die Affinität zu deren interagierenden Proteinen und ändert somit die molekulare Funktion der CaM-Bindeproteine. Eine Gruppe dieser Bindeproteine sind die pflanzenspezifischen IQ67-Domänen-Proteine (IQD), die über 33 Mitglieder in *Arabidopsis thaliana* verfügen. Die namensgebende IQ67-Domäne ist die CaM-Bindestelle und besteht aus sich wiederholenden bekannten CaM-Bindemotiven. Neben der höchstwahrscheinlich helikalen Struktur der IQ67-Domäne scheint der Rest der IQD-Proteine aus intrinsisch ungeordneten Regionen zu bestehen. Die meisten IQD-Proteine assoziieren mit Mikrotubuli (MT) und sind im Zellkern bzw. subnuklearen Strukturen wie dem Kernkörperchen lokalisiert. Neben der Bindung von CaM interagieren IQD Proteine auch mit Kinesin Light Chain-Related (KLCR) Proteinen. Die KLCR-Bindestelle ist direkt an die IQ67-domain anschließend und zeigt damit, dass sich die beiden Interaktoren gegenseitig beeinflussen könnten. Reverse genetische Analysen zeigten, dass IQDs höchstwahrscheinlich bei der Regulation der Zellform involviert sind und damit auch die Organ- bzw. Pflanzengestalt beeinflussen. Obwohl die IQD-Genfamilie in verschiedenen Pflanzengattungen untersucht wurde, ist über die biologische Rolle und über die molekulare Funktion wenig bekannt.

Diese Arbeit zeigt, dass IQD1 und generell IQD-Proteine unabhängig vom  $\text{Ca}^{2+}$ -Status mit CaM interagieren können. Es wird weiterhin gezeigt, dass IQD-Proteine direkt mit KLCRs und mit MT *in vitro* interagieren sowie KLCRs und CaM gleichzeitig an MT *in planta* rekrutieren können. Erste Hinweise zeigen, dass KLCR-Proteine mit  $\text{Ca}^{2+}$ -CaM interagieren und IQD-abhängig zu Apo-CaM rekrutiert werden können. *In vitro* und *in planta* Ansätze deuten darauf hin, dass IQD- und KLCR-Proteine durch Mitogen activated Protein Kinases (MPK) phosphoryliert werden und dass die Lokalisation von IQD1 durch diese Phosphorylierungen reguliert wird.

Zusammengefasst unterstützen die Ergebnisse dieser Arbeit die Hypothese, dass IQD-Proteine als Gerüstproteine fungieren, indem sie die CaM-vermittelte  $\text{Ca}^{2+}$  Signalweitergabe an spezifischen Stellen der Zelle verankern und somit eine schnelle und lokale molekulare Antwort zu ermöglichen.

# Table of contents

Abstract .....	i
Table of contents .....	iii
List of abbreviations.....	v
List of tables .....	viii
List of figures .....	ix
1. Introduction.....	1
1.1 Ca <sup>2+</sup> signaling in plants.....	1
1.2 IQ67-Domain proteins: plant specific CaM targets .....	3
1.3 Microtubules are ubiquitous hubs for cellular processes .....	4
1.4 Regulation and organization of MT dynamics.....	5
1.5 Kinesin Light Chain Related proteins – a class of IQD interacting proteins.....	8
1.6 IQDs within the nucleus.....	9
1.7 Posttranslational regulation of IQD proteins .....	10
1.8 Aims .....	12
2. Material and Methods .....	13
2.1.1 Cloning .....	13
2.1.2 Mobilization of genes and fragments .....	14
2.1.3 Site-directed mutagenesis .....	14
2.2.1 Protein Expression .....	16
2.2.2 Protein purification.....	16
2.2.3 GST-pulldown.....	17
2.2.4 SDS-PAGE .....	17
2.2.5 Western blotting and immuno-detection .....	18
2.3 Chemo-competent cells.....	19
2.4 MT spin-down.....	19
2.5 CaM pulldown.....	19
2.6 <i>In vitro</i> phosphorylation assays .....	20
2.7 Phosphoproteomics.....	20
2.8 Transient expression in <i>N. benthamiana</i> .....	21
2.9 Plant propagation .....	22
2.10 Microscopy .....	22
2.11 Stability assay.....	22
2.12 Yeast-two-hybrid.....	22
2.13 <i>In silico</i> analysis.....	23

2.14	Media.....	24
2.15	Buffers .....	25
3.	Results.....	28
3.1	Most IQD proteins interact with Apo- and Ca <sup>2+</sup> -CaM <i>in vitro</i> . .....	28
3.2	IQDs directly interact with KLCRs.....	30
3.3	IQD proteins recruit KLCRs to Apo-CaM .....	31
3.4	IQD1 interacts with the TPR-domain containing regions of KLCR1 .....	35
3.5	IQD proteins directly interact with MT .....	37
3.6	IQD proteins are <i>in vitro</i> MPK-targets.....	39
3.7	IQD1 interact with MPKs <i>in planta</i> .....	42
3.8	IQD1 changes its nucleolar localization upon phosphorylation....	43
3.9	KLCRs are <i>in vitro</i> MPK targets.....	45
3.10	KLCRs interact with MPKs <i>in planta</i> and recruit them to MT .....	47
3.11	MPKs interact with CaM <i>in planta</i> .....	50
4.	Discussion .....	52
4.1	IQD proteins as hubs for CaM-mediated Ca <sup>2+</sup> signaling .....	52
4.2	IQD proteins involved in MT linked processes.....	54
4.3	IQDs within the nucleus.....	56
4.4.	Regulating KLCRs .....	58
5.	Bibliography .....	60
6.	Supplements.....	68
7.	Publications .....	84
7.1	Oral Presentations.....	84
7.2	Poster Presentations .....	84
8.	Curriculum Vitae .....	86
9.	Danksagung .....	87
10.	Eidesstattliche Erklärung .....	88

## List of abbreviations

35S	cauliflower mosaic virus 35S promoter
<i>A. thaliana</i>	<i>Arabidopsis thaliana</i>
<i>A. tumefaciens</i>	<i>Agrobacterium tumefaciens</i>
ADE	adenine
amp <sup>(R)</sup>	ampicillin (resistance)
ANOVA	analysis of variance
APS	ammonium persulfate
AUX/IAA	auxin/indoleacetic acid
ARF	auxin response factor
ATP	adenosine triphosphate
BiFC	bimolecular fluorescent complementation
BSA	bovine serum albumin
CaBP	calcium binding protein
CaM	calmodulin
CAMTA	calmodulin-binding transcriptional activator
carb <sup>(R)</sup>	carbenicillin (resistance)
CBB	coomassie brilliant blue
CBL	calcineurin beta-like protein
CDPK	calcium dependent protein kinase
CFP	cyan fluorescent protein
CLASP	clip associated protein
CML	calmodulin like protein
CMU	cellulose microtubule uncoupling
CSC	cellulose synthase complex
CSI	cellulose synthase interacting
C-terminal	carboxyterminal
cYFP	C-terminal half of YFP
DAMP	damage associated molecular pattern
ddH <sub>2</sub> O	double distilled water
DFC	dense fibrillary center
DNA	deoxyribonucleic acid
dNTP	deoxy nucleoside triphosphate
DTT	dithiothreitol
EB1	end-binding protein
<i>E. coli</i>	<i>Escherichia coli</i>
EDTA	ethylenediaminetetraacetic acid
EGTA	ethylene glycol-bis(β-aminoethyl ether)-N,N,N',N'-tetraacetic acid
ER	endoplasmic reticulum
<i>et al.</i>	<i>et alii</i> – and others
EV	empty vector
FC	fibrillar centers
FWD	forward
GAL4-AD	GAL4 activation domain

## List of abbreviations

---

GAL4-DBD	GAL4 DNA binding domain
GC	granular component
GDP	guanosin diphosphate
gent <sup>(R)</sup>	gentamycin (resistance)
GFP	green fluorescent protein
GS	glucosinolate
GST	glutathion S-transferase
GTP	guanosin triphosphate
HEPES	4-(2-hydroxyethyl)-1-piperazineethanesulfonic acid
His	10 histidins fused to a protein
HIS	histidine
HRP	horseradish peroxidase
IgG	immunoglobulin G
IPTG	isopropyl $\beta$ -D-1-thiogalactopyranoside
kan <sup>(R)</sup>	kanamycin (resistance)
kb	kilo bases
KCBP	kinesin-like calmodulin binding protein
kDa	kilo dalton
KHC	kinesin heavy chain
KLC	kinesin light chain
KLCR	kinesin light chain related
LB	lysogeny broth
LEU	leucine
LSM	laser scanning microscopy
MPK	mitogen activated protein kinase
MKK	mitogen activated protein kinase kinase
MKKK	mitogen activated protein kinase kinase kinase
MKP	mitogen activated protein kinase phosphatase
mRFP	monomeric red fluorescent protein
MS	mass spectrometry
NEDD1	neuronal precursor cell Expressed, Developmentally Down-regulated protein 1
Ni-NTA	nickel nitrilotriacetic acid
NLS	nuclear localization signal
nYFP	N-terminal halve of YFP
OD <sub>600</sub>	optical density at 600nm
P	pellet
PAMP	pathogen associated molecular pattern
PC	pavement cell
PCR	polymerase chain reaction
PDB	protein database
PEG	polyethylene glycol
pH	<i>potentia hydrogenii</i>
PIPES	piperazine-N,N'-bis(2-ethanesulfonic acid)
pSP	phosphorylated serine followed by proline
PTM	post-translational modifications



pTP	phosphorylated tyrosine followed by proline
REV	reverse
RFP	red fluorescent protein
ROP	rhodopsin of plants
ROS	reactive oxygen species
rpm	rounds per minute
RNA	ribonucleic acid
rRNA	ribosomal ribonucleic acid
SCF	SKP, cullin, F-box containing protein
SDS	sodium dodecyl sulfate
SDS-PAGE	sodium dodecyl sulfate polyacrylamide gel electrophoresis
SKP	s-phase kinase-associated protein
SN	supernatant
spec <sup>(R)</sup>	spectinomycin (resistance)
SPR	spiral
ssDNA	single stranded DNA
T7	peptide derived from the T7 major capsid protein
TBS(-T)	tris-buffered saline (with Tween-20)
TE	Tris EDTA
TEMED	tetramethylethylenediamine
+TIP	plus end binding proteins
TPR	tetratricopeptide repeat
Tris	tris(hydroxymethyl)aminomethane
TRP	tryptophan
TuRC	tubulin ring complex
Ubi10	promotor of <i>UBI10</i>
UV	ultra violet
v/v	volume per volume
WRKY	WRKY transcription factor
WT	wild type
w/v	weight per volume
Y2H	yeast-two-hybrid
YFP	yellow fluorescent protein

## List of tables

Table 1: PCR conditions .....	13
Table 2: List of oligonucleotides used for PCR and SDM .....	14
Table 3: List of plasmids .....	16
Table 4: Antibodies used for immuno detection .....	19
Table S 1: Examples of MAP and their proposed function.....	82
Table S 2: Mass spectromic analysis of <i>in vitro</i> MPK-phosphorylated KLCR1 .	83

## List of figures

Figure 1 Calcium acts as a second messenger:.....	2
Figure 2: Structure and dynamics of MT .....	5
Figure 3: Microtubule Associated Proteins (MAPs) regulate and utilize the MT cytoskeleton .....	7
Figure 4: Most IQD proteins interact with Apo- and Ca <sup>2+</sup> -CaM <i>in vitro</i> .....	29
Figure 5: IQD1 and KLCR proteins directly interact <i>in vitro</i> .....	30
Figure 6: IQD2 and KLCR proteins directly interact <i>in vitro</i> .....	31
Figure 7: IQD1 protein recruits KLCRs to Apo-CaM .....	32
Figure 8: IQD2 protein recruits KLCR1 to Apo-CaM.....	32
Figure 9: CFP-IQD1 recruits the complemented nYFP-CaM2:cYFP-KLCR1 complex to the MT .....	33
Figure 10: TPR containing regions of KLCR1 interact with Ca <sup>2+</sup> -CaM.....	34
Figure 11: IQD1 interacts with the TPR domain containing regions of KLCR1 .	36
Figure 12: IQD proteins interact directly with MT .....	38
Figure 13: Most IQDs are phosphorylated .....	39
Figure 14: IQD2 is an <i>in vitro</i> MPK phosphorylation target.....	40
Figure 15: IQD1 interacts with MPKs <i>in planta</i> .....	42
Figure 16: IQD1 changes its localization upon phosphorylation .....	44
Figure 17: KLCRs are <i>in vitro</i> MPK targets.....	46
Figure 18: MPKs interact with KLCRs <i>in planta</i> .....	49
Figure 19: MPKs interact with CaM <i>in planta</i> .....	50
Figure 20: Proposed model of IQD1 as a CaM and KLCR scaffold .....	53
Figure 21: IQD proteins are most likely regulated via phosphorylation by MPK55	
Figure 22: KLCR and IQD proteins influence their localization mutually.....	57
Figure S 1: Structural features of IQD proteins.....	69
Figure S 2: mRFP-KLCR1 is recruited to the MT by nYFP-IQD1:cYFP-CaM2 complex .....	70
Figure S 3: IQD1 does not recruit RFP-tagged MPKs to MT. ....	71
Figure S 4: IQD1 is phosphorylated by MPKs <i>in vitro</i> .....	72
Figure S 5: MPK activity <i>in vitro</i> .....	73
Figure S 6: Overview of IQD1 features .....	74
Figure S 7: IQD1 does not interact with MPKs <i>in vitro</i> .....	75
Figure S 8: KLCRs do not interact with MPKs <i>in vitro</i> .....	76
Figure S 9: Phosphorylation of IQD1 might increase its stability .....	77
Figure S 10: Alignment of amino acid sequences of IQD1, IQD13 and IQD16.	78
Figure S 11: Predicted structure of IQD1 .....	79
Figure S 12: Structural prediction of IQD proteins .....	81



# 1. Introduction

## 1.1 Ca<sup>2+</sup> signaling in plants

Calcium (Ca<sup>2+</sup>) comprises around 4% of earth's crust. It is the fifth most abundant element. By forming insoluble complexes with phosphates, which are the main source in the energy metabolism of cells in the form of ATP, Ca<sup>2+</sup> is cytotoxic. To prevent the permanent precipitation of calcium phosphates, Ca<sup>2+</sup> is constantly exported into the extracellular space or intracellular storage compartments like the vacuole and the ER leading to a steep concentration gradient between the cytosol ([Ca<sup>2+</sup>]<sub>cyt</sub>) and apoplastic as well as compartmental Ca<sup>2+</sup> concentration (Bose et al. 2011). This gradient is a prerequisite for the cell to rapidly transduce signals by changing the [Ca<sup>2+</sup>]<sub>cyt</sub> making Ca<sup>2+</sup> ions ubiquitous second messengers involved in many aspects of plant defense, growth and development (Tuteja and Mahajan 2007). Upon various developmental and environmental cues Ca<sup>2+</sup>-specific ion channels are activated (Mori and Schroeder 2004) leading to the influx of Ca<sup>2+</sup> ions into the cytosol. The activation and inactivation of Ca<sup>2+</sup>-channels can occur in repetitive manners leading to Ca<sup>2+</sup>-oscillations (Evans, McAinsh, and Hetherington 2001) with stimulus specific oscillations that differ in length, amplitude and frequency referred to as Ca<sup>2+</sup> signatures (Evans, McAinsh, and Hetherington 2001; Smedler and Uhlen 2014). To decode the information encoded by changes in [Ca<sup>2+</sup>]<sub>cyt</sub> a vast number of Calcium Binding Proteins (CaBP) are present in plants. The most prominent Ca<sup>2+</sup> binding motifs, the EF-hands, are present in over 250 proteins (Bose et al. 2011; Day et al. 2002). EF-hands show a helix-loop-helix structure and bind Ca<sup>2+</sup> ions via a DxDxDG motif (Rigden and Galperin 2004). Two types of CaBPs have been described. Ca<sup>2+</sup>-responders like Ca<sup>2+</sup>-Dependent Protein Kinases (CDPK) change their enzymatic activity upon Ca<sup>2+</sup> binding and directly phosphorylate their targets and modify their activity (Cheng et al. 2002). Ca<sup>2+</sup>-sensor relays like Calcineurin B-like (CBL), CaM and CaM-like proteins (CML) change their affinity towards their interacting proteins after Ca<sup>2+</sup> binding (Fig. 1) (Batistic and Kudla 2009; Perochon et al. 2011). After Ca<sup>2+</sup> binding CBLs activate CBL interacting Protein Kinases (CIPK) which subsequently phosphorylate target proteins changing their biochemical properties leading to specific molecular responses (Luan 2009). The defining feature of CaM proteins is the presence of 2 globular domains containing 2 EF-hands each, which are connected by a flexible linker. The binding of Ca<sup>2+</sup> leads to conformational changes of CaMs, altering their affinity towards their interacting proteins, the CaM Binding Proteins (CaMBP). Interaction of CaMBPs with CaM can lead to inactivation, relief of auto-inhibition, active site

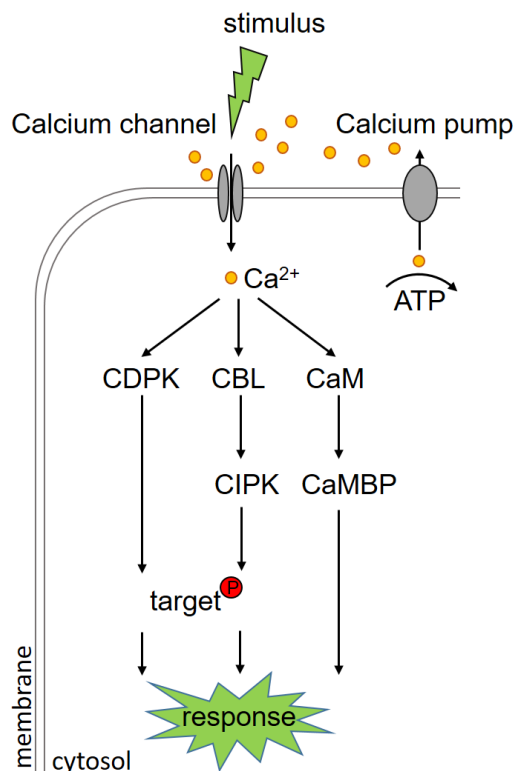


Figure 1 **Calcium acts as a second messenger**: Due to its cytotoxicity,  $\text{Ca}^{2+}$  is exported into the extracellular space or organelles by Calcium pumps. This gradient is used to transduce signals within the cell. The activation of calcium channels increases the intracellular  $\text{Ca}^{2+}$  concentration which is perceived by different Calcium Binding Proteins (CaBP). Calcium Dependent Protein Kinases (CDPKs) are activated after binding  $\text{Ca}^{2+}$ , leading to the phosphorylation of their target proteins. Calcineurin  $\beta$ -Like (CBL) proteins bind calcium, enabling them to interact with the CBL Interacting Protein Kinases (CIPK) leading to the phosphorylation of their target proteins and thereby change the activity of the targets. Calmodulin (CaM) and Calmodulin-like proteins bind calcium, which changes their conformation. This changes their affinity towards the CaM Binding Proteins (CaMBP) and by binding or dissociation, changes the activity of the CaMBPs. All those processes lead to specific responses enabling cells to adapt to their developmental status or to biotic as well as abiotic changes in the environment.

remodeling as well as dimerization or stabilization of multimeric complexes (Bouche et al. 2005). CaMBPs do not only show a great variety regarding their biochemical function but also play roles in various regulational pathways. CaM has been shown to interact with protein kinases like  $\text{Ca}^{2+}$ /CaM-dependent protein Kinases (CCaMK) in animals (Wang et al. 2015; Cerri et al. 2017), and Mitogen Activated Protein Kinases (MPK) in eukaryotes (Takahashi et al. 2011) and by this influencing the expression of specific genes. CaM also directly bind to and regulates transcription factors like the plant specific WRKY transcription factors (Park et al. 2005) and the CaM Transcription Activators (CAMTA) (Finkler, Ashery-Padan, and Fromm 2007). CAMTAs have different functions in the plant cell. CAMTA3 is involved in plant defense (Galon et al. 2008), CAMTA1 mediates drought responses (Pandey et al. 2013) and both have been reported to play roles in influencing cold-regulated gene expression (Doherty et al. 2009).

Computational analysis suggested that the interaction of Ca<sup>2+</sup>-CaM with CAMTAs and the subsequent expression responses could be part of the molecular machinery to decode the differences in Ca<sup>2+</sup> oscillations in the nucleus after different stimuli (Liu, Whalley, and Knight 2015).

The *Arabidopsis thaliana* genome encodes seven *bona fide* CaM and 50 CML genes indicating a high diversity in Ca<sup>2+</sup> perception via CaM and CML proteins. Taking into account that both Apo- and Ca<sup>2+</sup>-CaM have regulatory functions this underlines the versatility of CaM dependent Ca<sup>2+</sup> signaling.

## 1.2 IQ67-Domain proteins: plant specific CaM targets

Comprising of 33 members, the largest group of CaMBPs in *A. thaliana* are the plant specific IQ67-Domain (IQD) proteins. The hallmark of IQD proteins is the presence of the IQ67-Domain which consists of several known CaM-binding sites, the IQ-motif, the 1-5-10-motif and the 1-8-14-motif (Hoefflich and Ikura 2002; Abel, Savchenko, and Levy 2005a). The IQ-motif is known to mediate mainly binding to Apo-CaM whereas the latter ones are known to recruit Ca<sup>2+</sup>-CaM (Bahler and Rhoads 2002; Yap et al. 2000). Besides the CaM-binding motifs, Arabidopsis IQ67-domains also harbor a phase 0 intron within the first IQ-motif. Only IQD33 shows a truncated IQ67 domain due to an exon loss (Abel, Savchenko, and Levy 2005a). The IQ67-domain is the CaM binding site of IQD proteins and is sufficient to bind to Calmodulin (Burstenbinder et al. 2013). Overlay assays as well as *in vitro* pull down assays suggested that IQD proteins might interact with both states of CaM.

Besides the interaction with CaM further common features of IQD proteins are the association with microtubules (MTs) and/or the plasma membrane as well as the localization to the nucleus and nucle(ol)ar compartments.

The founding member of the IQD family, Arabidopsis IQD1 was identified in a forward genetic screen searching for plants with altered glucosinolate (GS) content and composition (Levy et al. 2005). *IQD1* overexpression lines showed increased levels of GS as well as increased levels of GS-biosynthesis related transcripts. *IQD1* overexpression lines were less frequented by *Trichoplusia ni* larvae and the larvae feeding on those lines showed a decreased bodyweight. This could be due to cytotoxic effects of GS towards herbivores (Kos et al. 2012). Besides the proposed role of IQD1 in plant defense, IQD proteins emerged to be involved in developmental processes. The adaxial epidermal pavement cells (PC) have a jigsaw like morphology. The overexpression of IQD25 in Arabidopsis led to reduced depth of PC indentations and by this to rounder PC. The overexpression of IQD16 results in elongated PC. In case of IQD16 the overexpression also led to twisting and elongation of leaves (Burstenbinder et al. 2017). This elongating effect has also been reported in other plant

species. In *Solanum lycopersicum* (tomato) the retrotransposon-based duplication of *IQD12/SUN* leads to pear-shaped fruits (Wu et al. 2011). In *Citrullus lanatus* (water melon) the deletion of a 159 bp long stretch of *IQD26* leads to elongated fruits (Dou et al. 2018). The same was reported for a 161 bp deletion within a *SUN* locus in *Cucumis sativus* (cucumber) (Pan et al. 2017).

For secondary cell wall formation, the cell wall compounds are transported within vesicles along the MT by kinesins and are released into the apoplast by exocytosis. During the development of meta xylem vessels Rhodopsin Of Plants 11 (ROP11) proteins act as local destabilizers of MT preventing secondary cell wall formation leading to the development of oval secondary cell wall pits. The MT associated IQD13 has been shown to act as a ROP11 repellent leading to the absence of cortical MT in areas where ROP11 is present. When IQD13 is missing, cortical MT are present in ROP11 membrane areas and rounder secondary cell wall pits were measured. The overexpression of IQD13 on the other hand leads to parallel aligned MT possibly due to its MT bundling activity suggested by its several MT associating domains (Sugiyama et al. 2017). 2017 Sugiyama *et al.* hypothesized that this leads to parallelly to the MT elongated cell wall pits and ROP11 containing membrane drafts.

Many developmental processes like stem cell maintenance, root and fruit development and hypocotyl elongation are regulated by the hormone auxin (Stewart and Nemhauser 2010). When low levels of auxin are present AUX/IAAs binding to the Auxin Response Factors (ARFs) and repress their function as transcription factors. When the auxin levels rises, AUX/IAAs are ubiquitinated by the SCF E3 ubiquitin ligase complex and subsequently are degraded by the proteasome. This releases the ARFs and enables them to initiate the expression of specific auxin response genes. The ARF5/MONOPTEROS (MP) is involved in the formation of the embryonic root. MP knock-lines showed miss-expression of the *IQD15-18* genes (Wendrich 2016; Moller et al. 2017) hinting to the fact that IQD proteins might be involved in the cross-talk between  $Ca^{2+}$  and auxin during root formation and maybe other developmental processes.

### 1.3 Microtubules are ubiquitous hubs for cellular processes

IQD proteins have been shown to associate with a specific subset of cytoskeletal structures in planta: the microtubules (MT). Due to the size of plant cells, diffusion becomes a limiting factor to target specific reactions at specific sites of the cell. In general, the cytoskeleton enables cells to transport the needed cargoes along those long tracks spanning throughout the cell. They also provide stability and function in numerous cellular processes. Lacking intermediate filaments (Goldberg 2013), plants have two sets of cytoskeletal components: the actin filaments and the microtubules (MT). The MT consist of hetero dimers of  $\alpha$ - and  $\beta$ -tubulins (Fig 2A). The dimers align in a head to toe fashion forming linear protofilaments (Fig 2D). This leads



to a polarization, meaning that at the +end the  $\beta$ -tubulins are exposed and at the –end the  $\alpha$ -tubulin is situated (Fig. 2C). The protofilaments form tubular structures consisting of 13 protofilaments (Fig. 2B). Although only *in vitro*, other types of MT have also been reported ranging from 8-20 protofilaments per tubulus (Sui and Downing 2010). Besides acting as tracks to transport cargoes throughout the cell MT play critical roles during cell division. There they act as tracks to separate the chromosomes (spindle apparatus) as well as define the site of cytokinesis (pre-prophase band, phragmoplast, cell division zone/site) (Van Damme, Vanstraelen, and Geelen 2007; Lee, Qiu, and Liu 2015). The common MT localization of IQDs and the growth-related phenotypes on *iqd* mis-expression lines suggest that IQDs might link  $\text{Ca}^{2+}$ -CaM signaling to regulation of the MT cytoskeleton.

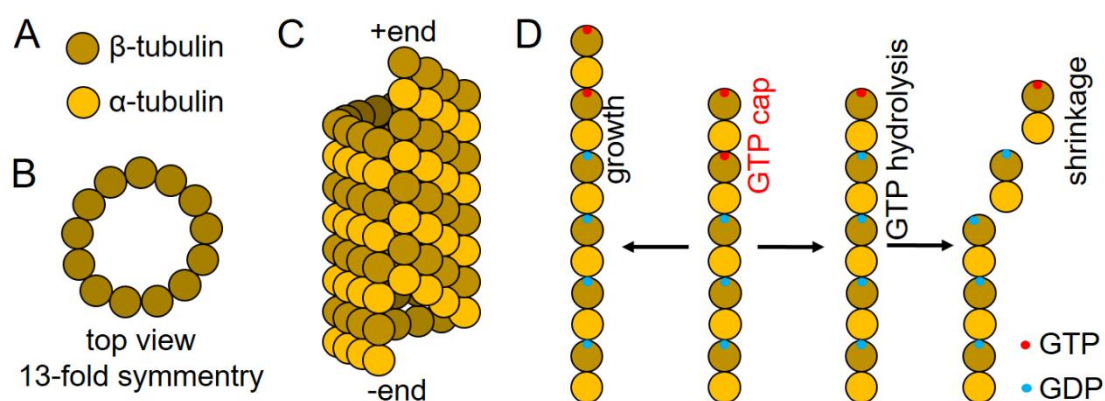


Figure 2: **Structure and dynamics of MT**

MTs consist of  $\alpha$ - and  $\beta$ -tubulins (A). They form tubular structures (B) and due to the head to tail arrangement have a polarity (C). Growth and shrinkage of MTs take place at the +end (D). The  $\beta$ -tubulins possess the ability to bind and hydrolyze GTP. The hydrolysis of GTP to GDP weakens the interaction between the individual protofilaments and prone them for depolymerization (adapted from (Hashimoto 2015)).

## 1.4 Regulation and organization of MT dynamics

The dynamics of MT are highly regulated. Tubulins themselves can only control the binding affinity of the protofilaments between each other and by this regulate the stability of MTs. Microtubule Associated Proteins (MAPs) are needed to mediate the diverse functions MTs are involved in and thereby integrate the ubiquitous MT network into the core processes of cellular functions (Fig. 3). The MT plus-end binding proteins (+TIPs) regulate growth, shrinkage and rescue of MT and by this define the fate of MT at specific sites and at specific times of cellular processes. The +TIP proteins End Binding protein 1 (EB1) are the most prominent +TIP protein family as they do not only influence MT at but also recruit other proteins to the plus end (Li et al. 2011). In *Arabidopsis* the three family members are proposed to be involved in a variety of different regulatory processes. EB1a seems to support polymerization of MT (Van Damme et

al. 2004), whereas EB1c regulates the alignment of spindle and phragmoplast MT (Komaki et al. 2010). EB1b together with Spiral1 (SPR1) is supposed to function in roots regulating MT dynamics after touch and gravity signals (Bisgrove et al. 2008; Galva et al. 2014). Loss of function mutants of SPR1 display twisted epidermal root cells and right-handed root skewing. Introducing the *eb1b* knock out mutation in the *spr1* mutant background enhanced the observed phenotypes, but the *eb1b* mutation alone resulted in a subtle left handed skewing. *In vitro* both proteins seem to either compete for the same MT-binding site or effect each other's MT binding affinities (Galva et al. 2014).

Nucleation of MT is organized by  $\gamma$ -tubulins and complex protein (GCP) 2 to GCP6 forming the so called  $\gamma$ -Tubulin Ring Complex ( $\gamma$ -TuRC). The  $\gamma$ -TuRC possesses 13  $\gamma$ -tubulins in a circular structure, which can interact with the  $\alpha$ -tubulin of the tubulin dimers. That leads to the exposition of  $\beta$ -tubulin establishing the polarity of MT (Hashimoto 2013). During Interphase, MT do not only form parallel structures but are also form branches influencing morphological outputs. For example, the Neuronal precursor cell Expressed, Developmentally Down-regulated protein 1 (NEDD1) is involved in recruiting the  $\gamma$ -TuRC to the MT allowing the formation of branches. NEDD1-RNAi plants showed a reduced number of branching events leading to parallel aligned MT in pavement cells, which subsequently do not show the jigsaw like structure of the WT (Walia et al. 2014). A similar phenotype has been described for plants overexpressing *IQD25* (Burstenbinder et al. 2017) and *iqd5* knock out lines (Burstenbinder et al. 2017).

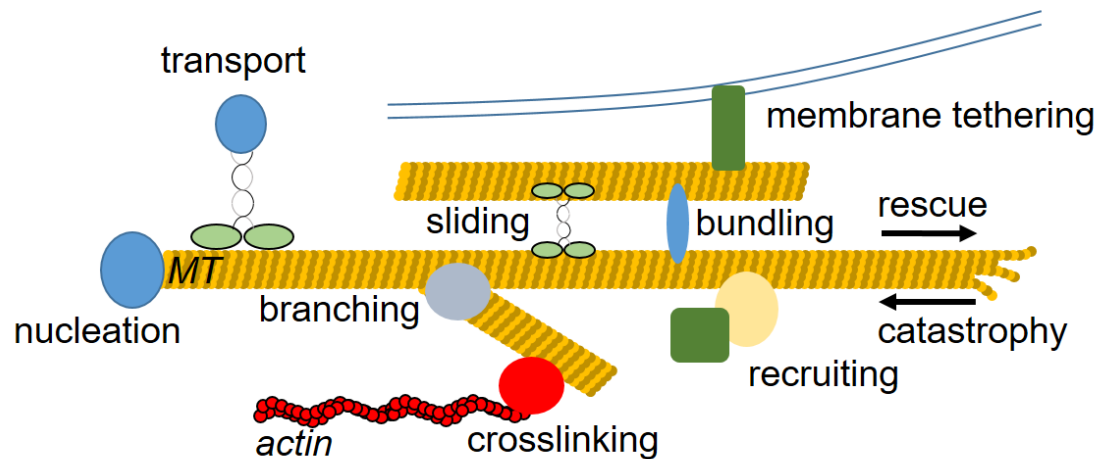


Figure 3: **Microtubule Associated Proteins (MAPs) regulate and utilize the MT cytoskeleton**

Examples of MAP functions and influence on the MT network. The many functions of MAP diversify the processes MT are involved in. MAPs can regulate the status of MT by forming sites for nucleation and branching but also influence the growth and shrinking of the MTs. Bundling of MT is also mediated by MAPs whereas some also let MT slide along each other. They can guide MT to specific sites of the cell by tethering them to specific domains at the plasma membrane or interconnect the MT network with the actin filaments. MT also act as tracks for proteins transporting cargoes along the MT network driven by the activity of the MT associated motor domain. Examples for MAP genes and their proposed function can be found in table S1.

Another important function of MAPs is to bundle and thereby align MT, influencing the trajectory direction of the MT network or connect them with the actin cytoskeleton. The plant specific Kinesin-Like Calmodulin Binding protein (KCBP/Zwichel) contains besides its MT binding motor domain an actin and a second MT binding site (Vinogradova et al. 2013). Its motor activity is negatively regulated by  $\text{Ca}^{2+}$ -CaM (Vos et al. 2000). Although KCBP labels MT of the mitotic array, mutant plants lacking KCBP do only show defects in trichome development and morphology (Oppenheimer et al. 1997).

In trichomes KCBP is believed to act as a MT crosslinker and to connect MT with actin filaments at different sites during trichome development (Tian et al. 2015). KCBP function is negatively regulated by interacting with  $\text{Ca}^{2+}$ -CaM or the KCBP-interacting  $\text{Ca}^{2+}$  Binding protein (KIC) which showed a higher degree of KCBP inhibition at lower  $\text{Ca}^{2+}$  concentrations compared to CaM (Reddy et al. 2004).

Cortical MT are situated right beneath the plasma membrane mediating processes like cell wall synthesis and cargo transport (see chapter 1.5). How MT are tethered to the membrane is not fully understood, nevertheless plants lacking the Clip-Associated Protein (CLASP) shows partial detachment of MT from the cortex leading to extensive waving of MTs (Ambrose and Wasteneys 2008). How CLASP is involved in MT membrane tethering is still under investigation.

How MT bundling proteins antagonize the mechanical forces attributed by MT sliding proteins as well as the entropic forces was analyzed by Lansky et al. 2015 using optical tweezers (Lansky et al. 2015). This highlights the complex dynamics regulating the MT network, which assures that cytoskeletal networks correctly modulate a morphological output.

Due to the regulatory role of  $\text{Ca}^{2+}$  within those processes, IQDs might play important parts in transducing external signals at specific sites of the network ensuring the correct modulation by the MAPs.

### **1.5 Kinesin Light Chain Related proteins – a class of IQD interacting proteins**

Besides the interaction with CaM little is known about interactor of IQDs. In a yeast-two hybrid (Y2H) based approach using a cDNA library, Kinesin Light Chain-Related 1 (KLCR1) was found to interact with IQD1 (Burstenbinder et al. 2013). The interaction between other IQDs and KLCRs has also been demonstrated in another Y2H approach. In search for central hubs in plant defense the Kinesin Light Chain Related protein (KLCR) 2 has been found to interact with effectors from two distinct plant pathogens. In search of interactors of those possible hubs for pathogen effectors it was found that KLCR2 interacts with IQD2 and IQD23 in yeast (Mukhtar et al. 2011). KLCRs, also known as Cortical Microtubule Uncoupling (CMU), are proteins showing similarities with mammal Kinesin Light Chains (KLC) (Burstenbinder et al. 2013). Mammalian KLCs together with the kinesin heavy chains (KHC) form type-1 kinesins. Kinesins are motor proteins which transport cargoes like vesicles and proteins along the MT network. The dimeric KHCs contain the motor domain and some cargo binding capacity, whereas the KLCs regulates kinesin activity as well as cargo binding and cargo specificity (Marx, Hoenger, and Mandelkow 2009; Reddy and Day 2001). The N-terminal part of KLCRs contains putative heptad repeats. In KLCs those repeats mediate the interaction with the coiled-coil structures of the dimeric KHC. The C-terminal part consists of several tetratricopeptide repeat domains (TPR). TPRs are protein-protein interaction domains and thereby could mediate cargo binding. In plants many kinesins have been identified based on sequence homologies with the motor domain of kinesins (Reddy and Day 2001). However, no functional KHC has been described in plants yet, leaving the question whether plant KLCRs have the same functions as their proposed animal counterparts, KLCs. What has been shown is that they are recruited towards MTs in an IQD dependent manner (Burstenbinder et al. 2013).

The cell wall not only gives plant cell its rigidity to cope with mechanical stresses but also controls the direction of growth and thereby dictates cell morphology. The major component of plant cell walls and the most common biopolymer is cellulose (Szymanski and Cosgrove 2009).

Cellulose fibrils are synthesized by the membrane localized Cellulose Synthase Complex (CSC). The complex is linked to MT via Cellulose Synthase Interacting 1 (CSI1) (Lei et al. 2013). This restricts the CSC to deposit cellulose only on the tracks given by cortical MT presence. In cells of the elongation zone of roots and hypocotyls cortical MT are aligned transversely to the growth direction. The cellulose microfibrils are synthesized surrounding the cell like a spring. This restricts the turgor driven cell expansion to only follow the longitudinal growth direction. The CSC itself has no motor domain but slides along the MT by the pushing forces of the forming cellulose. KLCR1/CMU1 is supposed to stabilize the cortical microtubules to the PM preventing a misplacing of those MT by the pushing forces of the CSC (Liu et al. 2016). This shows that KLCR1/CMU1, as suggested for IQD proteins, plays a crucial role in the cytoskeleton-PM nexus. The recruitment to MT *in planta* as well as the interaction in yeast suggests that IQD and KLCR proteins are direct interactors (Burstenbinder et al. 2013; Petzold et al. 2017; Mukhtar et al. 2011). But the biological role of this interaction is still elusive. Possibly, KLCR function is regulated via  $Ca^{2+}$  in a CaM dependent manner where IQD1 acts as a hub to mediate this interaction.

## 1.6 IQDs within the nucleus

Within the nucleus gene expression, replication, transcription, gene silencing and rRNA maturation is taking place. Many of those functions take place in sub-compartments within the nucleus (Cruz and Moreno Diaz de la Espina 2009). One of those compartments is the nucleolus. Besides rRNA biosynthesis, ribosome biogenesis and the maturation of ribonucleoproteins, the nucleolus functions in age control, sequestration of molecules and nuclear export (Stepinski 2014). To regulate those functions the nucleolus itself is divided into 3 compartments. The granular component (GC) builds a cortex-like structure around the dense fibrillar component (DFC) where the fibrillary centers (FC) are located (Thiry and Lafontaine 2005). All those compartments are known to locate different steps in rRNA biosynthesis and ribonucleoproteins maturation (Stepinski 2014).

IQD proteins show a diverse localization regarding their nuclear presence and a about half of these IQD family members localize to the nucleus. IQD6 and IQD18 are localizing to speckled spots within the nucleus whereas IQD1 and IQD15 are localizing to the nucleolus. IQD1 localizes to the cortex of the nucleolus suggesting a localization to the GC (Burstenbinder et al. 2017). It is proposed that within the GC the last steps of the rRNA maturation are taking place (Stepinski 2014). Compared to the nucleus the nucleolus shows a lower pH-value. This enables basic proteins to be targeted to the nucleolus, hence most nucleolar localization signals (NoLS) consist of basic stretches within the protein (Martin et al. 2015). Both is present in IQD1 and could explain its localization to the nucleolus. Besides its localization towards the

nucleolus nothing is known about the role of IQD1 within the nucleolus or the general role of IQDs within the nucleus and its compartments.

### 1.7 Posttranslational regulation of IQD proteins

IQDs contain long stretches comprising of basic amino acids. In general, such basic stretches can mediate functions found to be hallmarks of IQD proteins like MT- and PM-binding and the nuclear localization. Rendering the charge of those stretches via post-translational modifications (PTM) could regulate those processes. One class of PTM leading to the addition of a negatively charged group are phosphorylations taken out by kinases. One protein family of kinases are the Mitogen Activated Protein Kinases. Unrelated studies showed, that IQDs could be targets of MPKs {Feilner, 2005 #711}.

Like Calcium, the MPK cascade is involved transducing signals to regulate responses to biological (Meng and Zhang 2013) and abiological stresses (Moustafa et al. 2014) as well as developmental cues (Xu and Zhang 2015)). The activation of the classic MPK cascade starts from an extracellular signal like plant hormones, Damage Associated Molecular Patterns (DAMPs), Pathogen Associated Molecular Patterns (PAMPs) or Reactive Oxygen Species (ROS). Those signals are perceived by membrane localized receptor kinases. This leads to the activation of the intracellular kinase domain leading to the phosphorylation of a specific MPK Kinase Kinase (MKKK). The thereby activated MKKK phosphorylates specific MPK Kinases (MKK) which subsequently phosphorylates MPKs. In the classical canonical MAP cascade those MPKs are the kinases, phosphorylating the specific target proteins and by this changing their activity. Some MPKs have been reported to have an influence on cortical MT or MT of the spindle apparatus. MPK4 and MPK6 are involved in MT processes during cell division (Komis et al. 2011). During cytokinesis MAP65-1 bundles and stabilizes MT in the phragmoplast possibly to allow vesicle transport to the forming cell plate. AtMPK4 phosphorylates MAP65-1 leading to a decreased bundling which could lead to altered MT-dynamics and therefore the disassembly of the phragmoplast at positions where the cell plate has already been formed. Mutant lines lacking MPK4 or the corresponding MPKKK show oblique and incomplete cell plates and a dwarfed phenotype (Beck et al. 2011). MPK18 has been reported to affect cortical MT stability. mpk18 showed a decreased sensitivity towards MT destabilizing drugs. Interestingly, plants lacking the MPK-phosphatase Propyzamide-Hypersensitive 1 (PHS1) show a hypersensitivity towards MT destabilizing drugs. Introduction of mpk18 into the phs1 background could partially complement the phs1 root skewing phenotype (Walia et al. 2009). Interestingly the MPK18 phosphorylation seems not to be mediated by an MKK but directly by the MKKK20 (Benhamman et al. 2017). However the mode of MPK18 function and its influence on cortical MT stability is still unknown. Furthermore, the

MPK cascade is regulated by calcium. During wound responses MPK8 is activated by MKK3-dependent phosphorylation and interacts with  $\text{Ca}^{2+}$ -CaM. The full activation of MPK8 was only measured when both components, the phosphorylation and the  $\text{Ca}^{2+}$ -CaM interaction, were present (Takahashi et al. 2011). The MPK-Phosphatase 1 (MKP1) is involved in regulating responses to biotic and abiotic stresses (Anderson et al. 2011; Gonzalez Besteiro and Ulm 2013) and by interacting with CaM in a calcium dependent manner increase its phosphatase activity (Lee et al. 2008). Whether the known MT influencing MPKs and MKPs are also influenced by CaM is still elusive. Bimolecular Fluorescent Complementation (BiFC) experiments hint to an interaction of CaM4 with MPK16 and MPK17 but not MPK3, MPK4 and MPK6 (Takahashi et al. 2011). There is also a crosstalk between the MPK cascade and the Calcium Dependent Protein Kinases (CDPK) signaling. CDPK18 for example activates MPK5 by phosphorylation outside the classical MKK phosphorylation site (Xie et al. 2014). Furthermore MPKs and CDPKs could share target proteins phosphorylating them at specific sites at specific stages (Gao, Cox, and He 2014). Due to the fact that phosphorylations can differently regulate protein function, those phosphorylations could synergistically or antagonistically influence stress or developmental responses.

### 1.8 Aims

The founding member of the *Arabidopsis thaliana* IQD family, IQD1, was found in a screen aimed to identify genes affecting glucosinolate accumulation. Further studies showed that IQD proteins are *bona fide* Calmodulin (CaM) binding proteins due to the presence of the name giving IQ67-domain comprising of several known CaM binding motifs. CaMs are Ca<sup>2+</sup> sensor proteins and are part of the Ca<sup>2+</sup> signal transduction pathway. By characterizing other IQD proteins in *A. thaliana* it came clear that IQD1 and most IQD proteins associate with microtubules. Others are associated with the plasma membrane. Some of the IQD proteins also localize to the nucleus and subnuclear structures. By using reverse genetic approaches in *A. thaliana* and other plant species IQDs appeared to mainly be involved in influencing cell morphology and subsequently leading to altered organ shapes. Besides the ability to bind CaM, IQD1 also showed an interaction with Kinesin Light Chain Related proteins (KLCR) and can recruit both proteins to the MT. But little is known about the molecular mechanisms behind those interactions and how these interactions could influence cellular processes.

This work aims to analyze how IQD1 interacts with its known binding partners e.g. CaM and KLCRs. We will use *in vitro*, *in planta* and in yeast techniques to analyze those interactions. Moreover we are interested whether IQD proteins directly bind to MT and whether IQDs harbor the ability to interact with multiple proteins simultaneously. *In silico* analysis provided information that IQDs are post-translational modified via phosphorylation. We will analyze how these phosphorylations affect the fate of IQD1.

The resulting data will provide information about the molecular functions of IQD proteins and broaden our knowledge of IQD protein function during cellular processes.



## 2. Material and Methods

### 2.1.1 Cloning

All constructs were cloned by *in vitro* site-specific recombination (Hartley, Temple, and Brasch 2000). The gene or fragment of interest was amplified using Phusion Green High-Fidelity DNA Polymerase (ThermoFisher; #F-534L). The forward primer contained a CACC-overhang at the 5'-end. If truncated constructs were generated an additional start and/or stop codon was added. Primers used can be found in Tab. 2. The PCR was compiled of 0.1 µl template (e.g. purified vector), 0.5 µl of each primer, 4 µl 5xPhusion Green HF Buffer, 4 µl dNTPs (1 mM), 0.2 µl Phusion DNA polymerase and 10.7 µl ddH<sub>2</sub>O. The PCR was done using the thermocycler Mastercycler (Eppendorf; #6321000515). The cycles were programmed as followed:

Table 1: **PCR conditions**

Temperatures and cycle length and number used for amplification of coding sequences via PCR.

	Temperature	Duration	Number of cycles
Initial denaturing	95°C	5 min	1
Denaturing	95°C	15 sec	37-42, depending on efficiency
Annealing	primer dependent	15 sec	
Elongation	72°C	30 sec/kb	
Extension	72°C	5 min	1

The PCR product was separated using a 1% (w/v) agarose gel containing DNA Stain G (Serva; #39803.01) for visualization. Sizes were estimated by comparing with Gene Ruler 1k or 100bp, depending on the generated construct (ThermoFisher; #SM0313. #SM0241). The band was visualized by UV light and cut using a scalpel. The DNA was purified from the gel using the GeneJET Gel Extraction and DNA Cleanup Micro Kit (ThermoFisher; #0831) following the manufacturer's protocol. The purified DNA was cloned into the pENTRY vector using the pENTR/D-TOPO cloning kit (Invitrogen; #45-0218). 2 µl of the purified PCR product, 0.5 µl of salt solution and 0.5 µl of pENTR/D-TOPO vector were mixed and incubated at room temperature for >30 min. The solution was mixed with chemically competent Top10 cells (Genotype: F- *mcrA* Δ( *mrr-hsdRMS-mcrBC*) Φ80*lacZ*ΔM15 Δ *lacX74 recA1 araD139* Δ( *araleu*)7697 *galU galK rpsL* (StrR) *endA1 nupG*)(ThermoFisher; #C404010) and left on ice for 30 min. The mixture was heat shocked for 30 sec at 42°C and immediately put on ice. 400 µl of S.O.C.-medium was added and the solution was put on a shaker at 37°C for 1h. The bacterial solution was plated on LB-media agar plates containing 50µg/ml kanamycin and put

at 37°C over night. Colonies were picked and grown in 5 ml LB media containing 50µg/ml kanamycin over night. The plasmids were extracted using the GeneJET Plasmid Miniprep Kit (ThermoFisher, #K0503), following the manufacture's protocol. The correct insertion was analyzed by restriction digestion depending on the construct. The size of the plasmid fragments were analyzed by gel electrophoresis. For confirmation, plasmids were sent for sequencing.

### 2.1.2 Mobilization of genes and fragments

All constructs were mobilized into destination vectors by *in vitro* site-specific recombination (Hartley, Temple, and Brasch 2000). 2 µl of the plasmid solution containing the ENTRY-clone was mixed with 2 µl of the empty destination vector. 1 µl of Gateway LR-Clonase II (Invitrogen, #11791-100) was added and left for 2h at room temperature. Transformation, plasmid isolation and confirmation was achieved as described in chapter 3.1.1. Used plasmids are listed in Tab. 3.

### 2.1.3 Site-directed mutagenesis

Site directed mutagenesis was performed as stated in the manufacturers protocol of the AccuPrime Pfx DNA polymerase (Invitrogen; #12344-024). Primers used can be found in Tab. 2.

Table 2: List of oligonucleotides used for PCR and SDM

Oligonucleotides used for cloning and/or confirmation by colony PCR after ligation using Gateway technologies.

Primer:	Direction:	Sequence:
KLCR1	FWD	CACCATGCCAGCAATGCCAGGT
KLCR1	REV	TCAGAACTTGAAACCGAGGC
tr_KLCR1-I	FWD	TCAGAGATCAAGAACAGGTCCACCA
tr_KLCR1-II	REV	CACCATGGCTATGAGCCTTCATGTT
tr_KLCR1-II	FWD	TCATTTAGCCTCGCAGATAATTGCC
tr_KLCR1-III	FWD	GGGGACAAGTTTGTACAAAAAAGCAGGCTTCATGGGAGATTATGAAAACG
tr_KLCR1-III	REV	GGGGACCACTTTGTACAAGAAAGCTGGGTCTCAGCTCTGCTGTCC
tr_KLCR1-IV	FWD	CACCATGGCCATTGCAGGGTTAG
KLCR2	FWD	CACCATGGACGTAGGAGAGAGCAATG
KLCR2	REV	TCAATAAACCGGTCTCTGTCC
KLCR3	FWD	CACCATGGAAGGAGGGTCTGTTAATG
KLCR3	REV	TTAACGAAGAGCTGAAGAAGAAGTG
IQD1	FWD	CACCATGGTTAAAAAAGCGAAATGGC
IQD1	REV	TCACGGCGTTCTCTCTGC
IQD2	FWD	CACCATGGGGAAAAAAGCTAAATGGT

IQD2	REV	TCAGCTGCCTGCTCCGTT
IQD5	FWD	CACCATGGGAGCTTCAGGGAGATG
IQD5	REV	CTATGCAAGCCTCTGTTTTATTGG
IQD33	FWD	CACCATGGGTGTTACAGGAGATTAGTC
IQD33	REV	TTAGGTGCTGCTATTTAGCTTATGTG
IQD1-M2	FWD	CACC GAAGCAG GTATGTTGCA CAAGTAC
IQD1-M2	REV	TCAGGCTGTGG ATGATGCTGATGGGGTATTG
IQD1-C	REV	CACC AC CAGAAACCCG AGAAAGAAG
IQD1-phos-mimi-1-S16E	FWD	GTAAAAAGGCTTTTGAGCCAGATTCAAAGAAG
IQD1-phos-mimi-1-S16E	REV	CTTCTTTGAATCTGGCTCAAAGCCTTTTTAAC
IQD1-phos-mimi-2-S47E	FWD	CATCCAGAAGTTCTGAGCCTCAGTTTGAAGTTAG
IQD1-phos-mimi-2-S47E	REV	CTAACTCAAACCTGAGGCTCAGAACCTCTGGATG
IQD1-phos-mimi-3-4-S84E-S88E	FWD	TGTTCTTGTAGATGAGCCTCCATCTGAGCCTGAATCTGTC
IQD1-phos-mimi-3-4-S84E-S88E	REV	GACAGATTCAGGCTCAGATGGAGGCTCATCTACAAGAACA
IQD1 SDM PhosMim-8-S288E	FWD	CCACCAACAACGACAACCTCCGAGGTTAAGAAGCTCGAC
IQD1 SDM PhosMim-8S288E	REV	GTCGAGTTCTTAACCTCGGAGTTGTCGTTGTTGGTGG
IQD1 SDM PhosMim-9-10-S345E_S351E	FWD	CAAAGCGAGGATGATGAGGCCAAGGAGTCGGAGA
IQD1 SDM PhosMim-9-10-S345E_S351E	REV	TCTCCGACTCCTTGGCCTCATCATCCTCGCTTTTTG
IQD1 SDM PhosMim-11-S366E	FWD	GCTAGGCCATCGGTTGAGGATGACGAGACCCTGAG
IQD1 SDM PhosMim-11-S366E	REV	CTCAGGGTCTCGTCATCCTCAACCGATGGCCTAGC
IQD1-phos-mimi-5-T319E	FWD	GCTCGACTAAACCCAATGAGCCATCAGCATCATCCACAGCC
IQD1-phos-mimi-5-T319E	REV	GGCTGTGGATGATGCTGATGGCTCATTGGGTTTAGTCGAGC
IQD1-phos-mimi-6-T429E	FWD	CTCTCCACCTCGGCTGAGCCTGCACCCAAAC
IQD1-phos-mimi-6-T429E	REV	GTTTGGGTGCAGGCTCAGCCGAGGTGGAGAG
IQD1-phos-mimi-7-T453E	FWD	CGTTCTCAAGGCAGAGAGAGAGCCGTGAAAGGGTGG
IQD1-phos-mimi-7-T453E	REV	CCACCCTTTCACGGCTCTCTCTCTGCCTTGAGAACG
MPK3_fwd	FWD	ATGAACACCGGCGGTGGC
MPK3_rev	REV	CTAACCGTATGTTGGATTGAGTG
MPK4_fwd	FWD	ATGTCGGCGGAGAGTTGTTT
MPK4_rev	REV	TCACACTGTGTCTTGAGGATTG
MPK6_fwd	FWD	ATGGACGGTGGTTCAGGTCA
MPK6_rev	REV	CTATTGCTGATATTCTGGATTGAAAG
CaM2	FWD	ATGGCGGATCAGCTCACA
CaM2	REV	TCACTTAGCCATCATAACCTTCAC

Table 3: List of plasmids

Name	Resistance	Genotype	Reference
pENTR/D-TOPO	Kan <sup>R</sup>	attL1:TOPO:attL2; Kan <sup>R</sup>	ThermoFisher: #K240020
pDONR207	Gent <sup>R</sup>	attP1:ccdB:cm <sup>R</sup> :attP2;Gent <sup>R</sup>	Invitrogen: #12536-017
pDEST15	Carb <sup>R</sup>	T7::GST:attR1:cm <sup>R</sup> :ccdB:attR2; Amp <sup>R</sup>	ThermoFisher: #11802014
pDEST-N110	Amp <sup>R</sup>	7::lacO:10xHIS:attR1:cm <sup>R</sup> :ccdB:attR2, Amp <sup>R</sup> p35S::eGFP:attR1:cm <sup>R</sup> :ccdB:attR2; ba <sup>R</sup>	(Dyson et al. 2004) (Karimi, Inze, and Depicker 2002)
pB7WGF2	Spec <sup>R</sup>	p35S::mRFP:attR1:cm <sup>R</sup> :ccdB:attR2; ba <sup>R</sup>	(Nakagawa et al. 2007)
pGWB455	Spec <sup>R</sup>	35S::Venus <sup>C</sup> :HA:attR1:cm <sup>R</sup> :ccdB:attR2; Kan <sup>R</sup>	(Gehl et al. 2009)
pVYNE	Kan <sup>R</sup>	35S::Venus <sup>N</sup> :HA:attR1:cm <sup>R</sup> :ccdB:attR2; Kan <sup>R</sup>	
pVYCE	Kan <sup>R</sup>	pADH1::GAL4DBD:attR1:ccdB:cm <sup>R</sup> :attR2;	ProQuest Two-Hybrid System
pDEST32	Gent <sup>R</sup>	Gent <sup>R</sup> ;Leu2 ADH1::NLS:GAL4AD:attR1:ccdB:cm <sup>R</sup> :attR2;	with Gateway Technology (Invitrogen; # 10835)
pDEST22	Amp <sup>R</sup>	Amp <sup>R</sup> ;TRP1	

## 2.2.1 Protein Expression

Proteins were expressed using the KRX expression strain (Genotype: [F', *traD36*,  $\Delta ompP$ , *proA*<sup>+</sup>*B*<sup>+</sup>, *lacIq*,  $\Delta(lacZ)M15$ ]  $\Delta ompT$ , *endA1*, *recA1*, *gyrA96* (Nal<sup>r</sup>), *thi-1*, *hsdR17* (*r<sub>k</sub>*<sup>-</sup>, *m<sub>k</sub>*<sup>+</sup>), *e14*<sup>-</sup> (*McrA*<sup>-</sup>), *relA1*, *supE44*,  $\Delta(lac-proAB)$ ,  $\Delta(rhaBAD)$ ::T7 RNA polymerase)(Promega; #L3002). Cells were transformed with the expression vectors as described in chapter 3.1.1. Colonies were picked and used to inoculate LB-media containing the appropriate antibiotic. This pre-culture grew over night at 37°C. TB-media containing the appropriate antibiotic was inoculated with the pre-culture in a 1:20 ratio. This main culture was growing at 37°C for roughly 2 h. The main culture was monitored to not exceed an OD<sub>600</sub> value of 0.8-1. To induce expression 1 mM of IPTG and 0.1% rhamnose were added. Expression took place for 3 h at 37°C in a shaker at 140 rpm. To pellet the bacteria the culture was centrifuged for 20 min at 8000 g. The supernatant was removed and the pellet frozen at -80°C.

## 2.2.2 Protein purification

GST-tagged proteins were purified using purecube glutathione agarose (Cube Biotech; # 32103). His-tagged proteins were purified using Protino Ni-NTA Agarose (Macherey-Nagel; #745400.100). The pellet of a 100 ml main culture was resuspended using 8 ml of GST-lysis buffer or His-lysis buffer by pipetting. Greater main cultures were adjusted accordingly. The

bacterial slur was shaking in the cold room for 30 min. To disrupt the remaining cells and fragment bacterial DNA the slur was sonicated. The machine was set to pulse for 10 sec at 95% followed by 20 sec of pause for 10 cycles. If the extract still was viscous the extract was sonicated for 5 cycles. To remove cell debris the extract was centrifuged for 30 min at 18,000 g. The crude cleared crude extract was applied to the equilibrated resin (5 ml of extract was added to 50  $\mu$ l of resin). For equilibration the resin was washed with GST-washing or His-washing buffer. The mixture was left on an overhead shaker for 1h in the cold room. The mixture was poured into polypropylene columns (Qiagen; #34964) and unbound fraction was removed using gravitational flow. The resin was washed with 5 ml GST-washing or His-washing buffer for at least 3 times. The GST-elution buffer or His-elution buffer was applied 7 times. The buffer volume was the same as the bead volume. Elution was followed by testing each fraction for protein abundance using Bradford reagent (Serva; #39222.03). Normally the proteins appeared in the second and third fraction. The resin was washed using the remaining GST-elution or His-elution buffer followed by 10 bead volumes of GST-resin cleaning buffer or 0.5 M NaOH for Ni-NTA resin. For storage the cleaned resin was washed with 10 bead volumes ddH<sub>2</sub>O and stored with 10 bead volumes of ddH<sub>2</sub>O containing 20% ethanol. Purified GST-tagged proteins were aliquoted and stored at -80°C. To prevent imidazole derived protein precipitation the purified His-tagged proteins were dialyzed into a suitable buffer system, depending on the following experiments. After dialysis the proteins were aliquoted and stored at -80°C. To ensure no protein loss during dialysis the abundance of the proteins was analyzed by western-blotting.

### **2.2.3 GST-pulldown**

The pulldown was conducted as described for protein purification of GST-tagged proteins. After the washing, crude cleared extract of His-tagged proteins was added and incubated on an overhead shaker for at least one hour in the cold room. The agarose beads were washed at least 3 times with 10 bead volumes GST-washing buffer. One bead volume Laemmli-buffer was added and the beads were boiled for 5 min at 95°C. Protein detection was performed by western blotting.

### **2.2.4 SDS-PAGE**

Proteins were separated using SDS polyacrylamide gel electrophoresis (SDS-PAGE). Separation gel contained 15% acrylamide, 0.4% bis-acrylamide, 0.375 M Tris-HCl pH 8.8, 0.075% SDS, 0.083% APS and 0.0083% TEMED. The stacking gel contained 4.5% acrylamide, 0.12% bis-acrylamide, 0.1 M Tris-HCl pH 6.8, 0.1% SDS, 0.083% APS and

0.0083% TEMED. The protein samples were mixed with Laemmli-buffer and boiled for 5 min at 95°C. For size estimation the prestained protein ladder PageRuler (ThermoFisher; #26616) was loaded. Samples run at 90 V in SDS-running buffer until the running front left the gel. For the analysis of larger proteins the gel was run longer to increase resolution. After electrophoresis, the stacking gel was removed and the running gel was washed in towbin buffer. For direct protein staining, the gel was incubated in coomassie-stain solution. After 1 h of incubation the gel was rinsed with water. To remove unspecific stain, the gel was washed with coomassie-destain solution until no background stain was visible in the gel.

### **2.2.5 Western blotting and immuno-detection**

After SDS-PAGE the gels were incubated for 10 min in towbin buffer. 6 slices of gel blot paper (Sigma-Aldrich; # 10426890) and one slice of nitrocellulose membrane (GE Healthcare; #10600002) were cut according to the gel size and soaked with towbin buffer. 3 slides of gel blot paper one slide of nitrocellulose membrane the gel and then again 3 slides of gel blot paper were stacked and checked for air pockets. The semi-dry blotting took 1 h at 260 mA. After blotting the membrane was incubated in ponceau S stain for 5 min to check transfer efficiency and protein loading. The membrane was washed with ddH<sub>2</sub>O until no background stain was visible and scanned. The membrane was incubated in blocking solution and shook for 1 h in the cold room. After blocking the membrane was washed for 10 min in TBS buffer. Primary antibody was mixed with fresh blocking solution und applied tothe membrane shaking over night. After washing for 10 min in TBS the secondary antibody was mixed with blocking solution and applied to the membrane for >1 h under agitation in the cold room. To remove all remaining antibodies the membrane was washed for 1 h in TBS with at least 3 changes of the buffer. For the last 10 min TBST was used. After a last short wash with TBS the membrane buffer was removed. The HRP substrate was applied according to the manufacturer's protocol (GE-Healthcare; #RPN2232). The light emission was detected using the FlourChemQ Multimage III. The antibodies used are listed in Tab. 5.

Table 4: **Antibodies used for immuno detection**

<b>Antibody (source)</b>	<b>Manufacturer</b>	<b>Ordering Number</b>	<b>Dilution</b>
$\alpha$ -His (mouse)	GE-Healthcare	27-4710-01	1:3000
$\alpha$ -GST-HRP	SantaCruz	Sc-138	1:1000
$\alpha$ -mouse IgG (rabbit)	SigmaAldrich	A9044	1:40,000-80,000
$\alpha$ -GFP (mouse)	Living Colours	632381	1:2500

### 2.3 Chemo-competent cells

The pre-culture of the specific cells were grown at 37°C over night in LB media. 50 ml of the main culture was inoculated and grew for 3-4 h until an OD<sub>600</sub> value of 0.5 was reached. After cooling down the culture on ice the culture was transferred into a pre-cooled tube and centrifuged for 10 min, 4°C at 3,500 g. Supernatant was discarded and the bacterial pellet was resuspended in 25 ml pre-cooled 100 mM MgCl<sub>2</sub> solution and incubated for 1 h on ice. After centrifuging as described, the pellet was resuspended in 25 ml of 100 mM CaCl<sub>2</sub> solution and incubated for 1 h. This was repeated three times, the incubation times decreased 15 min for each repetition. The last pellet was resuspended in 4 ml of 100 mM CaCl<sub>2</sub> with 20% (v/v) glycerol. The bacterial solution was aliquoted, snap frozen using liquid nitrogen and stored at -80 °C. Antibiotic resistance was tested for spectinomycin, kanamycin, genthamycin and carbenicillin.

### 2.4 MT spin-down

The purified proteins were dialysed into the MT spin-down buffer over night. Protein abundance and purity was generally quite low. To ensure that the proteins were detectable via coomassie-staining, different volumes of the dialyzed proteins were tested via SDS-PAGE and subsequent coomassie-staining (see chapter 3.2.4). When bands were clearly visible, those amounts were used in the spin-down assay. MT polymerization and protein binding was performed as stated by the manufacturer's protocol (Cytoskeleton; #BK029). Sedimentation was performed in a Beckmann MAX-XP using a Beckmann TLA110 rotor and Beckmann microfuge tubes (#357448) at room temperature and a force of 100,000 g for 40 min at minimum acceleration and spin-out for deceleration. Separation was obtained by SDS-PAGE. Proteins were visualized by coomassie-staining or immuno-detection.

### 2.5 CaM pulldown

The CaM beads (GE-Healthcare; # 17052901) were equilibrated in CaM pulldown buffer either containing 5 mM EGTA or 1 mM CaCl<sub>2</sub>. Bacterial pellets were resuspended in CaM pulldown

buffer by pipetting and left on ice for 30 min. Cell disruption by sonication and centrifugation was obtained as described previously. The cleared crude extract was adjusted to either contain 5 mM EGTA or 1 mM CaCl<sub>2</sub>. The extracts were applied to the CaM agarose beads and incubated in an overhead shaker for 1 h in the cold room. The beads were washed 4 times with CaM pulldown buffer either containing EGTA or CaCl<sub>2</sub>. Protein samples were separated by SDS-PAGE. Proteins were visualized by immuno-detection using tag specific antibodies.

### 2.6 *In vitro* phosphorylation assays

GST-tagged KLCR, IQD and MPK proteins were expressed and purified as described. To average the different enzymatic activities of the MPKs the known substrate MBP was tested with different amounts of MPK proteins. The MPKs were activated using a constitutively active MKK5 variant (Feilner et al. 2005). Experiments were conducted as described by (Lee et al. 2004)). Briefly, 1  $\mu$ L purified MBP, 8  $\mu$ L of 5x MPK-buffer, 0.1  $\mu$ L of  $\gamma$ P<sup>32</sup>-ATP and the different amounts of the activated MPKs were mixed and ddH<sub>2</sub>O added to a total volume of 40  $\mu$ L. The mixture was incubated at 37°C for 30 min. Laemmli buffer was added and the mixture was boiled for 5 min at 95°C. Proteins were separated using SDS-PAGE. To control protein loading gels were stained using CBB. Afterwards the autoradiograph was taken using the Typhoon FLA 9000 (GE-Healthcare)(Fig. S3). For the *in vitro* phosphorylation of GST-tagged IQD2 and KLCR proteins 0.2  $\mu$ L of MPK3, 2  $\mu$ L of MPK4 and 10  $\mu$ L of MPK6 were used. The *in vitro* reaction and visualization was performed as described for MBP.

### 2.7 Phosphoproteomics

Proteins were separated with SDS-PAGE, in-gel digested with trypsin and desalted as described in (Majovsky et al. 2014). Dried peptides were dissolved in 5% acetonitrile, 0.1% trifluoroic acid, and 0.1  $\mu$ g were injected into an EASY-nLC II liquid chromatography system (Thermo Fisher Scientific). Peptides were separated using C18 reverse phase chemistry employing a pre-column (EASY column SC001, length 2 cm, ID 100  $\mu$ m, particle size 5  $\mu$ m) in line with an EASY column SC200 with a length of 10 cm, an inner diameter (ID) of 75  $\mu$ m and a particle size of 3  $\mu$ m (both from Thermo Fisher Scientific). Peptides were eluted into a Nanospray Flex ion source (Thermo Fisher Scientific) with a 60 min gradient increasing from 5% to 40% acetonitrile in ddH<sub>2</sub>O and a flow rate of 300 nL/min and electrosprayed into an Orbitrap Velos Pro mass spectrometer (Thermo Fisher Scientific). The source voltage was set to 1.9 kV, the S Lens RF level to 50%. The delta multipole offset was -7.00. Phosphopeptides were measured with a Top 20 targeted data acquisition (TDA) scan strategy with inclusion list to specifically target IQD1 or KLCR1 peptides bearing an MPK phosphorylation site motif



potentially phosphorylated by MPK3, MPK4 and MPK6 for MS/MS peptide sequencing. The AGC target value was set to 1e06 and the maximum injection time (max IT) to 500 ms in the Orbitrap. The parameters were set to 1e04 and 100 ms in the LTQ with an isolation width of 2 Da for precursor isolation and MS/MS scanning. Multi stage activation (MSA) was applied to further fragment ion peaks resulting from neutral loss of the phosphate moiety by dissociation of the high energy phosphate bond to generate b- and y- fragment ion series rich in peptide sequence information. MS/MS spectra were used to search the TAIR10 database with the Mascot software v.2.5 integrated in Proteome Discoverer v.1.4. The enzyme specificity was set to trypsin and two missed cleavages were tolerated. Carbamidomethylation of cysteine was set as a fixed modification and oxidation of methionine and phosphorylation of serine and threonine as variable modifications. The precursor tolerance was set to 7 ppm and the product ion mass tolerance was set to 0.8 Da. A decoy database search was performed to determine the peptide false discovery rate (FDR). Only peptide spectral matches (PSMs) with a Mascot ion score surpassing the significance threshold  $\alpha = 0.05$  were considered true. The phosphoRS module was used to localize the phosphorylation site in the peptide's primary structure.

## 2.8 Transient expression in *N. benthamiana*

For transient expression of constructs for BiFC assays the *A. tumefaciens* strain GV3101 (pMP90 (pTiC58DT-DNA)) was used. For all other experiments the strain GV3101pK (pMP90RK (pTiC58DT-DNA)) was used. To suppress post transcriptional gene silencing all constructs were co-infiltrated with *A. tumefaciens* containing the p19 gene ('Retraction: "An enhanced transient expression system in plants based on suppression of gene silencing by the p19 protein of tomato bushy stunt virus" 2015)(although retracted, the authors state that the conclusions of this publication are correct). The *A. tumefaciens* strain harboring the specific binary vectors were grown for 2 days at 28 °C in 5 ml LB-media containing the specific antibiotic and 50 µg/ml rifampicillin. The bacteria were pelleted at 10,000 g at room temperature and resuspended in tobacco transformation buffer, followed by the same step to wash the bacteria. The pellet was resuspended in 1 ml of tobacco transformation buffer and the OD<sub>600</sub> was adjusted to 0.8 using the tobacco transformation buffer. All strains were mixed in a 1:1 ration with the p19 strain and incubated for 1 h at 18°C shaking. The mixture was infiltrated into young *N. benthamiana* leaves using a needleless syringe.

### 2.9 Plant propagation

*N. benthamiana* seeds were propagated on standard soil (45% white peat, 20% clay, 15% sod peat, 20% coconut fiber) for 14 days and then pricked onto standard soil. Infiltration was performed about 5 weeks after. Plants were grown under 16 hour light and 8 hours night cycles. During day the temperatures were set to 23°C-25°C and 19°C-24°C during night. Relative humidity was kept between 55% and 75%.

### 2.10 Microscopy

For investigating BiFC experiments the confocal laser scanning microscope Zeiss LSM 780 was used. Excitation of Venus was 514 nm, emission was detected between 519 and 594 nm. For the co-expression experiments including BiFC constructs, CFP was excited with 458 nm and detected at the wavelengths between 463 and 502 nm, mRFP was excited with 594 nm and detected between 599 and 648 nm. For KLCR1 recruitment experiments the Zeiss LSM 700 was used. GFP was excited with a 488 nm laser and emission was detected between 493 and 543 nm. Excitation of mRFP was obtained with a 555 nm laser and its emission was detected between 560 and 605 nm. For all co-expression and co-localization experiments images were generated in the sequential mode. Due to different expression levels not all investigated constructs showed the same emission intensity. The contrast of the images of the low expressed constructs was enhanced. The degree of enhancement of the image of the lowest expressed construct was also applied to the negative controls.

### 2.11 Stability assay

*Arabidopsis thaliana* protoplasts derived from mesophyll cells were isolated as previously described (Yoo, Cho, and Sheen 2007). Aliquots of 300 µl were incubated over night in the dark at room temperature. Cells were treated with 5 µM cycloheximide. After 2 h or 5 h the cells were pelleted and boiled in Laemmli-buffer. Protein separation was performed by SDS-PAGE. Proteins were visualized by immuno-detection.

### 2.12 Yeast-two-hybrid

200 ml YPDA media was inoculated with a fresh colony of *S. cerevisiae* PJ69-4a strain. The culture grew over night at 28°C and 150 rpm. If an OD<sub>600</sub> of 0.8 was reached the culture was centrifuged at 20°C and 5000 rpm. The pellet was resuspended by shaking with sterile 10 ml ddH<sub>2</sub>O and again centrifuged as described. This was repeated once with 1 ml. The pellet was resuspended in 1 ml of LiOAc/TE-buffer, centrifuged and resuspended in 0.25 ml of LiOAc/TE-

buffer. ssDNA from salmon sperm (SigmaAldrich; # D9156) was boiled for 20 min at 95°C. 400 ng of each plasmid was pipetted into a 96 well plate. The ssDNA was mixed with the cell suspension in a 5:1 ratio. 24 µl of the mix was pipetted into the 96 well plate. The cells in the wells were carefully mixed with 100 µl buffered PEG. The plate was shaking for 1 h at 30°C with an agitation of 120 rpm. The cells were heat shocked for 15 min at 42°C in an incubator. Cells were pelleted at 1,800 rpm for 5 min. 100 µl of the supernatant was discarded. 200 µl of TE-buffer was added and directly 150 µL were removed to wash the pellet. The remaining cells were resuspended into the remaining 50 µl of TE-buffer. 10 µl of the mixture was pipetted onto a SD Medium-LEU-TRP plate and incubated at 29°C for 3 days. Colonies were picked and resuspended into 200 µl of TE-buffer. The cells were shaking over night at 28°C. 10 µl of the co-transformed cells were spotted onto SD Medium-HIS-LEU-TRP and the more stringent SD Medium-ADE-HIS-LEU-TRP plates. The plates grew for 2-4 days.

### 2.13 *In silico* analysis

To predict the putative CaM-binding sites the Calmodulin target database was used <http://calcium.uhnres.utoronto.ca/ctdb/ctdb/home.html> (Yap et al. 2000). To predict the tertiary structure of IQDs and KLCRs phyre2 database was used <http://www.sbg.bio.ic.ac.uk/~phyre2/html/page.cgi?id=index> (Kelley et al. 2015). Analysis and image acquisition of the modeled proteins was done using pymol <https://pymol.org/2/> (DeLano 2009). The structure of the IQ67 domain was aligned with the CaM-binding site of myosin (green) binding to Apo-CaM (PDB: 2XI7). The position of CaM was changed by hand to fit the interaction between IQ-motifs of IQD1/IQD33 with CaM as described for the IQ-motifs of myosin and CaM (Houdusse et al. 2006).

Since no reasonable sequence similarity to any X-ray structure could be found to allow protein homology modelling with standard methods like YASARA the sequence was sent to the *ab initio* protein structure prediction server QUARK (<http://zhanglab.ccmb.med.umich.edu/QUARK/>, (Xu and Zhang 2012, 2013). Herewith for the complete sequence of IQD1 also no satisfying model could be obtained. Subsequently, the sequence was divided into an N-terminal part (aa 1-180) and a C-terminal part (aa 160 – 500). For each of the partial sequences 10 models were produced with the help of the *ab initio* modelling server. The quality of all predicted models was evaluated with PROSA II (Sippl 1990, 1993). The best evaluated ones of each sequence part were manually linked by superposition of the overlapping region (aa 160-180). Finally, the model was refined using YASARA (Krieger et al. 2009; Krieger and Vriend 2014) and applying the MD-refinement tool which is a simulated annealing procedure which heats and cools the structure 20times in a 500 ps molecular dynamics simulation. The final quality inspection of the obtained model with PROSA II and

PROCHECK (R. A. Laskowski 1993) indicated a satisfying model with regard to stereochemical quality and native folding.

### 2.14 Media

#### LB media:

Component	Concentration
Bacto Trypton	10 g/l
Yeast Extract	5 g/l
NaCl	10 g/l

#### TB media:

Component	Concentration
Bacto Trypton (BD; #288620)	12 g/l
Bacto Yeast Extract (BD; #211705)	24 g/l
Glycerol	0.4%

Add ddH<sub>2</sub>O to 90% of final volume and autoclave. Additionally a phosphate buffer solution for TB media must be added after autoclaving to 100% final volume.

Component	Concentration
KH <sub>2</sub> PO <sub>4</sub>	10 g/l
K <sub>2</sub> HPO <sub>4</sub>	5 g/l

#### YPDA media:

Component	Concentration
Bacto Peptone (BD; #211677)	20 g/l
Yeast extract (AppliChem; #A1552,1000)	10 g/l
Adenine hemisulfate(Sigma, #A3159-25G))	100 mg/l
Glucose (add after autoclaving)	2%

#### SD-Media:

Provided as mixture from manufacturer, for solid media plates 17 g/l agar were added.

Component
SD Medium-LEU-TRP (MP; #4823-065)
SD Medium-HIS-LEU-TRP (MP; #4830-065)
SD Medium-ADE-HIS-LEU-TRP (MP; #4842-065)

#### S.O.C. media:

Component	Concentration
Tryptone (AppliChem; #A1553,1000)	20 g/l
Yeast extract (AppliChem; #A1552,1000)	5 g/l
NaCl	8.5 mM
KCl	2.5 mM
MgCl <sub>2</sub>	10 mM
Glucose	20 mM

## 2.15 Buffers

### GST-lysis buffer:

Component	Concentration
Tris-HCl, pH 7.4	125 mM
NaCl	150 mM
DTT	1 mM
EDTA	1 mM
Lysozyme	1 mg/ml
Triton X-100	1% (v/v)
Protease Inhibitor	1x

### GST-washing buffer:

Component	Concentration
Tris-HCl, pH 7.4	125 mM
NaCl	150 mM
DTT	1 mM
EDTA	1 mM

### GST-elution buffer:

Component	Concentration
Tris-HCl, pH 7.4	125 mM
NaCl	150 mM
Triton X-100	0.1% (v/v)
Reduced Glutathione (Cube Biotech; #61033)	50 mM
DTT	1 mM

After adding the reduced glutathione the pH-value needs be adjusted with NaOH to 7.4 again.

### GST-resin cleaning buffer:

Component	Concentration
Tris-HCl, pH 7.4	125 mM
NaCl	150 mM
DTT	1 mM

### His-lysis buffer:

Component	Concentration
NaH <sub>2</sub> PO <sub>4</sub>	50 mM
NaCl	300 mM
Imidazol	10 mM

### His-washing buffer:

Component	Concentration
NaH <sub>2</sub> PO <sub>4</sub>	50 mM
NaCl	300 mM
Imidazol	20 mM

### His-elution buffer:

Component	Concentration
NaH <sub>2</sub> PO <sub>4</sub>	50 mM
NaCl	300 mM
Imidazol	250 mM

### Towbin buffer:

Component	Concentration
Tris-HCl pH 8.3	25 mM
Glycin	192 mM
Methanol	20%
SDS	1.3 mM

### SDS running buffer:

Component	Concentration
Tris-HCl pH 8.3	25 mM
Glycin	192 mM
SDS	0.1 %

### TBS:

Component	Concentration
Tris-HCl pH 7.8	50 mM
NaCl	150mM
MgCl <sub>2</sub>	1mM

For preparation of TBST, 0.05% of Tween 20 was added.

### Blocking solution:

Component	Concentration
TBS-buffer	
BSA	2%
Skimmed milk powder	2%

### Ponceau S:

To ensure solubility of the stain a pre-mixture with higher acid concentration was prepared. 10 ml of ddH<sub>2</sub>O, 0.3 ml of glacial acetic acid and 33 mg of Ponceau S was mixed. ddH<sub>2</sub>O was added to a final volume of 30 ml.

### MT spin-down buffer:

Component	Concentration
PIPES pH 7.3	80 mM
MgCl <sub>2</sub>	5 mM

### Coomassie staining solution

Component	Concentration
Coomassie Brilliant Blue G-250	0.1%
Methanol	50%
Glacial acetic acid	10%

### Coomassie destaining solution

Component	Concentration
Methanol	40%
Glacial acetiv acid	10%

### CaM pulldown buffer

Component	Concentration
Tris-HCl	5.8 mM
KCl	2.7 mM
NaCl	137 mM

Tween 20	0.1%
Sodium azide	0.002%
EGTA/CaCl <sub>2</sub>	5 mM/ 1 mM

**MPK-buffer**

Component	Concentration
HEPES	20 mM
MgCl <sub>2</sub>	15 mM
EGTA	10 mM
DTT	2 mM
ATP	40 μM

**Tobacco transformation buffer**

Component	Concentration
MES pH 5.3	10 mM
MgCl <sub>2</sub>	10 mM
Acetosyringone	150 μg/ml

**LiOAc**

Component	Concentration
Lithiumacetate pH7.5	100 mM

**TE-buffer**

Component	Concentration
Tris-HCl pH 7.5	10 mM
EDTA	1 mM

**LiOAc/TE-buffer**

Component	Concentration
Tris-HCl pH 7.5	10 mM
EDTA	1 mM
Lithiumacetate pH7.5	100 mM

**Buffered PEG**

Component	Concentration
PEG	40%
Tris-HCl pH 7.5	10 mM
EDTA	1 mM
Lithiumacetate pH7.5	100 mM

**6x Protein loading buffer**

Component	Concentration
Tris-HCl pH 6.8	60 mM
SDS	12% (m/v)
DTT	9.3% (m/v)
Bromphenol blue	0.06% (m/v)
Glycerol	47% (v/v)

## 3. Results

### 3.1 Most IQD proteins interact with Apo- and Ca<sup>2+</sup>-CaM *in vitro*.

The Ca<sup>2+</sup> dependency of IQD-CaM interaction showed ambiguous results dependent of the experimental setup. In CaM-overlay assays T7-IQD1 and T7-IQD20 interacted only with Apo-CaM (Burstenbinder et al. 2013). When beads with immobilized Strep-CaM were used, T7-IQD1 only interacted with Ca<sup>2+</sup>-CaM (Levy et al. 2005) whereas IQD20 interacted with Apo- and Ca<sup>2+</sup>-CaM (Abel, Savchenko, and Levy 2005a). T7-IQD33 showed no interaction with CaM *in vitro* (Burstenbinder et al. 2013) but *in planta* using BiFC assays (Burstenbinder et al. 2017). For a conclusive analysis of clade III IQD-CaM interaction IQD1 and its closest homologue IQD2 as well as IQD5 were chosen. IQD33 was analyzed due to its truncated IQ67 domain. We investigated the interaction using recombinantly expressed tagged proteins and CaM linked to sepharose beads. The proteins were applied as crude extracts. To specify the state of CaM, the beads were treated either with Ca<sup>2+</sup> to generate the Ca<sup>2+</sup>-CaM or with the bivalent cation chelator EGTA to form Apo-CaM. To ensure that the state of CaM is constant throughout the experiment the crude extract as well as the washing buffer were applied containing either Ca<sup>2+</sup> or EGTA. We observed that all tested clade III IQDs interacted with Apo- and Ca<sup>2+</sup>-CaM (Fig. 4A). IQD33 exclusively interacted with Ca<sup>2+</sup>-CaM but not Apo-CaM. The IQ67-domain of IQD33 only consists of the first 16 amino acids most likely due to exon loss (Abel, Savchenko, and Levy 2005a). This compromises the first IQ-motif (Fig 4B). The IQ67-domain is predicted to form a helical structure. This would fit with the current model of CaM-CaMBP interaction, where CaM interacts with amphiphilic helices. Myosin shows in its CaM binding site a similar IQ-motif patterning like IQDs. The IQ-motifs in the IQ67 domain are interspaced by 11 aa whereas the IQ-motifs in myosin are interspaced by 12 aa. Aligning the IQ67-domain of IQD1 into the structure of myosin binding to Apo-CaM shows high similarity due to the presence of the IQ-motif (Fig. 4C). As shown in the alignment of the IQ67-domain of IQD33 into the myosin structure the last arginine of the IQ-motif is missing (Fig. 4D). Little is known about the structural features of IQD proteins. We found that IQD proteins show a high degree of intrinsic disorder (Fig. S1; for IQD1 see Fig. 13). Regions of intrinsic disorder are highly flexible regions and are commonly found in scaffolds proteins which do bind multiple proteins of common or interlinked pathways allowing a fast transduction of signals (Cortese, Uversky, and Dunker 2008). We also modelled the structure of IQD proteins with special emphasis on IQD1 (Fig. S11; Fig S12). We found that all predicted structures showed, that the IQD67 domain forms a long but sometimes interrupted  $\alpha$ -helix. We could observe, that IQD proteins potentially only form helices as well as unstructured regions. The conserved motifs of IQD1 are mostly the sites of helical structures, expanding the helical structure of the IQ67 domain C-terminally. The



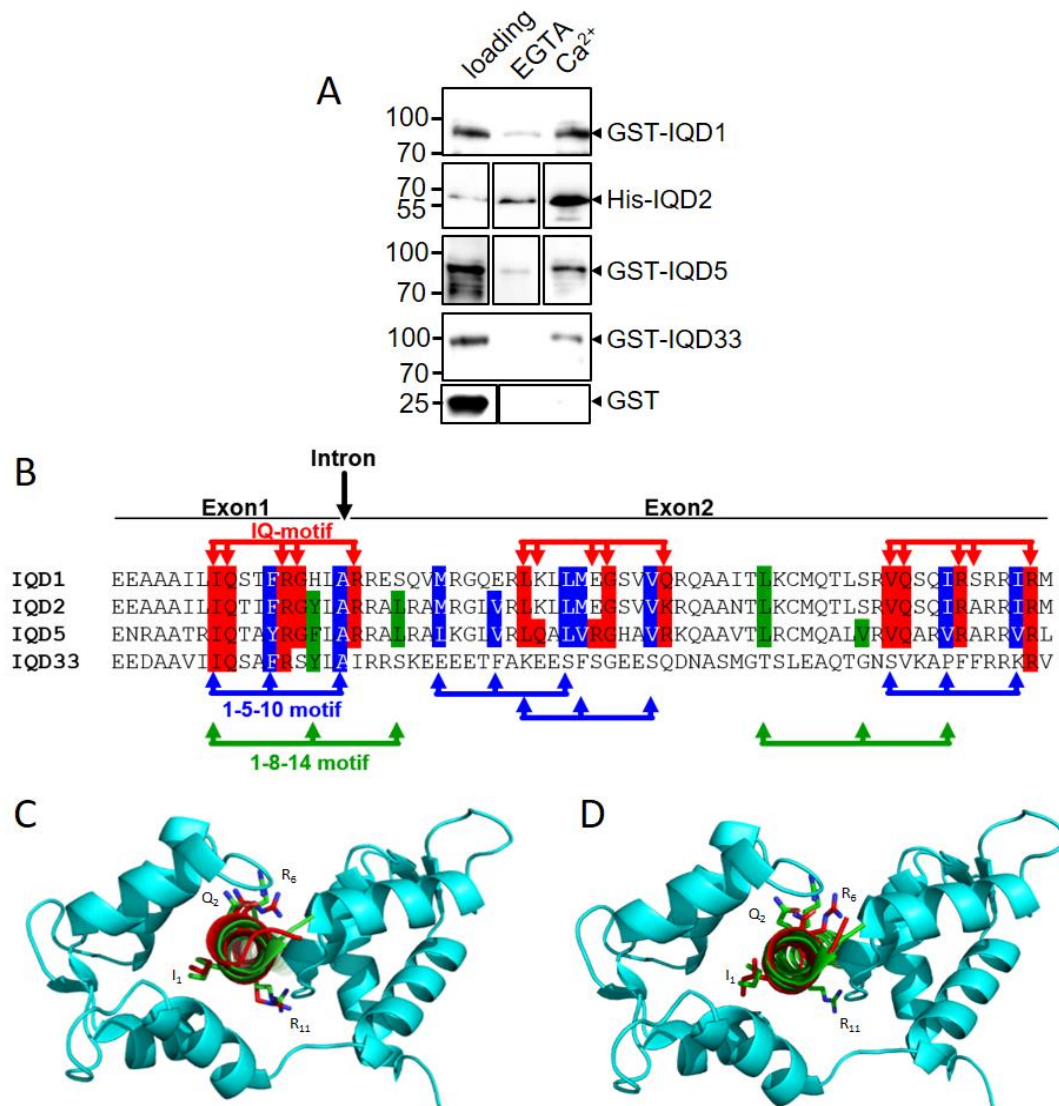


Figure 4: Most IQD proteins interact with Apo- and  $\text{Ca}^{2+}$ -CaM *in vitro*

Pulldown using CaM bound to agarose beads (GE-Healthcare). Proteins were recombinantly expressed in *E. coli*. IQD2 was expressed containing N-terminal His-tag using the pDESTN110 vector. Less soluble IQD-proteins were expressed containing N-terminal GST-tag to increase solubility using the pDEST15 vector. Crude cleared extracts were applied to the beads either in the presence ( $\text{Ca}^{2+}$ ) or absence (EGTA) of calcium. After three times washing, the beads were boiled in Laemmli-buffer. Protein detection was performed via western blotting using tag-specific antibodies (A) (for IQD2, IQD5 and GST the blots were cut. All bands originate from one individual blot and the signals intensities were not altered separately) All *in vitro* experiments were repeated at least twice, representative images are shown. Schematic representation of the IQ67 domain (B)(altered from (Abel, Savchenko, and Levy 2005a). Predicted structure of IQ67-domains of IQD1 (C) and IQD33 (D) are depicted in red. Structural modeling was conducted using the phyre2 database (Kelley et al. 2015). The IQ67 domains were aligned into the structure of the IQ-motif containing region of myosin (green) binding to Apo-CaM (cyan)(PDB: 2X17). The aa of the IQ-motifs are marked to their relative position in the IQ-motif  $I_1Q_2XXXR_6G_7XXXR_{11}$ . Alignment and visualization was done using Pymol (DeLano 2009).

other IQD proteins are also proposed to form long helical stretches including the IQ67 domain surrounded by unstructured regions.

### 3.2 IQDs directly interact with KLCRs

The interaction of IQD and KLCR proteins has been studied *in planta* and in yeast (Burstenbinder et al. 2013). To analyze whether those observed interactions are direct or are mediated by unknown linker proteins, *in vitro* pulldown experiments using glutathion-agarose beads and GST-tagged variants have been conducted. Recombinantly expressed GST-tagged IQD1 was bound to Glutathione beads. As a negative control, the glutathione beads were incubated with recombinantly expressed GST. After washing, the beads were incubated with His-tagged KLCR proteins. His-tagged KLCRs could be pulled down using GST-tagged IQD1, but not with GST alone. This shows that IQD1 directly interacts with KLCR proteins (Fig. 5). To further analyze whether this interaction is truly due to direct interaction we investigated the interaction between the sister gene of IQD1, e.g. IQD2 and KLCRs. We additionally swapped the tags between KLCR and IQD proteins and again used GST alone as a negative control.

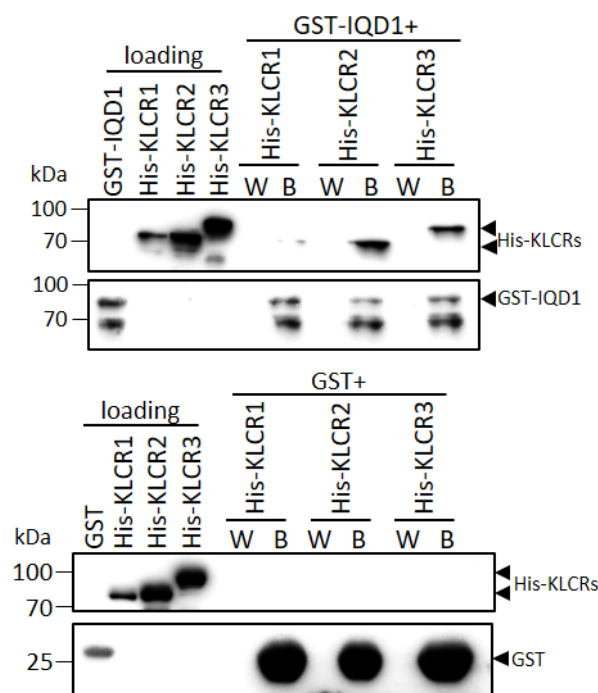


Figure 5: **IQD1 and KLCR proteins directly interact *in vitro***

GST-pulldown assay, was performed using crude GST-tagged IQD1 protein containing cleared crude extracts, which were applied to glutathione beads. After washing, His-tagged KLCR proteins were added. The beads were again washed three times. The last washing step was used as the washing control (W). Beads (B) and last washing step were boiled in Laemmli buffer. Detection of proteins was conducted by western blotting using tag specific antibodies. GST was used as a negative control. Experiments were repeated three times showing similar results. A representative image is shown.

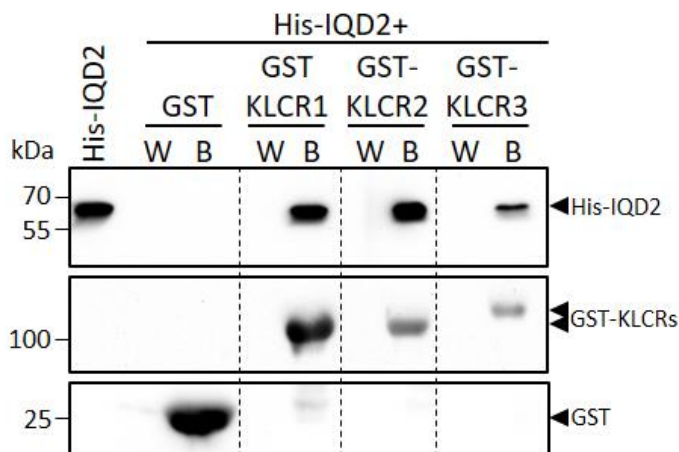


Figure 6: **IQD2 and KLCR proteins directly interact *in vitro***

GST-pulldown assay was performed with GST-tagged KLCR protein containing cleared crude extracts, that were applied to glutathione beads. After washing, His-tagged IQD2 protein extract was added. The beads were again washed three times. The last washing step was used as the washing control (W). Beads (B) and last washing step were boiled in Laemmli buffer. Detection of proteins was conducted by western blotting using tag specific antibodies. GST was used as a negative control. Experiments were repeated two times. A representative image is shown.

Only the GST-tagged KLCRs but not GST alone could pull down the His-tagged IQD2 (Fig. 6). These results show that there is a true and direct interaction between IQD1/IQD2 and KLCRs underlying the importance of this interaction. This further suggests that IQD proteins might recruit KLCRs to MTs directly and therefore possibly guide them to their site of action.

KLCR1 was interacting weakly with IQD1 as demonstrated due to the reduced amount of pulled down KLCR1 compared to KLCR2 and KLCR3. This was also observed in previous experiments using a yeast-two hybrid approach (not published). Those differences were not observed when analyzing the *in vitro* interaction between IQD2 and KLCR. This might hint to the fact that KLCR-binding IQD proteins might bind KLCR proteins with different affinities which might be part of IQD function.

### 3.3 IQD proteins recruit KLCRs to Apo-CaM

KCBP and other kinesins are known CaM binding proteins (Reddy et al. 1996; Rogers et al. 1999). Also Kinesin Light Chains (KLC) from mammals have been reported to modify the ATPase activity of KHC after CaM binding (Matthies, Miller, and Palfrey 1993). KLCRs show structural similarity with KLCs and could therefore also be regulated via CaM. Using the Calmodulin database (Yap et al. 2000) we found at least one possible CaM binding site for each KLCR.

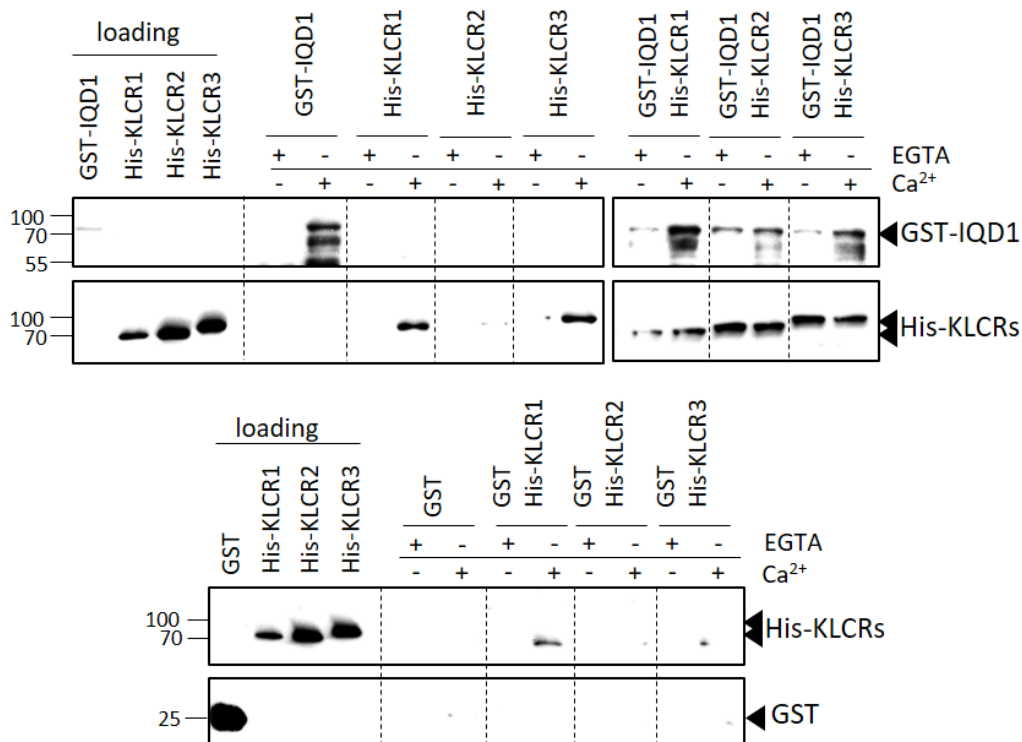


Figure 7: IQD1 protein recruits KLCRs to Apo-CaM

IQD1-KLCR pulldown assay was performed using CaM bound to agarose beads (GE-Healthcare). GST-tagged IQD1 and/or His-tagged KLCR protein-containing cleared crude extracts were applied to the beads either in the presence (Ca<sup>2+</sup>) or absence (EGTA) of calcium and incubated for 1h. After 4 times washing beads were boiled in Laemmli-buffer. GST was used as a negative control. Protein detection was performed via western blotting using tag-specific antibodies. Experiments were repeated three times. A representative image is shown.

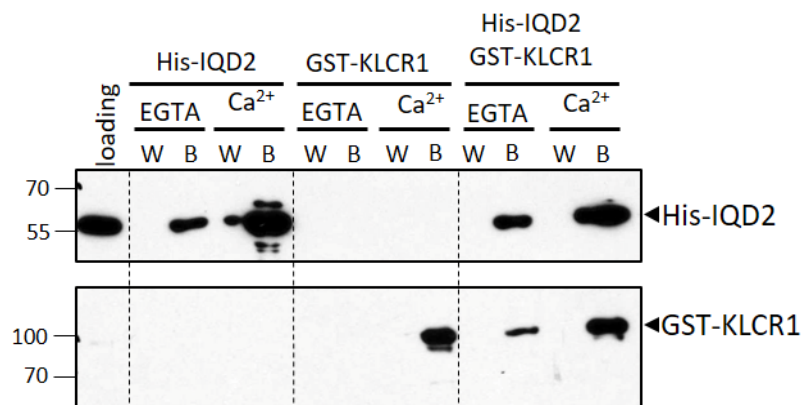


Figure 8: IQD2 protein recruits KLCR1 to Apo-CaM

IQD2-KLCR1 pulldown assay was performed, using CaM bound to agarose beads (GE-Healthcare). His-tagged IQD2 and/or GST-tagged KLCR1 protein containing cleared crude extracts were applied to the beads either in the presence (Ca<sup>2+</sup>) or absence (EGTA) of calcium and incubated for one h. After four times washing beads were boiled in Laemmli-buffer. Protein detection was performed via western blotting using tag-specific antibodies. Experiments were repeated two times. A representative image is shown.

To confirm the predicted CaM-interaction *in vitro* assays using CaM-beads were performed as previously described. His-tagged KLCRs alone only interacted with Ca<sup>2+</sup>-CaM. When His-KLCRs and GST-IQD1 were applied simultaneously both proteins were found to be associated with Apo- and Ca<sup>2+</sup>-CaM (Fig. 7). To test whether this is mediated by IQD1 or influenced by the fusion tags, we again used the IQD1 sister gene IQD2 and switched tags. As demonstrated

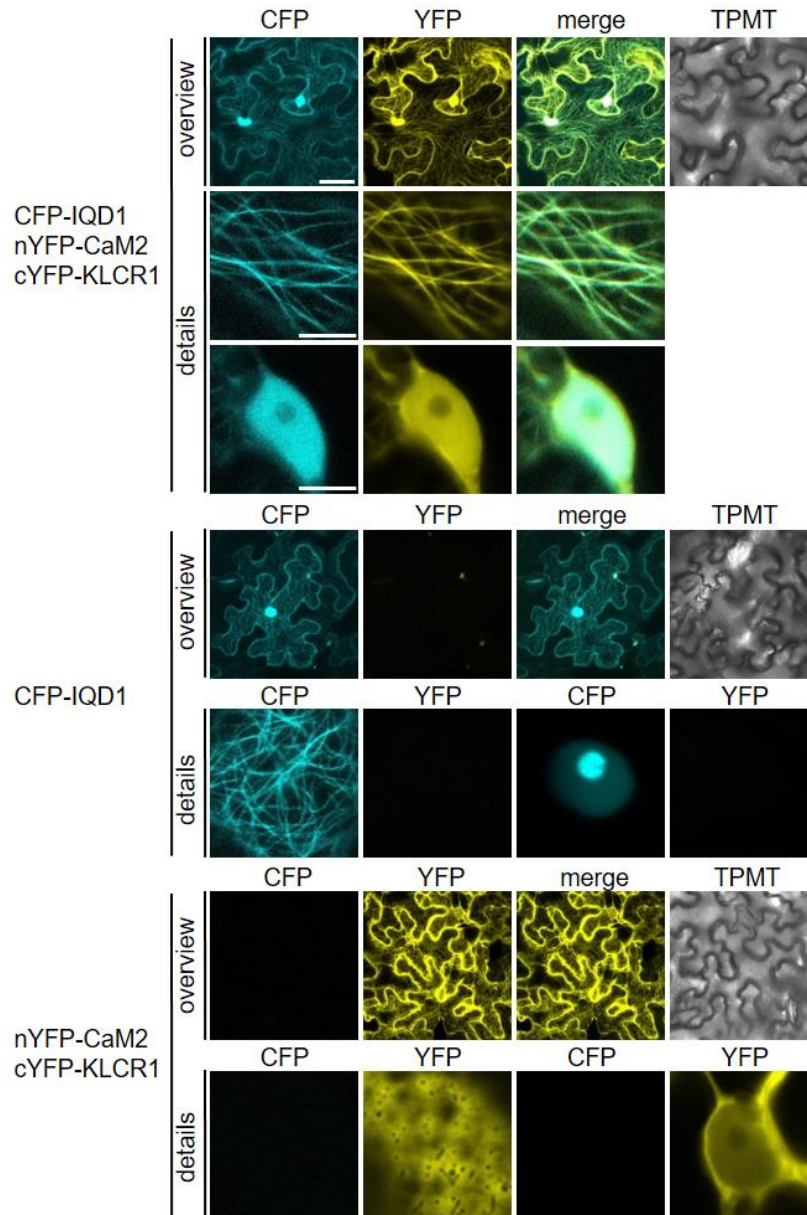


Figure 9: **CFP-IQD1 recruits the complemented nYFP-CaM2:cYFP-KLCR1 complex to the MT Stacks** (overview) and single optical sections (details) of YFP-signals after bimolecular fluorescent complementation (BiFC) and CFP signals after coexpression with CFP-tagged IQD1. Coexpression was performed by Agrobacterium mediated transient transformation of CaM2 fused to the N-terminal part of the fluorescence protein Venus (nYFP), KLCR1 fused to the C-terminal part of Venus (cYFP) and CFP-IQD1 in tobacco under the control of the 35S promoter. Single expression of CFP-IQD1 and the BiFC constructs were used as controls. Bars: overview = 50  $\mu$ m, details = 10  $\mu$ m. Experiment was repeated 3 times. At least 3 cells were analyzed per experiment and infiltration. Representative images are shown.

for GST-IQD1, His-IQD2 recruited GST-KLCR1 to Apo-CaM and GST-KLCR1 only interacted with  $\text{Ca}^{2+}$ -CaM (Fig. 8). Whether this is due to recruitment of KLCRs to Apo-CaM via IQDs or a changed affinity of KLCRs towards CaM due to IQD binding needs to be addressed in future experiments.

We previously could show that IQD1 recruits KLCR1 and CaM2 to the MT *in planta* when transiently co-expressed in tobacco. To get first ideas whether a possible trimeric complex is formed *in planta* and where this complex is localized subcellularly, co-expression analysis of BiFC constructs and CFP-tagged IQD1 have been conducted. BiFC assays are based on the association of two fragments of Venus, the N-terminal fragment nYFP and the C-terminal fragment cYFP. When expressed together those two fragments do not reconstitute Venus and no fluorescence can be measured. When fused to interacting proteins, the two halves are brought into proximity. This enables the re-formation of Venus and a fluorescence signal can be detected. CFP-IQD1 could recruit the reconstituted Venus-CaM2-KLCR1 complex to the MT (Fig. 9). The reconstituted Venus-CaM2-KLCR1 complex alone localized to the cell plasma and only showed a weak nuclear localization. As described previously, CFP-IQD1 is strongly localizing to the nucleolus.

When co-expressed with the CaM2 and KLCR1, IQD1 was absent from the nucleolus but remained in the nucleus. The reconstituted CaM2-KLCR1 complex showed a higher nuclear presence when IQD1 was co-expressed when comparing the overview pictures. But due to the changes in localization and the subsequent changes in the fluorescence intensity the contrast of the detailed pictures of the nuclei was adjusted and are therefore not comparable. Due to

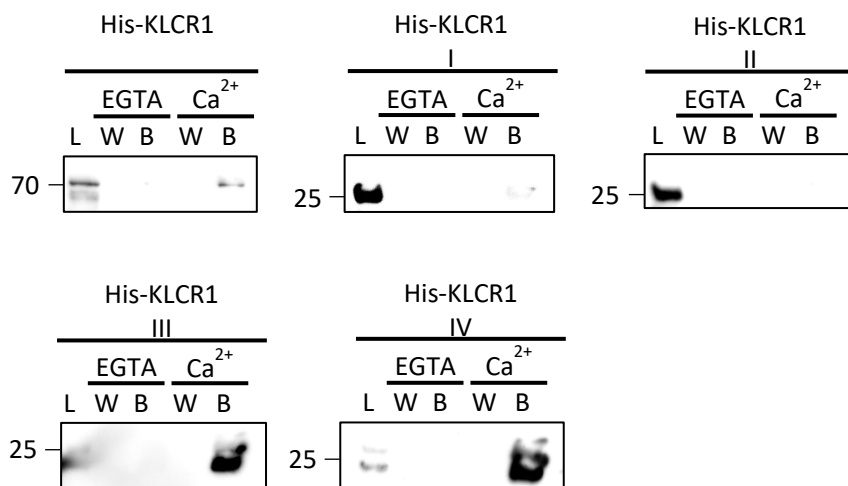


Figure 10: **TPR containing regions of KLCR1 interact with  $\text{Ca}^{2+}$ -CaM**

Pull-down of KLCR1 fragments (see Fig. 11A) was done with CaM bound to agarose beads (GE-healthcare). Cleared crude extracts were applied to the CaM-beads either in the presence ( $\text{Ca}^{2+}$ ) or absence (EGTA) of  $\text{Ca}^{2+}$ . After washing, the beads were boiled in Laemmli buffer. Protein detection was performed via western blotting. Experiments were repeated two times. A representative image is shown.

this strong complexation of the Venus constructs we could not exclude an influence on the localization. We therefore changed the arrangement of the tags and co-expressed mRFP-KLCR1 with the nYFP-IQD1 and cYFP-CaM2. The VENUS-IQD1-CaM2 complex associated with MT and the nucleus. mRFP-KLCR1 alone localized to the cytosol but got recruited to the MT when co-expressed with the Venus-IQD1-CaM2 complex (Fig. S2). In both set-ups a recruitment to the MT was only visible when IQD1 was either part of the VENUS complex or was expressed separately, showing the necessity of IQD1 for subcellular changes of KLCR1 and CaM2. To narrow down the possible CaM-binding site of KLCR1, truncated variants (see Fig. 11A) of KLCRs were tested for their *in vitro* CaM interaction. As shown for the full length KLCRs, none of the tested fragments interacted with Apo-CaM. The strongest interaction with Ca<sup>2+</sup>-CaM was detectable for the two C-terminal fragments (Fig. 10). This indicates that Ca<sup>2+</sup>-CaM interacts with the structured areas of the TPR containing regions and could therefore directly influence KLCR function.

### 3.4 IQD1 interacts with the TPR-domain containing regions of KLCR1

The IQ67-domain is the site of CaM-binding of IQD proteins. The C-terminal adjacent motifs are responsible for KLCR1 interaction (data not published). To better understand the complexes IQD proteins are forming with their interacting proteins the site of IQD1 binding of KLCR1 was mapped using truncated variants of KLCR1. The truncations were chosen to not interrupt helix-loop-helix structures of the TPR-domains containing stretches of KLCR1, based on the predicted structure (Fig. 11A) (Burstenbinder et al. 2013). To analyze the interaction *in planta*, mRFP-tagged KLCR1 fragments and GFP-IQD1 were transiently co-expressed in *N. benthamiana*. An IQD1-dependent recruitment of the fragments to the MT indicate *in planta* interaction. We observed that only the long KLCR1-I-II-III-fragment as well as the II-III-IV-fragment were co-localizing with IQD1. The overlapping II-III-fragment was not recruited (Fig. 11B). We further tested the interaction in an independent yeast-two hybrid screen. Interaction of IQD1 and the KLCR1 fragments would lead to the reconstitution of the GAL4 transcription factor leading to the expression of selection markers and subsequently to cell growth. We could only observe cell growth when GAL4-DBD-IQD1 and GAL4-AD-KLCR1-I-II-III were co-expressed (Fig. 11C). In both experiments only TPR domain containing fragments were able to interact with IQD1. KLCR1 contains several TPRs in its C-terminal half. Those TPRs can form super-helical structures which can form convex and concave formed structures. Those structures mediate the specific ligand binding via hydrophobic and electrostatic interaction with short stretches of their ligand (Zeytuni and Zarivach 2012). Truncating the TPR domain containing regions of KLCR1 did not break up individual TPRs but might have impaired the

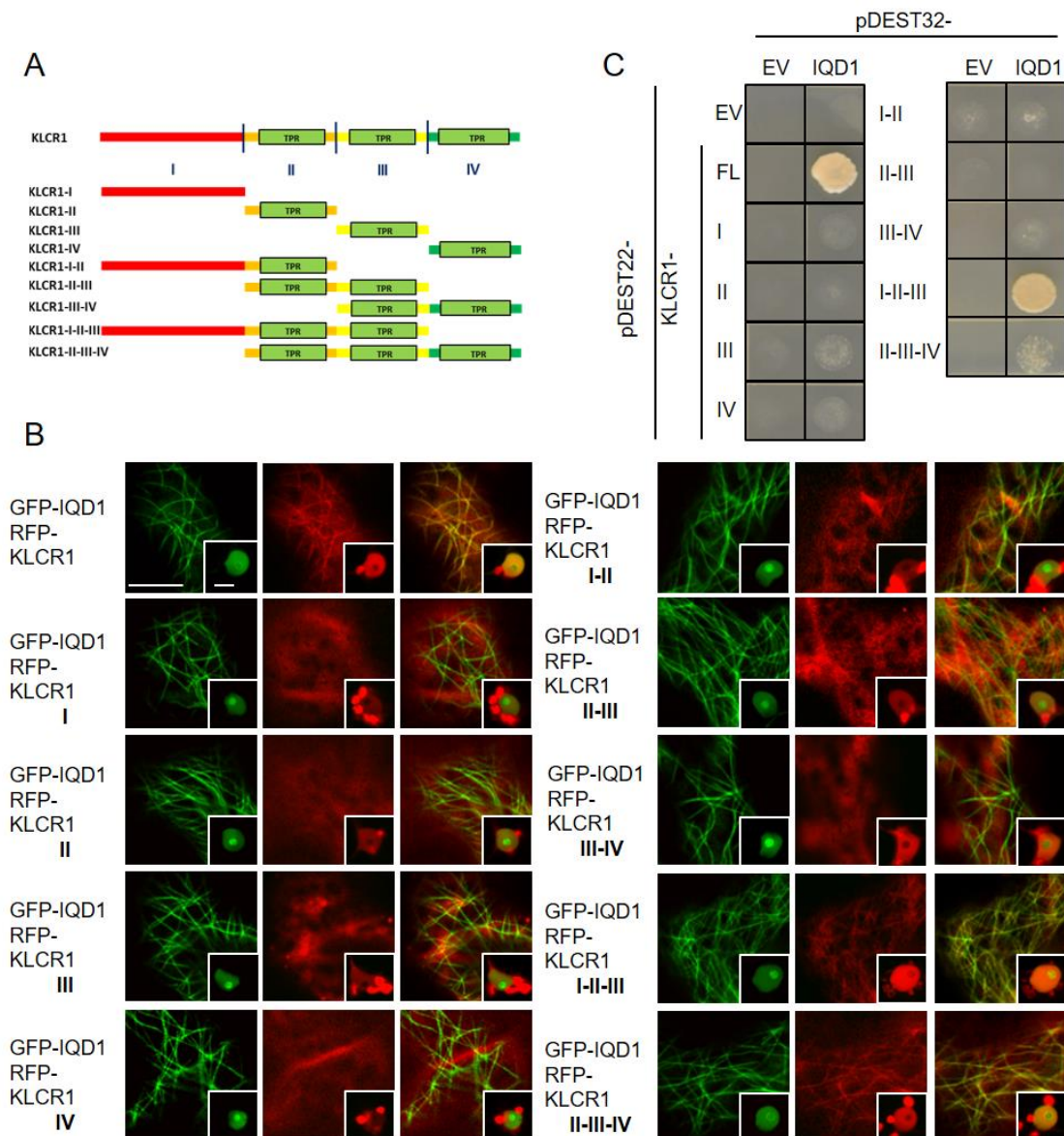


**Figure 11: IQD1 interacts with the TPR domain containing regions of KLCR1**

Truncated fragments of KLCR were selected to not interrupt the helix-loop-helix structures of the TPR domains based on the predicted structure of KLCR1 (A)(Burstenbinder et al. 2013). *In planta* interaction of KLCR1 fragments and IQD1 was analyzed by transient co-expression of GFP-tagged IQD1 and mRFP-tagged KLCR1 fragments via *Agrobacterium* mediated transient transformation into tobacco under the control of the 35S promoter. Recruitment of mRFP-KLCR1 fragments to MT via GFP-IQD1 indicates interaction (B); Bars=10 $\mu$ m. The experiment was repeated three times. At least three cells were analyzed per infiltration, representative images are shown. Yeast-two hybrid assay co-expressing GAL4-DBD-IQD1 (pDEST32) and GAL4-AD-KLCR1 fragments (pDEST22) in yeast strain PJ69-4a. Pictures were taken 3 days after plating on LB media lacking leucine, tryptophane and histidine. Growth indicates interaction (C). Empty vectors (EV) were used as a negative control. Experiment was repeated two times showing similar results.

super-helical structure. This could explain that the longer I-II-III and II-III-IV fragments still interacted with IQD1 but not the overlapping II-III fragment. Additionally, the interaction within the yeast-two hybrid screen takes place in the nucleus. This might not be the endogenous site of interaction and therefore the proteins are in a different state due to different post-



translational modification, dependent on their site of localization. This might lead to false negative results.

### 3.5 IQD proteins directly interact with MT

When co-expressed *in planta* IQD1 localizes and recruits KLCR1 and CaM to MT. This suggests that IQD1 is directly binding to MT. Studies using truncated fragments of IQD1 showed, that the C-terminal part of IQD1 (IQD1-C) is sufficient for the association with MT. The middle part IQD1-M2 showed only a partial MT localization (Fig. 12A). To test whether this interaction is direct or mediated by an unknown adaptor protein, *in vitro* MT-spin down assays were conducted. These experiments are based on the sedimentation of polymerized MT using ultracentrifugation. MT-binding proteins co-sediment with the MT whereas cytosolic proteins remain in the supernatant. The functionality of the assay was tested using the manufacturer's controls; Bovine Serum Albumin (BSA) as a non-MT binding protein and the MT Associated Protein Fraction (MAPF) as a positive MT binding control (Fig. 12B). BSA was not found in the MT fraction whereas the MAPF was co-sedimenting with the *in vitro* polymerized MT showing the functionality. The tested proteins and protein fragments were recombinantly expressed in *E. coli* using the pDEST15 expression vector introducing an N-terminal GST tag. The proteins were purified using affinity chromatography. Due to the lability of the MT regarding  $\text{Ca}^{2+}$  ions and the buffering agent the proteins were dialyzed into the MT spin-down buffer. The middle fragment IQD1-M2 was found to be enriched in the MT fraction but was also found in the supernatant fraction, pointing to a reduced MT binding affinity in comparison to the C-terminal fragment. This resembles the data from the localization studies hinting to the idea that the IQD1-M2 could have lower affinity towards MT. IQD1-C was found exclusively in the MT fraction showing that this is the region where the stronger MT binding domain might be located (Fig. 12C). Full-length IQD1 was not co-sedimenting with MT. This non-binding could be an effect of the *in vitro* conditions. Another explanation would be, that IQD1 binding proteins e.g. CaM are necessary to conformationally change IQD1 to free the c-terminus from a locked state. Experiments using purified IQDs and CaM were conducted but did not show conclusive results (not shown). The MT-binding capacity of KLCR1 and IQD2 have already been tested (Liu et al. 2016; Liu 2016). In a similar assay KLCR1 but not IQD2 interacted with MT *in vitro* (Liu 2016). Contrary to the published results we show that IQD2 but not KLCR1 are interacting with MT *in vitro* (Fig. 12D). The differences could be due to the different buffers used. The

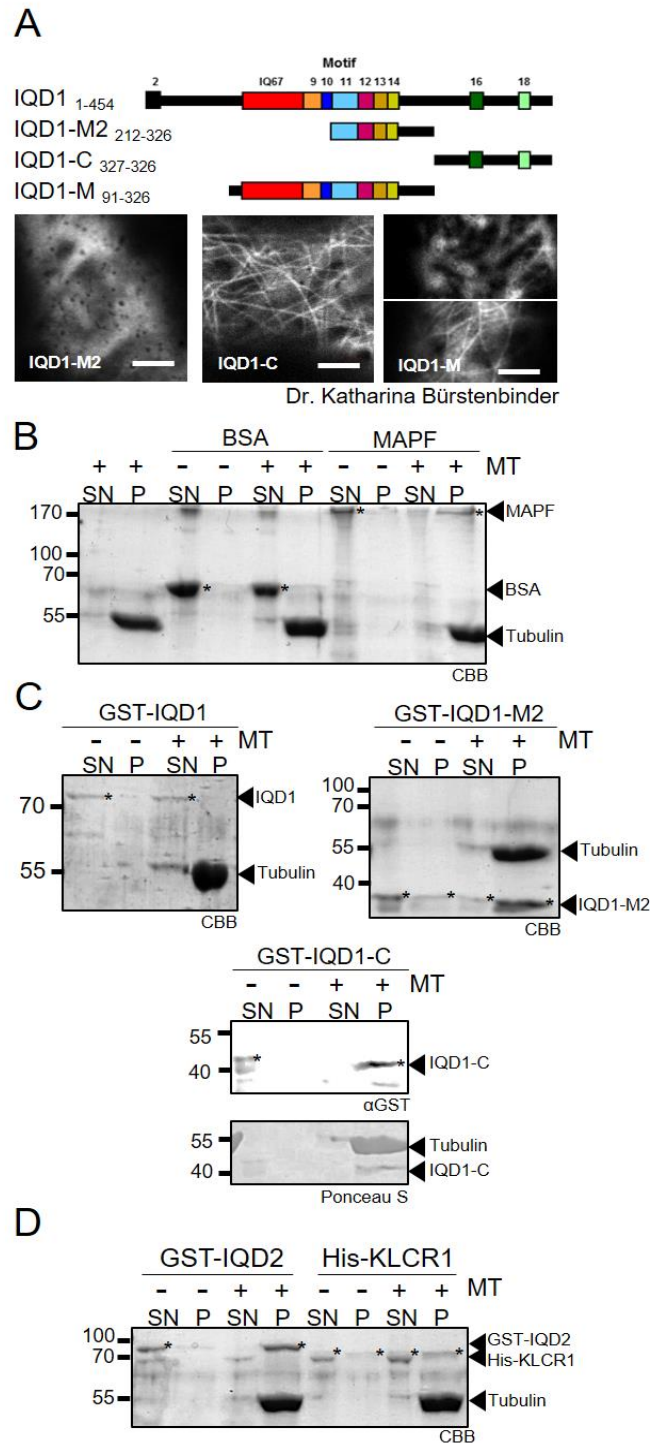


**Figure 12: IQD proteins interact directly with MT**

Single optical planes of GFP fused to truncated fragments of IQD1 transiently expressed in *N. benthamiana* under the control of the 35S promoter (A) (Bars=10 $\mu$ m). *In vitro* MT-spin down assays (B-D) using controls provided by the manufacturer (B) and purified proteins (C, D) (Asterisks mark the regarding band). Proteins were expressed recombinantly in *E. coli*. Protein purification was carried out as described by the manufacturer of the corresponding resins. After *in vitro* polymerization of tubulins, proteins were applied and incubated for 1h. After centrifugation at 100.000xg the supernatant and the pellet were boiled in Laemmli-buffer. Proteins were detected using CBB-staining or via immune detection (IQD1-C). The *in vitro* experiments were repeated two times showing similar results. Representative images are shown.

buffering agent, the ion strength and the  $\text{Ca}^{2+}$  concentration within the buffer system have strong influences on those assays. We conclude that IQD1 harbors multiple MT binding sites and that IQDs are bona fide MT binding proteins (for in silico MT-binding site prediction see Fig. S1). This further implies a function of IQDs as site specific hubs for  $\text{Ca}^{2+}$ /CaM mediated signal transduction.

### 3.6 IQD proteins are *in vitro* MPK-targets

The activity, localization and affinity of proteins towards their interactors can be altered via post-translational modifications (PTMs) enhancing the regulational flexibility of cells beyond protein abundance (Prabakaran et al. 2012). One of those PTMs is the phosphorylation of serine, tyrosine and threonine by specific kinases. Mitogen activated Protein Kinases (MPK) are one group of those kinases specifically phosphorylate the serine and threonine of TP and SP motifs of their targets. After a stimulus a phosphorylation cascade is activated resulting in the phosphorylation and subsequently activation of a specific MPK (Rodriguez, Petersen, and Mundy 2010). The MT binding affinity of the Microtubule Associated Protein 65-1 (MAP65-1) is regulated by phosphorylation via MPKs and Cyclin-Dependent Kinases. The C-terminal tail of MAP65-1 directly interacts with the acidic tail of  $\alpha$ -tubulin via static interaction. The

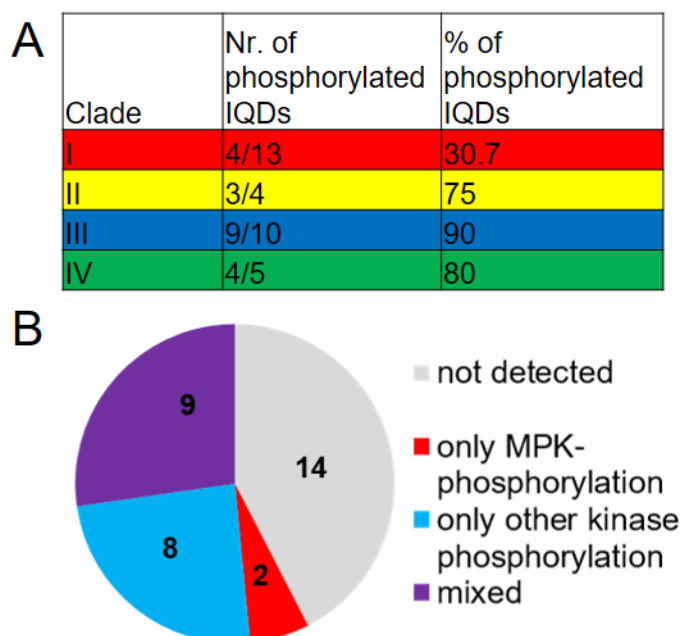
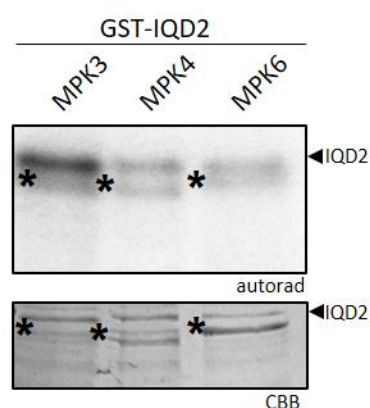


Figure 13: **Most IQDs are phosphorylated**

Total number and percentage of IQDs showing at least one phosphorylated peptide in PhosPhAt-database (A). Distribution of phosphorylation sites (B). IQDs found in the PhosPhAt database showing only the typical pTP/pSP MPK target sites (red), other unknown kinase target sites (blue), both (purple), or are not found in the database (grey).

phosphorylations take place in this basic patch altering the overall charge leading to a loss of the MT binding capacity. Taking into account that IQD proteins might be MAPs and that they show an overall basic charge, localization of IQD proteins might also be regulated via phosphorylation. In a high-throughput screen searching for potential *in vitro* MPK targets IQD23 has been found to be phosphorylated by MPK3 (Feilner et al. 2005). To gain insight whether other IQDs might also be regulated by phosphorylation we used the PhosPhAt-database (Durek et al. 2010) in search for phosphorylated IQD specific peptides. We found phosphorylated peptides of more than half of the IQDs (Fig. 13A; Fig. S1). The evolutionary conserved clade III showed the highest percentage of phosphorylated IQDs indicating a conserved mode of regulation of clade III IQD proteins. We analyzed the sites of phosphorylation and separated them in typical MPK phosphorylation (TP and SP motifs) and “other” phosphorylation sites. We found two IQD proteins, whose peptides were only phosphorylated at MPK specific sites (IQD6 and IQD10). The largest group of IQDs showed mixed peptides phosphorylated at MPK specific sites and sites where the kinase cannot be determined. We further mapped those phosphorylations to see where they would take place in the IQD proteins. We found that with the exception IQD3 all phosphorylations take place in the unstructured regions and not within the IQ67-domain (Fig. S1). It also appeared that clade III IQD proteins did not show phosphorylations in conserved motifs C-terminally of the IQ67 domain which is supposed to mediate the interaction with KLCRs.

We further investigated if those phosphorylations also take place *in vitro*. Previous studies showed, that IQD1 is an *in vitro* MPK target and MPK4 showing the highest phosphorylation capacity (Fig. S4). The multiple MPK target sites within IQD1 raised the question which of those sites are phosphorylated and whether the phosphorylation pattern differs regarding the



**Figure 14: IQD2 is an *in vitro* MPK phosphorylation target**

*In vitro* phosphorylation assays were carried out using recombinantly expressed and purified proteins. MPKs were activated using a constantly active MKK5. The active MPKs were incubated with the IQD2 protein including  $^{32}\text{P}$ - $\alpha$ -ATP. After 30 min, proteins were applied to SDS-PAGE. Loading of gel was analyzed by CBB staining. Phosphorylation was visualized via a phosphoimager. Experiments were repeated two times. A representative image is shown.

interacting MPK. So we further mapped the *in vitro* MPK target sites of IQD1. *In vitro* phosphorylated recombinantly expressed IQD1 was separated using SDS-PAGE. The corresponding band was cut and digested using trypsin. The peptides were analyzed via MS/MS analysis (Tab. S2, for visualization see Fig. S6). Five out of seven possible MPK-target sites were phosphorylated by MPK3, six were phosphorylated by MPK4 whereas MPK6 seems to phosphorylate only two TP/SP motifs.

To gain insight whether the *in vitro* phosphorylation is a common feature we performed the *in vitro* assay using GST-IQD2 (Fig. 14). We found that all used MPKs hold the capacity to phosphorylate IQD2 *in vitro* and MPK3 showing the strongest activity towards IQD2.

Besides the phosphorylations found in the *in vitro* assay for IQD1 we found several peptides in the PhosPhAt-database where the phosphorylating kinase cannot be predicted (Fig. 13). Those phosphorylations took place mostly in the N- and C-terminal regions surrounding the IQD67 domain and adjacent motifs (Fig. S7). Those regions are also the ones being intrinsically disordered and also harboring basic patches and with regard to the C-terminal part also harbor the possible MT binding domain (Fig. S6; Fig. S1).

### 3.7 IQD1 interact with MPKs *in planta*

To test whether an interaction of MPKs and IQD1 could take place *in planta* we performed bimolecular fluorescence complementation (BiFC) assays transiently in *N. benthamiana* using nYFP-IQD1 and cYFP-MPK fusion constructs. The YFP signal could be restored showing a possible interaction of nYFP-IQD1 and cYFP-MPKs (Fig. 15). The subcellular sites of fluorescent complementation were the MT and nucleus. For MPK6 a complementation could also be observed in the nucleolus. Previous interaction studies of MPKs using BiFC assays showed that reconstituted complexes were localizing to the nucleus and the cytosol (Schweighofer et al. 2014). Most likely the possible IQD1-MPK complex was directed to the MT via IQD1 in this experiment in an IQD1 dependent fashion. Since in this method the

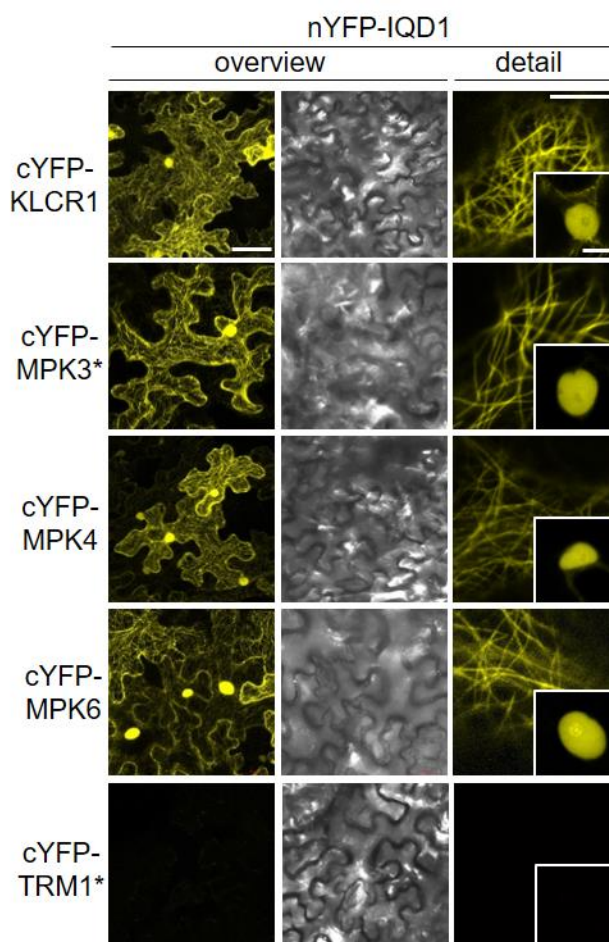


Figure 15: **IQD1 interacts with MPKs *in planta***

Stacks (overview) and single optical sections (details) of YFP-signals after bimolecular fluorescent complementation are shown. Transient coexpression of IQD fused to the N-terminal part of Venus (nYFP) and MPK fused to the C-terminal part of Venus (cYFP) under the control of 35S promotor was done via *Agrobacterium* mediated transformation. cYFP fusions of KLCR1 and TRM1 were used as positive and negative controls, respectively. Bars: overview = 50µm, details = 10µm. Microscopy was conducted two dpi, asterisks mark constructs analyzed three dpi. Experiments were repeated two times. At least 3 cells were analyzed per infiltration. Representative images are shown.

maturation of the YFP Venus after reconstitution of the two halves leads to a strong complex (Kerppola 2008), it could not be determined whether the interaction of the proteins is permanent or only temporary. To have a first look on the dynamics of the IQD1-MPK interaction, GFP-tagged IQD1 and mRFP-tagged MPKs were transiently co-expressed in *N. benthamiana*. The co-localization of the two proteins would only rely on the interaction of proteins itself and be influenced by the reconstitution of the tags. Three days after transformation we did not see a recruitment of the RFP-tagged MPKs to the MT via GFP-IQD1 (Fig. S3). This might show that the interaction is transient and might only take place during the phosphorylation of IQD1. This shows that IQD proteins might be regulated by MPK phosphorylation, but do not act as hubs for MPK derived signaling.

### 3.8 IQD1 changes its nucleolar localization upon phosphorylation

As described for MAP65-1 it was of interest for us to elucidate the role of the phosphorylations regarding the subcellular localization of IQD1. Therefore we generated phospho-mutants by changing the phosphorylated aa to glycine. Additionally we generated phospho-mimicry mutants, where the phosphorylated aa was exchanged to glutamate, imitating the acidic phosphate group (Fig. 16A). Different degrees of phosphorylation were mimicked. We generated and analyzed a variant where all possible MPK specific SP/TP sites were changed to glutamate (1-7 S/T -> E) or where only the C-terminal MPK target sites were mutated to glutamate (5-7 S/T -> E). To analyze the effect of the mutations we transiently expressed the GFP tagged mutants in *N. benthamiana* and observed the localization using laser scanning microscopy. We did not detect any changes in the MT localization of those phospho-mimicries. To get an idea whether other kinases might regulate the MT localization of IQD1 we mutated additional aa found to be phosphorylated in the PhosPhAt database. Due to MT localization of the C-terminal half of IQD1 we choose to mutate the aa situated C-terminally of the IQ67 domain (5-11 S/T -> E). Similar to the other phospho-mimicry mutants no changes in the MT localization were visible. The MPK phospho-mutant (1-7 S/T -> G) did also not show an altered MT localization. However, we observed a reduced nucleolar localization of the mimicry-mutants, but not the phospho-mutant, compared to the WT (Fig. 16B+C). To estimate the degree of shifted localization the relative fluorescence intensity between the nucleus and nucleolus was calculated (Fig. 16D). The phospho-mutant showed the same degree of

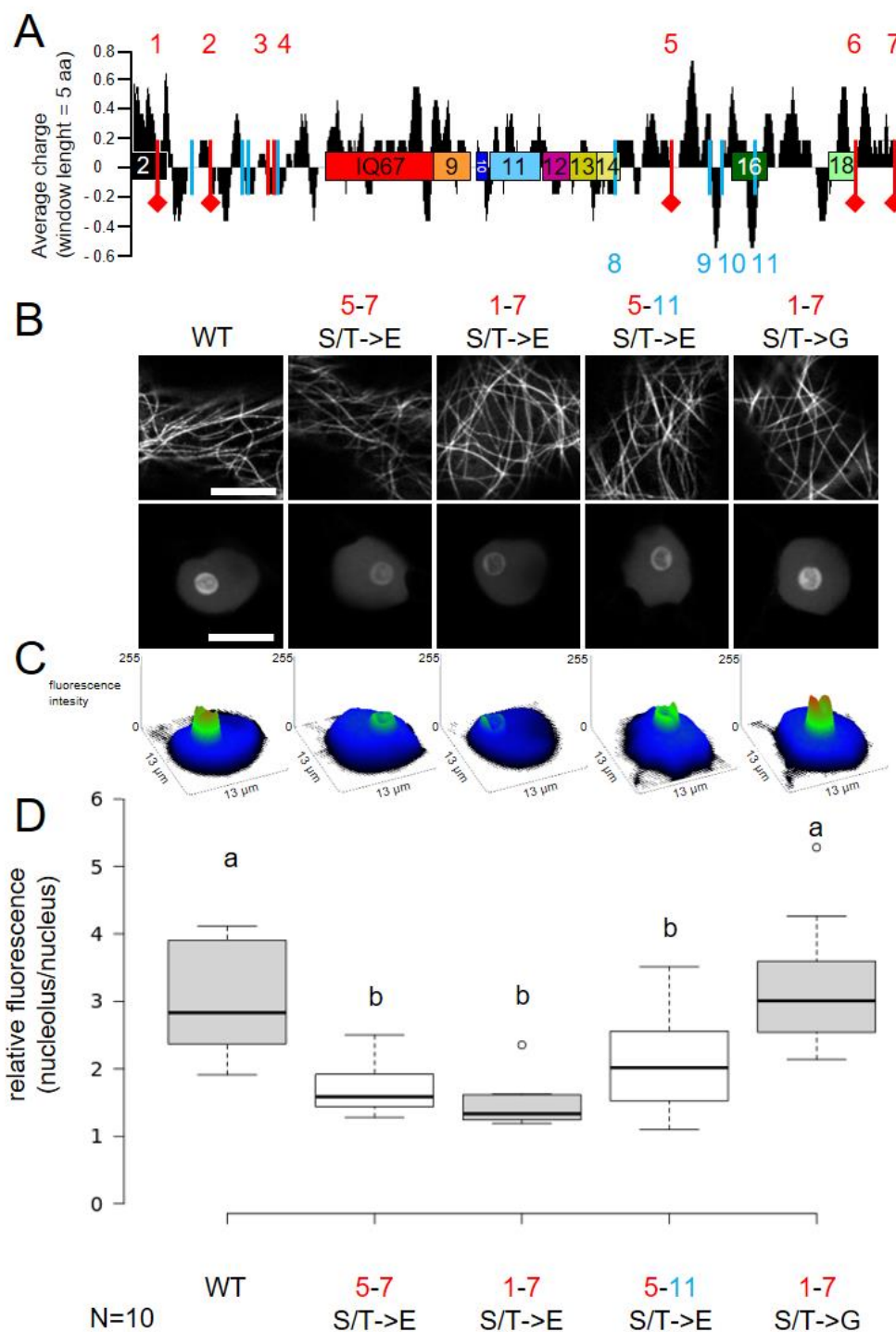


Figure 16: **IQD1 changes its localization upon phosphorylation**

Distribution of possible phosphorylation sites (red bars = MPK target sites (TP/SP), blue bars depict phosphorylated peptides found in PhosPhAt-database; red diamonds mark aa phosphorylated *in vitro*; boxes indicate conserved motifs including their respective number, red box depicts IQ67 domain; black graph represents charged stretches) (A). GFP fused to phospho-mimicries (S/T->E) and -mutants (S/T->G) of IQD1 were expressed under the control of the 35S promoter in *N. benthamiana*, transiently transformed via *Agrobacterium*, single optical sections are shown (B) (bars = 10  $\mu$ m). Visualization of fluorescence intensity within the nucleus (surface plot) (C). Pictures were analyzed using ImageJ, 8bit images were colored in "Rainbow RGB" and analyzed via "surface plot". Relative fluorescence of the nucleolus (D). "Mean grey values" of the nucleolus and the nucleus were measured and the quotient was calculated. For information about the positions see table 2. Experiments were repeated two times with 5 cells analyzed per infiltration.



nucleolar localization compared to the WT indicating that exchanging the aa at those specific sites does not alter the localization due to aa exchange per se. All the phospho-mimicry mutants on the other hand showed a significantly reduced nucleolar localization compared to the WT and the phospho-mutant. The phospho-mutants showed no difference between each other suggesting that the C-terminal phosphorylation via MPKs is sufficient to reduce the nucleolar localization of IQD1. To ensure that the observed changes are not caused by altered stability or turnover rate of the phospho-mimicry mutants, stability assays have been conducted (Fig. S10). All the mutated variants were detectable in the assay. The WT showed a low level of expression compared to the mutants. All variants were detectable up to 5 hours after cycloheximide treatment suggesting a high stability. We conclude that the MPK-derived phosphorylations in the c-terminus lead to a reduced nucleolar localization of IQD1. Half of all human NoLS signals show an overall basic charge which is a feature of IQD proteins (Scott et al. 2010). A phosphorylation could change the charge in those patches and influence the nucleolar localization similar to the system described for the MT binding sites. Here we show that the IQD1 mediated  $\text{Ca}^{2+}$ /CaM signaling within the nucleolus could be regulated via phosphorylation.

### 3.9 KLCRs are *in vitro* MPK targets

When analyzing the sequence of KLCR proteins we found several putative MPK target TP/SP motifs (Fig. 17C). Several of them were found to be phosphorylated in the PhosPhAt-database as well as additional phosphorylated non-TP/SP motifs. We were interested whether KLCRs are phosphorylated only by specific MPKs. As described for IQD1 and IQD2, we performed *in vitro* phosphorylation assays using activated MPKs and  $\gamma\text{P}^{32}$ -ATP (Fig. 17A). After incubation, we could detect a MPK3 derived  $\text{P}^{32}$  labeling of all KLCRs. MPK4 labeled KLCR1 and KLCR2 radioactively whereas MPK6 seemed to only phosphorylate KLCR1. The strongest radioactive signals were observed for the phosphorylation of KLCR1 by MPK3 and MPK4. The weakest signals were seen for KLCR3. This suggests that the tested MPKs mainly target KLCR1 and KLCR2 and that KLCR3 might only be phosphorylated due to the artificial *in vitro* conditions.

Due to the strong signal and the 4 MPK specific phosphorylation sites found *in silico* for KLCR1, we were interested whether the different MPKs would phosphorylate KLCR1 at specific sites or whether MPKs indifferently phosphorylate KLCR1. We again performed *in vitro* phosphorylation assays but with unlabeled ATP. After incubation the proteins were separated by SDS-PAGE, and the corresponding bands were cut (Fig 17B). After tryptic digestion the peptides were analyzed via MS/MS directly targeting phosphorylated peptides (Tab. S2). We found that all MPKs phosphorylated threonine at position 35 (T35) (Fig. 17C, orange diamond; Tab. S2).

Interestingly this specific aa was not found to be phosphorylated within the PhosPhAt database. This suggests that other MPKs might be more relevant regarding KLCR phosphorylation as only 3 out of 20 putative Arabidopsis MPKs were tested in this assay.

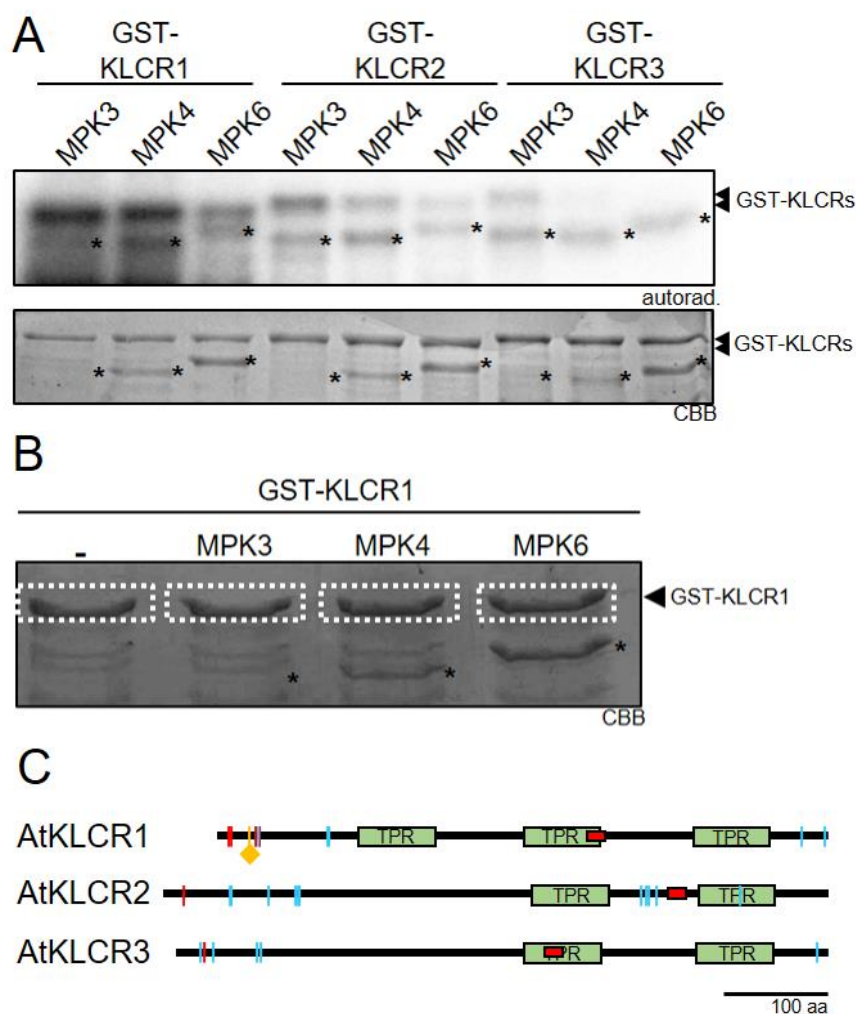


Figure 17: **KLCRs are *in vitro* MPK targets**

*In vitro* phosphorylation assays were done using recombinantly expressed and purified proteins (A). MPKs were activated using a constantly active MKK5. The active MPKs were incubated with the KLCR proteins including  $^{32}\text{P}$ - $\alpha$ -ATP. After 30min proteins were applied to SDS-PAGE. Loading of gel was analyzed by CBB staining. Phosphorylation was visualized using a phosphorimager. Mapping of phosphorylation sites of KLCR1 are shown (B+C). MPKs were activated using a constantly active MKK5. The active MPKs were incubated with the KLCR proteins including ATP. After 30min proteins were applied to SDS-PAGE. Loading of gel was analyzed by CBB staining. Bands of the corresponding size were cut (B), digested with trypsin and analyzed via a targeted MS/MS approach. Map of phosphorylated peptides derived from the PhosPhAt-database and *in vitro* phosphorylation site (C). Red bands mark putative MPK target sites (SP/TP motifs), blue bands mark putative phosphorylated non-TP/SP sites. The orange band marked with a diamond marks the *in vitro* phosphorylated T35. The green boxes show TPR-domains predicted using the Pfam-database (<https://pfam.xfam.org/>). The red box marks the CaM binding site predicted by the Calmodulin target database (<http://calcium.uhnres.utoronto.ca/ctdb/>). Experiment was performed once.

### 3.10 KLCRs interact with MPKs *in planta* and recruit them to MT

The interaction between KLCRs and MPKs have not been described yet. To get a first impression whether the tested MPKs do interact with KLCRs *in planta* we conducted BiFC assays using nYFP-MPK and cYFP-KLCR constructs transiently expressed in *N. benthamiana* (Fig. 18). The VENUS fluorescence could be re-constituted using all MPK-KLCR combinations, but not using the negative control TRM1. This indicates that KLCRs interact with MPKs *in planta* and are possibly regulated via MPK derived phosphorylation.

We further could observe tubular structures in cells showing a reduced level of fluorescence indicating low levels of expression. Due to the previous experiments, showing an IQD-dependent recruitment of KLCRs to the MT and their similarity with animal kinesin subunits, those tubular structures are most likely MT. But whether the KLCR-MPK complex is recruited to the MT via IQDs or other MAPs needs to be tested. The observation that the tubular structures were only visible under low expression conditions shows that KLCRs are most likely recruited to MT by MAP. The amount of KLCR recruiting MAPs would be the limiting factor in those experiments. If every IQD or MAP is occupied with a KLCR, but much more KLCRs are expressed due to the use of the high expression CaMV35-promotor than this would lead to a masking effect due to high fluorescence emitted from cytosolic KLCRs. Under low expression conditions all IQDs or MAPs are still occupied but the masking effect would be highly reduced. This is conclusive with previous experiments expressing GFP-tagged KLCRs under the control of the weaker UBI10 promotor (not published). Furthermore, all combinations except the ones containing cYFP-KLCR3 constructs showed a fluorescence signal within in the nucleus. Previous experiments showed that N-terminal KLCR3 fluorescence fusions are not found in the nucleus whereas C-terminal fusions did. Hence the fact that the BiFC-fusion constructs are N-terminal fusions this might also be the case in this experiment. Most likely a NLS is masked by the fusion construct but future experiments need to be conducted to confirm this.

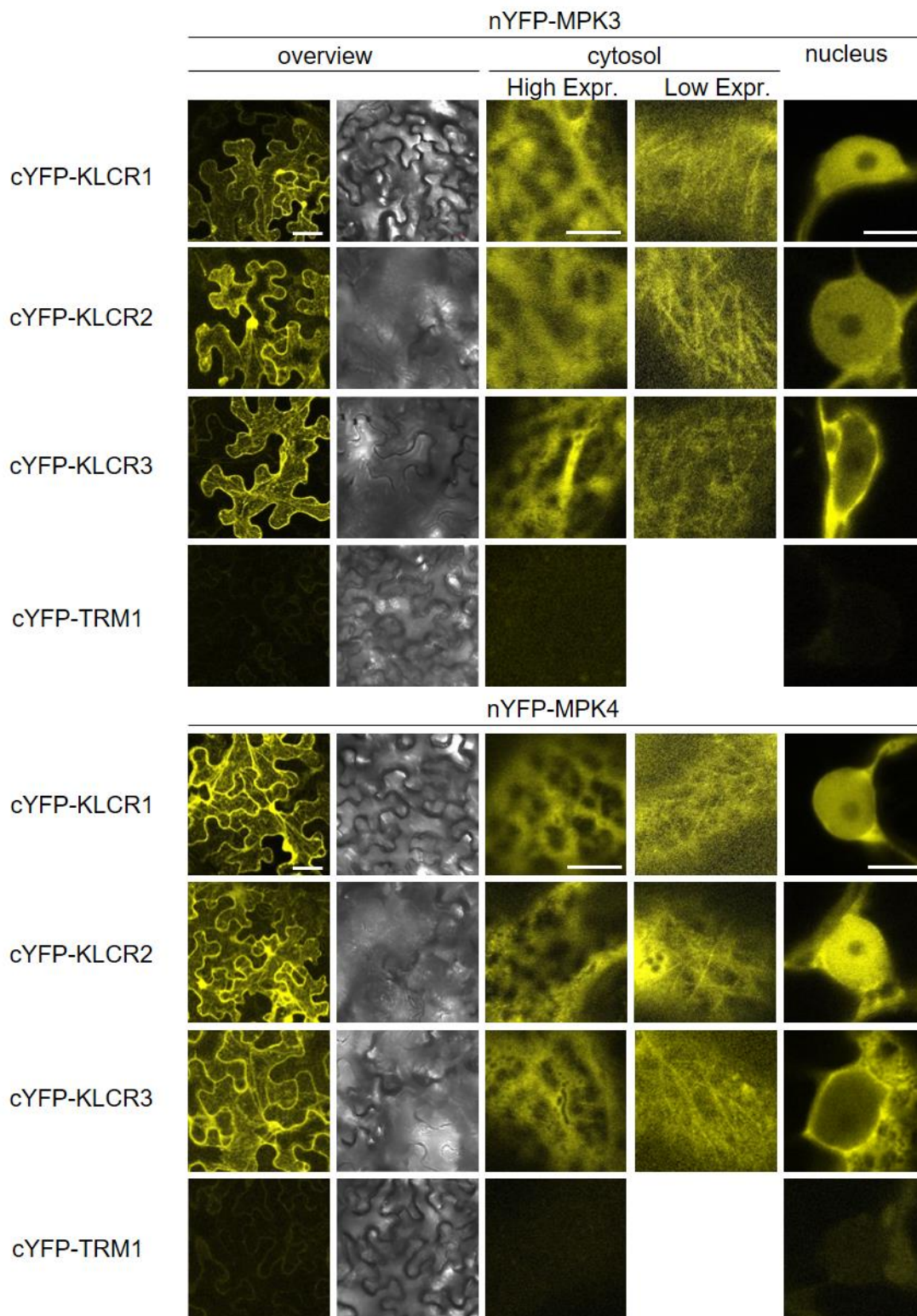


Figure 18: For description see next page.

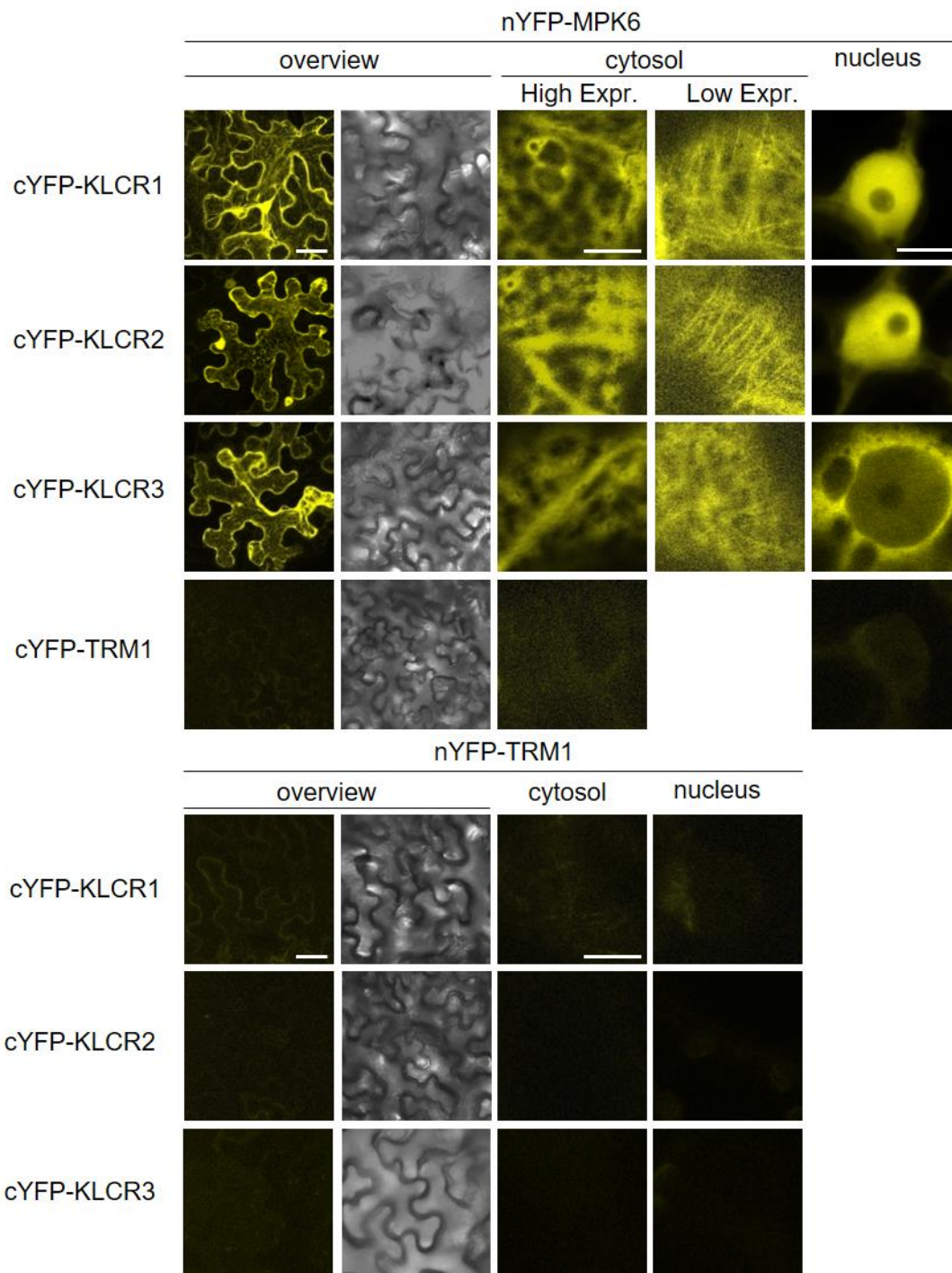


Figure 18: **MPKs interact with KLCRs in planta**

Stacks (overview) and single optical sections (cytosol and nucleus) of YFP-signals after BiFC are shown. MPKs fused to the N-terminal part of Venus (nYFP) and KLCRs fused to the C-terminal part of Venus (cYFP) were transiently coexpressed in tobacco under control of CaM35S promoter via Agrobacterium mediated transient transformation. Different strength of fluorescence was observed. Cells showing low expression and fluorescence were analyzed with a stronger laser intensity. TRM1 was used as a negative control. Bars: overview = 50  $\mu\text{m}$ , cytosol and nucleus = 10  $\mu\text{m}$ . Experiments were repeated two times. At least three cells were analyzed per infiltration. Representative images are shown.

### 3.11 MPKs interact with CaM *in planta*

CaM has been reported to regulate MPK8 function in ROS homeostasis after wounding. Full function of MPK8 is only obtained after phosphorylation by MKK3 and Ca<sup>2+</sup>-CaM binding (Takahashi et al. 2011). The C-terminal two EF-hands of CaM were sufficient for MPK8 binding. The deactivation of MPKs is regulated by MPK-phosphatases (MKPs). The activation of MKP function through Ca<sup>2+</sup>-CaM binding has been reported as well (Lee et al. 2008). Those results integrate the classical canonical MPK cascade and its regulation via MKPs into the ubiquitous Ca<sup>2+</sup>-signaling. Based on those ideas and the fact that IQDs and KLCRs are CaM

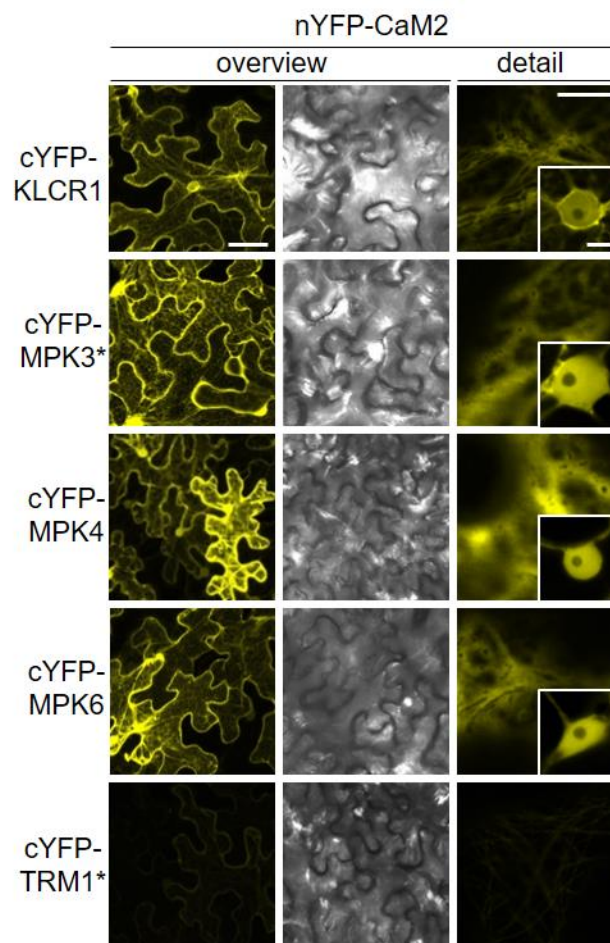


Figure 19: **MPKs interact with CaM *in planta***

Stacks (overview) and single optical sections (details) of YFP-signals after BiFC are shown. CaM2 fused to the N-terminal part of Venus (nYFP) and MPKs fused to the C-terminal part of Venus (cYFP) were transiently coexpressed under the control of the 35S promoter in tobacco via *Agrobacterium* mediated transformation. cYFP fusions of KLCR1 and TRM1 were used as positive and negative controls, respectively. Bars: overview = 50µm, details = 10µm. Microscopy was conducted two dpi, asterisks mark constructs analyzed three dpi. Experiments were repeated two times. At least three cells were analyzed per infiltration. Representative images are shown.

binding proteins and are regulated via MPK we were interested whether the tested MPKs are as well CaM binding proteins. To gain a first insight we tested the interaction of CaM and MPKs in a BiFC assay *in planta*. We observed a complementation of the VENUS signal in tobacco leaves transiently co-expressing nYFP-CaM and cYFP-MPKs, indicating an interaction of those proteins. We did not observe an interaction of nYFP-CaM with the negative control cYFP-TRM1. Fluorescence was detectable in the cytosol and the nucleus (Fig. 19). Takahashi *et al.* (2010) showed the interaction of MPK8 and CaMs *in planta* using BiFC assays. However, they could not observe an interaction between MPK3, MPK4, MPK6 and CaM4 using C-terminal fusions of those proteins. It is often described that the C-terminal globular domain containing two EF-hands of CaM are most important for the interaction with the CaMBP. In our experiments N-terminal fusions of CaM2 were used. This could explain the discrepancy of our results and might point to future prospects to analyze whether MPKs are CaMBP in general and if calcium somehow regulates MPK derived processes.

## 4. Discussion

### 4.1 IQD proteins as hubs for CaM-mediated Ca<sup>2+</sup> signaling

The analysis of CaMBP focuses mostly on the influence of Ca<sup>2+</sup>-CaM on the CaMBP. In many screens searching for potential CaMBP those interacting with Apo-CaM are either not found (Reddy, Ali, and Reddy 2002) or are excluded from the experimental setup. Protein extracts are often applied to CaM resins in the presence of Ca<sup>2+</sup>. The eluting of those CaMBP is often achieved using EGTA (Reddy, Ben-Hur, and Day 2011) leaving the Apo-CaMBPs bound to the CaM resin or losing them in the first place by pulling down interactors only with Ca<sup>2+</sup>-CaM. By directly analyzing the cases for both states we could show that IQD proteins potentially interact with both states of CaM, except for IQD33 (Fig. 4). The IQ-motif is known for its capability to interact with both states of CaM (Jang, Ban, and Lee 2011; Bahler and Rhoads 2002). Structural analysis of Apo-CaM interacting with IQ-motifs of myosin showed that the last arginine of the IQ-motif interacts with the N-lobe of Apo-CaM and is therefore important for Apo-CaM binding (Houdusse et al. 2006). The truncated IQ67-domain of IQD33 is missing this arginine. This could describe that IQD33 showed no interaction with Apo-CaM *in vitro*. This hints to the fact that at least the first IQ-motif most likely mediate Apo- and Ca<sup>2+</sup>-CaM binding. Whether the other CaM-binding motifs interact with only one state of CaM or are also indifferent CaM interactors is still elusive. The bifunctional CaM-binding and the overall intrinsically disordered structure of IQD proteins hint to the fact that they might be scaffold proteins, acting as hubs or mediators for protein interaction (Cortese, Uversky, and Dunker 2008). One could think of that IQDs bind their interacting proteins using the structured helical regions of the IQ67-domain and the adjacent motifs. The unstructured regions would act as free-floating anchors attaching the scaffold to specific sites of the cell. On the other hand, not many IQD interactors have been described yet, but interacting with multiple proteins is the defining feature of scaffold proteins. CaM and KLCRs show stable *in vitro* interaction with IQD1 and IQD2. MPKs on the other hand do not seem to be static interactors of IQDs. IQD1 and IQD2 recruit KLCRs to Apo-CaM *in vitro*. It also recruits KLCR1 and CaM to MT *in planta* (Burstenbinder et al. 2013). A possible trimeric state of IQD1 recruiting CaM and KLCRs simultaneously to the MT has been demonstrated *in planta*. One could assume that IQD1 scaffolds Apo-CaM and KLCRs to the cortical MT. This would allow CaM and KLCRs to reside in the proximity of the plasma membrane where the Ca<sup>2+</sup>-channels are located. This guidance towards the cortex would increase the competitiveness to bind influxing Ca<sup>2+</sup> to the IQD1 bound Apo-CaM ensuring that the Ca<sup>2+</sup>-signal could be transduced to IQD-bound proteins in a quick way.

If this reaction takes place there are two possibilities. KLCRs could bind to IQDs and form a resting state until [Ca<sup>2+</sup>]<sub>cyt</sub> increases. The forming Ca<sup>2+</sup>-CaM could bind to KLCR and



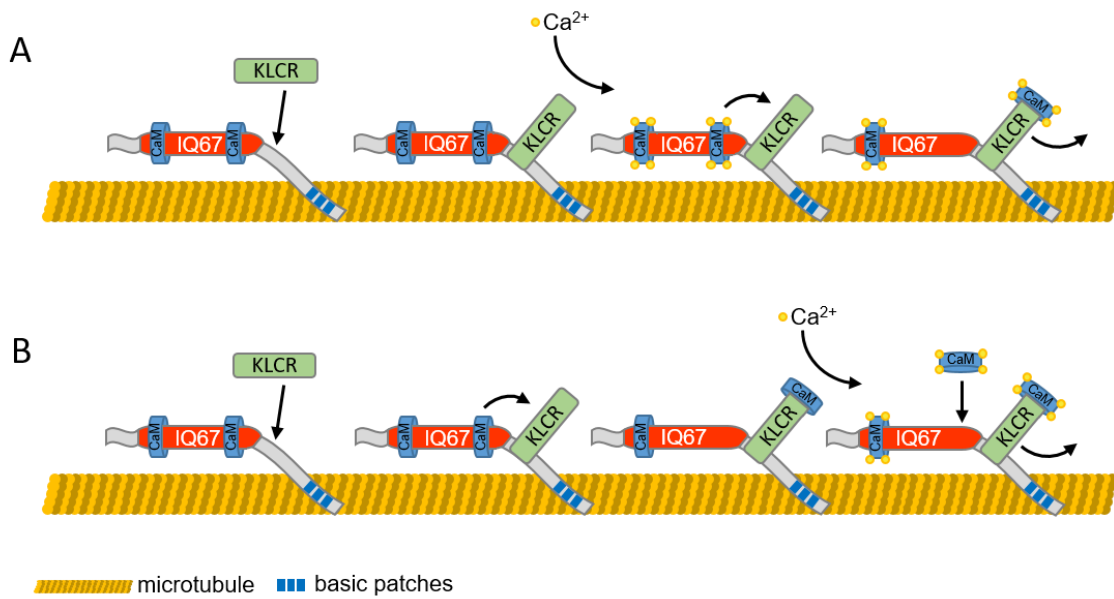


Figure 20: **Proposed model of IQD1 as a CaM and KLCR scaffold**

IQD1 recruits KLCR and CaM to the MT and recruits KLCR to Apo-CaM. IQD1 interacts directly with MT via its basic patches. The first possible mechanism of IQD scaffold function could be that KLCRs and Apo-CaM are brought into proximity of each other to ensure the transfer of Ca<sup>2+</sup>-CaM to KLCRs after Ca<sup>2+</sup>-influx (A) Second possible scenario would be that IQD1 renders KLCRs affinity towards Apo-CaM and even might transfer Apo-CaM to KLCRs. Ca<sup>2+</sup>-CaM could then either out compete KLCRs or KLCRs affinity towards IQDs is rendered due to the interaction with Ca<sup>2+</sup>-CaM.

subsequent KLCR-mediated responses could take place (Fig. 20A). Another possibility would be that the IQD-KLCR interaction changes the CaM-binding property of KLCRs enabling them to also interact with Apo-CaM. Elevating  $[Ca^{2+}]_{cyt}$  would get perceived directly by the KLCR bound CaM. Subsequently the bound Ca<sup>2+</sup>-CaM, could alter the affinity of KLCRs to IQDs. Alternatively, due to the proximity of the IQD67 domain and the KLCR binding site, free Ca<sup>2+</sup>-CaM could affect the KLCR-IQD interaction by binding to the IQ67 domain (Fig. 20B). The hypothesized destabilizing effect of Ca<sup>2+</sup> regarding this multimeric state need to be investigated in future experiments.

A similar scaffolding protein has been reported for eukaryotes, although no homologue has been described in plants. The Ras GTPase-activating-like proteins (IQGAP) interact with the actin cytoskeleton, both states of CaM and with MPKs (Smith, Hedman, and Sacks 2015). Briggs and Sacks hypothesized that IQGAP1 recruits the guanine nucleotide exchange factor Cdc24 to the actin filaments only under low  $[Ca^{2+}]_{cyt}$ . After Ca<sup>2+</sup> influx, Ca<sup>2+</sup>-CaM would change the conformation of IQGAP1 leading to a dissociation from the actin filaments and thereby to a dissociation of Cdc24 from the actin cytoskeleton which subsequently would affect the actin cytoskeleton (Briggs and Sacks 2003). It could be likely that IQD1 could act in a similar way but linking CaM-mediated Ca<sup>2+</sup> signaling towards the MT network.

The Arabidopsis Receptor for Activated C Kinase 1 (RACK1) protein on the other hand is described as a scaffold protein assembling the core components of the MPK-signaling cascade to ensure a fast immune response upon pathogen attack (Cheng et al. 2015). It was shown that RACK1 could interact with the MPKs, MPKK as well as MPKKK. However, due to the lacking *in vitro* interaction of MPKs with IQD1 as well as KLCR1 (Fig. S5 and S7) such a mechanism seems unlikely. The *in vitro* phosphorylation as well as the *in planta* interaction suggest that IQDs and KLCRs indeed are MPK interactors but might only interact with MPKs during the enzymatic process of phosphorylation but are not static interactors of those proteins. As shown *in vivo* and *in vitro*, IQD2 and possibly IQD1 seem to be MAPs. The *in silico* analysis using the MAPalyzer tool (Zhou et al. 2015) showed that 29 out of 33 IQD proteins contain putative MT binding sites and roughly half of the IQD proteins have at least two putative MT binding sites (Fig. S1). *In planta* IQD1 associates with MT, but full length IQD1 did not interact with MT *in vitro*. However, using truncated variants of IQD1 suggested that IQD1 seem to have at least two MT binding sites (Fig. 12). Using *in planta* experiments, multiple MT binding sites have also been reported for IQD13 (Sugiyama et al. 2017) suggesting that this is a feature of at least some IQDs. The presence of multiple MT binding sites enables proteins to interact with multiple MT (Tulin et al. 2012) suggesting that at least some IQDs might have MT bundling capacities. Additionally, the overexpression of IQD16 leads to parallel aligned MT which could be a result of its MT bundling capacities subsequently leading to an elongated cell shape (Burstenbinder et al. 2017). Another possibility is that IQD16 leads to a suppression of MT branching events as reported for NEDD1.

We wanted to analyze whether those regions of MT binding might be conserved among the reported MT binding IQDs. The sequences of IQD1, IQD13 and IQD16 share only a low sequence homology (Fig. S10). The C-terminal MT binding site containing regions of IQD1 and IQD13 does overlap but do not show a distinguishable increased degree of similarity. This suggests that the interaction with MT is not driven by conserved motifs but likely driven by the overall charge and structure of those regions.

### 4.2 IQD proteins involved in MT linked processes

The observation that overexpression as well as knock out of IQDs does not lead to a homogenous phenotype, but to subtle changes in morphology either contradicts the possibility of IQDs as general MT bundling proteins or shows a high level of functional redundancy among IQD proteins. Due to the high number of sister genes within the IQD family the latter one is more likely (Abel, Savchenko, and Levy 2005a). Nevertheless, IQDs not only associate with MT but also nuclear structures. For several IQDs, the localization towards the plasma

membrane has been shown (Burstenbinder et al. 2017). Taken this together with the fact that most IQDs label MT uniformly and are able to recruit other proteins towards the MT, have the potential to interact with multiple MT due to multiple MT binding sites and some show a possible plasma membrane binding one could hypothesize that IQDs act as lime twigs sitting on the MT. It would allow the recruitment of MT influencing proteins which do not directly bind to MT, the connection of the cytoskeleton via possible MT bundling activities as well as anchoring MT right on the cortex by tethering MT towards the plasma membrane. Such a mechanism could influence cell morphology by recruiting or restricting MT at specific sites and by this influencing cell wall deposition by the cellulose synthase complex. The latter one has been described for the MT severing protein of katanin (KTN1), which gets recruited by Rhodopsin Of Plants 6 (ROP6) and ROP-Interactive Crib motif-containing protein 1 (RIC1) to the MT. It is hypothesized that ROP6 activates RIC1 in an auxin dependent manner leading to a RIC1 dependent potentiation of KTN1, which then severs MT. It is believed that those effects occur at sites, which later on are the lobes of pavement cells. MT at the soon to be established indentations are unaffected, leading to growth restrictions only at the sites of KTN1 residence

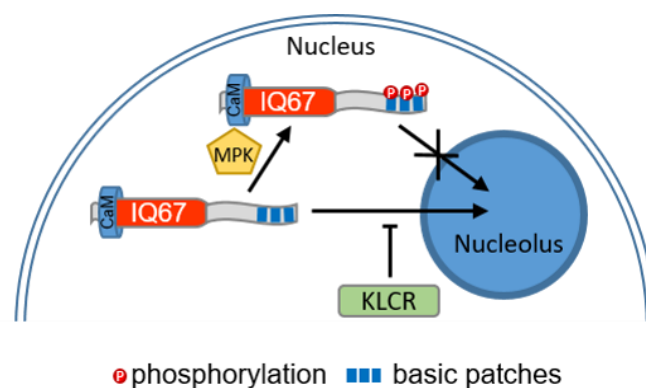


**Figure 21: IQD proteins are most likely regulated via phosphorylation by MPK**

The phosphorylation of the C-terminal region of IQD leads to a reduced localization to the nucleolus. The c-terminus harbors basic patches, which most likely harbor the nucleolar localization signals. Co-expression experiments showed that IQD1 can recruit CaM to the nucleolus. Co-expression with KLCR proteins on the other hand excludes IQD1 from locating to the nucleolus.

(Lin et al. 2013; Hamant 2013). This leads to the jigsaw like structure of pavement cell. However, due to recent problems in Auxin Binding Protein 1 mutant lines the influence of auxin within this process needs to be readdressed in future experiments (Gao et al. 2015).

Interestingly, QTL based screens in search for genes involved in regulatory mechanisms regarding the central metabolism showed that the loss of IQD22 leads to a higher starch to sucrose ratio and a reduced number of leaves and an earlier flowering time (Fusari et al. 2017). The authors suspected that IQD22 might be regulating the allocation of carbohydrates during cell expansion, pointing to the importance of IQDs during growth processes. These findings are supported by metabolic measurements in *S. lycopersicum* harboring a duplicated SUN/IQD locus. The duplication of the *SUN* genes in the SUN lines not only leads to elongated fruits but

also to changes in the central metabolism like decreased levels of sucrose and fructose (Clevenger et al. 2015). Additionally, in experiments analyzing different apple cultivars regarding their malate contents and the underlying genetic cause, *IQD2* has been found to be co-regulated with different alleles believed to be involved in regulating the malate content. There *IQD2* is proposed as a hub and regulatory genes regarding those alleles (Bai et al. 2015).

Those findings suggest that IQDs might not only regulate cell division and cell growth directly by influencing the localization of other proteins but might also influence the metabolic state of the cell and subsequently could regulate the availability of cell wall pre-cursors and thereby the rate of cell wall biosynthesis. An accelerated cell wall synthesis could restrict the expansion growth and thereby change cell morphology and the rate of differentiation. However, one has to consider that IQD proteins have not been shown to act as enzymatic or transcriptomic regulators or being directly involved in any metabolic processes. IQD proteins could just influence cell wall deposition positively or negatively and by this drain or restrain UDP-glucose changing the metabolic state of the cell. The published metabolic changes in IQD misexpression lines could also occur due to pleiotropic effects.

### 4.3 IQDs within the nucleus

Besides the MT association *IQD1* strongly localizes to the nucleolus. This localization is mediated by motifs at the c-terminus, probably by basic stretches within those motifs. Although IQD proteins show diversity in their molecular masses and the distribution of motifs, the physicochemical parameters are uniform. They share a high iso-electrical point and an overrepresentation of arginine, lysin and serine. These parameters are shared with RNA processing proteins, which led to the hypothesis that IQD proteins might be involved in intracellular trafficking of RNA along the MT (Burstenbinder et al. 2013). Due to their function, nucleoli contain high amounts of RNA (Stern, Johnston, and Setterfield 1959). Therefore the localization of *IQD1* to the nucleolus could just be a side effect of *IQD1* binding to the nucleolar rRNA. On the contrary, not all IQDs are localizing to the nucleolus or the nucleus despite their physicochemical uniformity. Additionally, *IQD1* can recruit CaM to the nucleolus and the co-expression of *IQD1* and *KLCR1* effects the nucleolar localization of *IQD1*. This could be part of another *IQD1* re-localization mechanism ensuring that *IQD1* is absent from nucleolus of only present at the MT when *KLCR* proteins are present (Fig. 22). It also supports the fact that the nucleolar localization might also be part of the biological function of *IQD1*. Most nucleolar proteins are involved in ribosome biosynthesis and maturation. More specifically *IQD1* seem to reside in granular component, which is the outer layer of the nucleolus. The granular component hosts the last steps of rRNA and ribosome assembly. Such a function is not

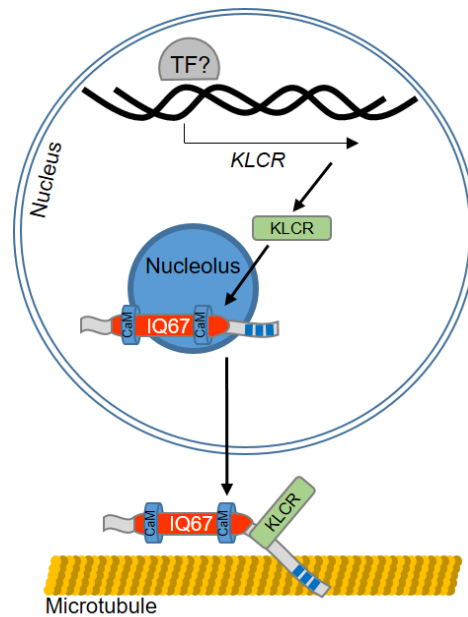


Figure 22: **KLCR and IQD proteins influence their localization mutually**

KLCR proteins when overexpressed reside in cytosol. IQD1 proteins are found associated with MT and within the nucleolus. When co-expressed IQD1 recruits KLCR1 to the MT whereas KLCR1 excludes IQD1 from the nucleolus.

proposed for IQD1 or IQD proteins in general. Little is known about nucleolar proteins involved in other functions than ribosome maturation, especially in plants. Proteomic analysis of animal nucleoli showed, that half of the nucleolar localized proteins are unrelated to the ribosomal production. Some of those proteins have proposed roles in cell cycle regulation (Andersen et al. 2002; Pederson and Tsai 2009). Although the phenotypic characterization does not support a role of IQD1 during mitosis, the MT localization might hint to such function. MT are of relevance at all stages of a cells life. Especially during mitosis MT are of special importance building the spindle apparatus, that separates the chromosomes (Mayer and Jurgens 2002). In plants MT also define the site of cytokinesis as part of the plant specific preprophase band and the later forming phragmoplast which acts as a hub for exocytotic deposition of cell wall material in a centrifugal manner. However, during mitosis, specifically in the prophase, the nucleolus disassembles completely and reassembles during the early G1-phase. Although IQD1 does not seem to be expressed in cells of the proliferating zones of the root tip and the apical meristem, it would be of interest how the subcellular localization of IQD1 changes during those phases. For other IQDs, especially from clade Ic a localization at the root tip as well as in the embryo has been shown. Some members of this clade show a nucleolar localization when transiently overexpressed in *N. benthamiana* (Burstenbinder et al. 2017) but not under the native promotor in *A. thaliana* (Wendrich et al. 2018). This might be due to different posttranslational modifications of those IQDs. One possibility could be that in Arabidopsis those IQDs are phosphorylated and subsequently acidified by Arabidopsis-specific protein kinases in the basic stretches of the NoLS, leading to a reduced nucleolar localization (Fig.

22). We could observe such a behavior for IQD1 by the use of phospho-mimicry mutants. The residing, but reduced presence of the IQD1 phospho-mimicry mutants within the nucleolus might hint to still undetected phosphosites within IQD1. Taking into account that some IQDs might be involved in the cell cycle, Cyclin Dependent Protein Kinases (CDPK) might be responsible for the phosphorylation of those sites.

Similar to the NoLS, basic stretches have been shown to mediate the interaction between the MAPs and the acidic tail of  $\alpha$ -tubulins. Phosphorylation within those regions were shown to reduce the MT binding capacity of MAPs. Although the proposed main MT binding site of IQD1 is situated in the same C-terminal region as the NoLS is most likely situated, no changes in the MT binding capacity of the IQD1 phospho-mimicry or phospho-mutants were observed. Either the localization of IQD1 is not regulated by phosphorylation or, as suggested for the residing presence of the IQD1 phospho-mimicry mutants within the nucleolus, yet unknown phosphorylations need to take place to regulate the MT binding of IQD1. The low abundance of IQD proteins and the fact that dividing cells are underrepresented when analyzing whole plants for their protein phosphorylation status could lead to a blind eye regarding those phosphosites within the used databases.

Another explanation could be that some phosphorylations have opposing effects than described for other proteins (Wang, Pei, et al. 2007; Mylona et al. 2016) meaning only a specific combination of phosphorylations lead to an absolute change of IQD1 localization. Phosphorylations do not only change the charge of proteins but also can influence their secondary structure. The human prolyl-isomerase Protein Interacting with NIMA (PIN1) specifically targets prolines in TP and SP motifs. It catalyzes the change between the *cis*- and *trans*-isomeration of those prolines which normally is a slow process (Lu and Zhou 2007). Computational analysis suggested that the phosphorylation of prolines within TP and SP motifs lead to a favored  $\alpha$ -helical structure and to a decreased change of the *cis*- or *trans*-conformation (Hamelberg, Shen, and McCammon 2005). Taken into account that the structured regions of IQD1 only contain  $\alpha$ -helices and that most phosphorylations are found outside of those structured regions, one could assume that the phosphorylations might lead to an overall structural change influencing the ability of IQD1 to bind to its interactors or changes its capacity to interact with multiple proteins.

### 4.4. Regulating KLCRs

KLCRs also seem to be phosphorylated by MPKs at the N-terminal end. This region does not seem to be the site for binding of IQD1. The function of human KLCs is regulated via MPK derived phosphorylation at the TPR containing C-terminal part (Vagnoni et al. 2011). KLC1 phospho-mimicry mutants showed a reduced binding towards a specific protein cargo but did

not affect the interaction to several other cargoes. The *in vitro* MPK phosphorylation site of KLCR1 is not situated in the TPR containing region and might therefore not be regulating cargo specificity. If KLCR1 has the same function like KLC1 acting as a kinesin subunit, the phosphorylation in the N-terminal part might regulate its interaction with an unknown kinesin. It could control the association with the KHC regulating the activity of the kinesin. Although we could see a MT association of KLCRs in cells expressing low amounts of GFP- (not shown) or nYFP-tagged KLCRs, we could not observe any movement along cytoskeletal tracks or punctuated structures often seen for active kinesins. The same was true when KLCRs were co-expressed with MPKs. Apparently all KLCR could recruit MPKs to the MT when expressed at low levels. Immunofluorescence co-localization studies of MPK6 and MT (Samajova, Komis, and Samaj 2014) as well as localization studies expressing GFP tagged MPK6 under the endogenous promotor (Dokocilova et al. 2014) did not show any MT association of MPK6. The localization to the MT observed in the BiFC assay is most likely due to the co-recruitment of the bound KLCR via the endogenous IQDs. When comparing the localization of different KLCR:MPK combinations one can see that the KLCR:MPK6 BiFC constructs seem to be less strongly localized to the nucleus than the other combinations. This was also visible in other BiFC experiments conducted with other MPK interacting proteins (Schweighofer et al. 2014). Using GFP-tagged MPKs from *Brassica napus L.* also showed, that comparing to the other *Bna*MPKs, MPK6 seemed generally less present in the nucleus (Liang et al. 2013). Why MPK6 seem to be more prone to reside in the cytosol than other MPKs or whether the GFP is cleaved or is not discussed in the literature.

Taken together this studies provides insights into the hypothesized scaffolding properties of IQD proteins linking  $Ca^{2+}$  signaling with MT functions. The results further imply that the localization and thus the site of IQD function might be regulated via MPK derived phosphorylation and the interaction with its known binding proteins.

## 5. Bibliography

- Abel, S., T. Savchenko, and M. Levy. 2005a. 'Genome-wide comparative analysis of the IQD gene families in *Arabidopsis thaliana* and *Oryza sativa*', *Bmc Evolutionary Biology*, 5.
- . 2005b. 'Genome-wide comparative analysis of the IQD gene families in *Arabidopsis thaliana* and *Oryza sativa*', *Bmc Evolutionary Biology*, 5: 72.
- Ambrose, J. C., and G. O. Wasteneys. 2008. 'CLASP modulates microtubule-cortex interaction during self-organization of acentrosomal microtubules', *Molecular Biology of the Cell*, 19: 4730-7.
- Andersen, J. S., C. E. Lyon, A. H. Fox, A. K. Leung, Y. W. Lam, H. Steen, M. Mann, and A. I. Lamond. 2002. 'Directed proteomic analysis of the human nucleolus', *Current Biology*, 12: 1-11.
- Anderson, J. C., S. Bartels, M. A. Gonzalez Besteiro, B. Shahollari, R. Ulm, and S. C. Peck. 2011. 'Arabidopsis MAP Kinase Phosphatase 1 (AtMKP1) negatively regulates MPK6-mediated PAMP responses and resistance against bacteria', *Plant J*, 67: 258-68.
- Asada, T., R. Kuriyama, and H. Shibaoka. 1997. 'TKRP125, a kinesin-related protein involved in the centrosome-independent organization of the cytokinetic apparatus in tobacco BY-2 cells', *Journal of Cell Science*, 110 ( Pt 2): 179-89.
- Bahler, M., and A. Rhoads. 2002. 'Calmodulin signaling via the IQ motif', *FEBS Lett*, 513: 107-13.
- Bai, Y., L. Dougherty, L. Cheng, G. Y. Zhong, and K. Xu. 2015. 'Uncovering co-expression gene network modules regulating fruit acidity in diverse apples', *Bmc Genomics*, 16: 612.
- Batistic, O., and J. Kudla. 2009. 'Plant calcineurin B-like proteins and their interacting protein kinases', *Biochimica Et Biophysica Acta-Molecular Cell Research*, 1793: 985-92.
- Beck, M., G. Komis, A. Ziemann, D. Menzel, and J. Samaj. 2011. 'Mitogen-activated protein kinase 4 is involved in the regulation of mitotic and cytokinetic microtubule transitions in *Arabidopsis thaliana*', *New Phytologist*, 189: 1069-83.
- Benhamman, R., F. Bai, S. B. Drory, A. Loubert-Hudon, B. Ellis, and D. P. Matton. 2017. 'The Arabidopsis Mitogen-Activated Protein Kinase Kinase Kinase 20 (MKKK20) Acts Upstream of MKK3 and MPK18 in Two Separate Signaling Pathways Involved in Root Microtubule Functions', *Front Plant Sci*, 8: 1352.
- Binarova, P., V. Cenklova, J. Prochazkova, A. Doskocilova, J. Volc, M. Vrlik, and L. Bogre. 2006. 'Gamma-tubulin is essential for acentrosomal microtubule nucleation and coordination of late mitotic events in *Arabidopsis*', *Plant Cell*, 18: 1199-212.
- Bisgrove, S. R., Y. R. J. Lee, B. Liu, N. T. Peters, and D. L. Kropf. 2008. 'The microtubule plus-end binding protein EB1 functions in root responses to touch and gravity signals in *Arabidopsis*', *Plant Cell*, 20: 396-410.
- Bose, J., Pottosin, II, S. S. Shabala, M. G. Palmgren, and S. Shabala. 2011. 'Calcium efflux systems in stress signaling and adaptation in plants', *Front Plant Sci*, 2: 85.
- Bouche, N., A. Yellin, W. A. Snedden, and H. Fromm. 2005. 'Plant-specific calmodulin-binding proteins', *Annu Rev Plant Biol*, 56: 435-66.
- Briggs, M. W., and D. B. Sacks. 2003. 'IQGAP1 as signal integrator: Ca<sup>2+</sup>, calmodulin, Cdc42 and the cytoskeleton', *FEBS Lett*, 542: 7-11.
- Burstenbinder, K., B. Moller, R. Plotner, G. Stamm, G. Hause, D. Mitra, and S. Abel. 2017. 'The IQD Family of Calmodulin-Binding Proteins Links Calcium Signaling to Microtubules, Membrane Subdomains, and the Nucleus', *Plant Physiology*, 173: 1692-708.
- Burstenbinder, K., T. Savchenko, J. Muller, A. W. Adamson, G. Stamm, R. Kwong, B. J. Zipp, D. C. Dinesh, and S. Abel. 2013. 'Arabidopsis Calmodulin-binding Protein IQ67-



- Domain 1 Localizes to Microtubules and Interacts with Kinesin Light Chain-related Protein-1', *Journal of Biological Chemistry*, 288: 1871-82.
- Cerri, M. R., Q. Wang, P. Stolz, J. Folgmann, L. Frances, K. Katzer, X. Li, A. B. Heckmann, T. L. Wang, J. A. Downie, A. Klingl, F. de Carvalho-Niebel, F. Xie, and M. Parniske. 2017. 'The ERN1 transcription factor gene is a target of the CCaMK/CYCLOPS complex and controls rhizobial infection in *Lotus japonicus*', *New Phytologist*, 215: 323-37.
- Cheng, S. H., M. R. Willmann, H. C. Chen, and J. Sheen. 2002. 'Calcium signaling through protein kinases. The Arabidopsis calcium-dependent protein kinase gene family', *Plant Physiology*, 129: 469-85.
- Cheng, Z., J. F. Li, Y. Niu, X. C. Zhang, O. Z. Woody, Y. Xiong, S. Djonovic, Y. Millet, J. Bush, B. J. McConkey, J. Sheen, and F. M. Ausubel. 2015. 'Pathogen-secreted proteases activate a novel plant immune pathway', *Nature*, 521: 213-6.
- Clevenger, J. P., J. Van Houten, M. Blackwood, G. R. Rodriguez, Y. Jikumaru, Y. Kamiya, M. Kusano, K. Saito, S. Visa, and E. van der Knaap. 2015. 'Network Analyses Reveal Shifts in Transcript Profiles and Metabolites That Accompany the Expression of SUN and an Elongated Tomato Fruit', *Plant Physiology*, 168: 1164-78.
- Cortese, M. S., V. N. Uversky, and A. K. Dunker. 2008. 'Intrinsic disorder in scaffold proteins: getting more from less', *Prog Biophys Mol Biol*, 98: 85-106.
- Cruz, J. R., and S. Moreno Diaz de la Espina. 2009. 'Subnuclear compartmentalization and function of actin and nuclear myosin I in plants', *Chromosoma*, 118: 193-207.
- Day, I. S., V. S. Reddy, G. Shad Ali, and A. S. Reddy. 2002. 'Analysis of EF-hand-containing proteins in Arabidopsis', *Genome Biol*, 3: RESEARCH0056.
- DeLano, W. L. 2009. 'PyMOL molecular viewer: Updates and refinements', *Abstracts of Papers of the American Chemical Society*, 238.
- Doherty, C. J., H. A. Van Buskirk, S. J. Myers, and M. F. Thomashow. 2009. 'Roles for Arabidopsis CAMTA transcription factors in cold-regulated gene expression and freezing tolerance', *Plant Cell*, 21: 972-84.
- Doskocilova, A., I. Luptovciak, V. Smekalova, and J. Samaj. 2014. 'Fluorescent protein tagging of Arabidopsis MAPKs for in vivo localization studies', *Methods Mol Biol*, 1171: 131-45.
- Dou, J., S. Zhao, X. Lu, N. He, L. Zhang, A. Ali, H. Kuang, and W. Liu. 2018. 'Genetic mapping reveals a candidate gene (CIFS1) for fruit shape in watermelon (*Citrullus lanatus* L.)', *Theor Appl Genet*.
- Drevensek S., Goussot M., Duroc Y., Christodoulidou A., Steyaert S., Schaefer E., Duvernois E., Grandjean O., Vantard M., Bouchez D., Pastuglia M. 2012. 'The Arabidopsis TRM1-TON1 Interaction Reveals a Recruitment Network Common to Plant Cortical Microtubule Arrays and Eukaryotic Centrosomes', *The Plant Cell*, 24: 178-91.
- Durek, P., R. Schmidt, J. L. Heazlewood, A. Jones, D. MacLean, A. Nagel, B. Kersten, and W. X. Schulze. 2010. 'PhosPhAt: the Arabidopsis thaliana phosphorylation site database. An update', *Nucleic Acids Res*, 38: D828-34.
- Dyson, M. R., S. P. Shadbolt, K. J. Vincent, R. L. Perera, and J. McCafferty. 2004. 'Production of soluble mammalian proteins in *Escherichia coli*: identification of protein features that correlate with successful expression', *BMC Biotechnol*, 4: 32.
- Evans, N. H., M. R. McAinsh, and A. M. Hetherington. 2001. 'Calcium oscillations in higher plants', *Current Opinion in Plant Biology*, 4: 415-20.
- Feilner, T., C. Hultschig, J. Lee, S. Meyer, R. G. Immink, A. Koenig, A. Possling, H. Seitz, A. Beveridge, D. Scheel, D. J. Cahill, H. Lehrach, J. Kreuzberger, and B. Kersten. 2005. 'High throughput identification of potential Arabidopsis mitogen-activated protein kinases substrates', *Mol Cell Proteomics*, 4: 1558-68.
- Finkler, A., R. Ashery-Padan, and H. Fromm. 2007. 'CAMTAs: calmodulin-binding transcription activators from plants to human', *FEBS Lett*, 581: 3893-8.
- Fusari, C. M., R. Kooke, M. A. Lauxmann, M. G. Annunziata, B. Enke, M. Hoehne, N. Krohn, F. F. M. Becker, A. Schlereth, R. Sulpice, M. Stitt, and J. J. B. Keurentjes. 2017.

- 'Genome-Wide Association Mapping Reveals That Specific and Pleiotropic Regulatory Mechanisms Fine-Tune Central Metabolism and Growth in Arabidopsis', *Plant Cell*, 29: 2349-73.
- Galon, Y., R. Nave, J. M. Boyce, D. Nachmias, M. R. Knight, and H. Fromm. 2008. 'Calmodulin-binding transcription activator (CAMTA) 3 mediates biotic defense responses in Arabidopsis', *FEBS Lett*, 582: 943-8.
- Galva, C., V. Kirik, J. J. Lindeboom, D. Kaloriti, D. M. Rancour, P. J. Hussey, S. Y. Bednarek, D. W. Ehrhardt, and J. C. Sedbrook. 2014. 'The Microtubule Plus-End Tracking Proteins SPR1 and EB1b Interact to Maintain Polar Cell Elongation and Directional Organ Growth in Arabidopsis', *Plant Cell*.
- Gao, X., K. L. Cox, Jr., and P. He. 2014. 'Functions of Calcium-Dependent Protein Kinases in Plant Innate Immunity', *Plants (Basel)*, 3: 160-76.
- Gao, Y., Y. Zhang, D. Zhang, X. Dai, M. Estelle, and Y. Zhao. 2015. 'Auxin binding protein 1 (ABP1) is not required for either auxin signaling or Arabidopsis development', *Proc Natl Acad Sci U S A*, 112: 2275-80.
- Gehl, C., R. Waadt, J. Kudla, R. R. Mendel, and R. Hansch. 2009. 'New GATEWAY vectors for high throughput analyses of protein-protein interactions by bimolecular fluorescence complementation', *Molecular Plant*, 2: 1051-8.
- Goldberg, M. W. 2013. 'Nucleoskeleton in Plants: The Functional Organization of Filaments in the Nucleus, in Annual Plant Reviews: Plant Nuclear Structure, Genome Architecture and Gene Regulation, Volume 46', *Annual Plant Reviews: Plant Nuclear Structure, Genome Architecture and Gene Regulation, Volume 46*.
- Gonzalez Besteiro, M. A., and R. Ulm. 2013. 'Phosphorylation and stabilization of Arabidopsis MAP kinase phosphatase 1 in response to UV-B stress', *Journal of Biological Chemistry*, 288: 480-6.
- Hamant, O. 2013. 'Integrative cell biology: katanin at the crossroads', *Current Biology*, 23: R206-8.
- Hamelberg, D., T. Shen, and J. A. McCammon. 2005. 'Phosphorylation effects on cis/trans isomerization and the backbone conformation of serine-proline motifs: accelerated molecular dynamics analysis', *J Am Chem Soc*, 127: 1969-74.
- Hartley, J. L., G. F. Temple, and M. A. Brasch. 2000. 'DNA cloning using in vitro site-specific recombination', *Genome Research*, 10: 1788-95.
- Hashimoto, T. 2013. 'A ring for all: gamma-tubulin-containing nucleation complexes in acentrosomal plant microtubule arrays', *Current Opinion in Plant Biology*, 16: 698-703.
- . 2015. 'Microtubules in plants', *Arabidopsis Book*, 13: e0179.
- Hoeflich, K. P., and M. Ikura. 2002. 'Calmodulin in action: diversity in target recognition and activation mechanisms', *Cell*, 108: 739-42.
- Houdusse, A., J. F. Gaucher, E. Kremontsova, S. Mui, K. M. Trybus, and C. Cohen. 2006. 'Crystal structure of apo-calmodulin bound to the first two IQ motifs of myosin V reveals essential recognition features', *Proc Natl Acad Sci U S A*, 103: 19326-31.
- Jang, D. J., B. Ban, and J. A. Lee. 2011. 'Characterization of novel calmodulin binding domains within IQ motifs of IQGAP1', *Mol Cells*, 32: 511-8.
- Karimi, M., D. Inze, and A. Depicker. 2002. 'GATEWAY vectors for Agrobacterium-mediated plant transformation', *Trends Plant Sci*, 7: 193-5.
- Kelley, L. A., S. Mezulis, C. M. Yates, M. N. Wass, and M. J. Sternberg. 2015. 'The Phyre2 web portal for protein modeling, prediction and analysis', *Nat Protoc*, 10: 845-58.
- Kerppola, T. K. 2008. 'Bimolecular fluorescence complementation (BiFC) analysis as a probe of protein interactions in living cells', *Annu Rev Biophys*, 37: 465-87.
- Komaki, S., T. Abe, S. Coutuer, D. Inze, E. Russinova, and T. Hashimoto. 2010. 'Nuclear-localized subtype of end-binding 1 protein regulates spindle organization in Arabidopsis', *Journal of Cell Science*, 123: 451-9.
- Komis, G., P. Illes, M. Beck, and J. Samaj. 2011. 'Microtubules and mitogen-activated protein kinase signalling', *Current Opinion in Plant Biology*, 14: 650-7.

- Kos, M., B. Houshyani, R. Wietsma, P. Kabouw, L. E. Vet, J. J. van Loon, and M. Dicke. 2012. 'Effects of glucosinolates on a generalist and specialist leaf-chewing herbivore and an associated parasitoid', *Phytochemistry*, 77: 162-70.
- Kozlowski, L. P., and J. M. Bujnicki. 2012. 'MetaDisorder: a meta-server for the prediction of intrinsic disorder in proteins', *Bmc Bioinformatics*, 13: 111.
- Krieger, E., K. Joo, J. Lee, J. Lee, S. Raman, J. Thompson, M. Tyka, D. Baker, and K. Karplus. 2009. 'Improving physical realism, stereochemistry, and side-chain accuracy in homology modeling: Four approaches that performed well in CASP8', *Proteins*, 77 Suppl 9: 114-22.
- Krieger, E., and G. Vriend. 2014. 'YASARA View - molecular graphics for all devices - from smartphones to workstations', *Bioinformatics*, 30: 2981-2.
- Lansky, Z., M. Braun, A. Ludecke, M. Schlierf, P. R. Ten Wolde, M. E. Janson, and S. Diez. 2015. 'Diffusible Crosslinkers Generate Directed Forces in Microtubule Networks', *Cell*.
- Lee, J., J. J. Rudd, V. K. Macioszek, and D. Scheel. 2004. 'Dynamic changes in the localization of MAPK cascade components controlling pathogenesis-related (PR) gene expression during innate immunity in parsley', *Journal of Biological Chemistry*, 279: 22440-8.
- Lee, K., E. H. Song, H. S. Kim, J. H. Yoo, H. J. Han, M. S. Jung, S. M. Lee, K. E. Kim, M. C. Kim, M. J. Cho, and W. S. Chung. 2008. 'Regulation of MAPK phosphatase 1 (AtMKP1) by calmodulin in Arabidopsis', *Journal of Biological Chemistry*, 283: 23581-8.
- Lee, Y. R., H. M. Giang, and B. Liu. 2001. 'A novel plant kinesin-related protein specifically associates with the phragmoplast organelles', *Plant Cell*, 13: 2427-39.
- Lee, Y. R., W. Qiu, and B. Liu. 2015. 'Kinesin motors in plants: from subcellular dynamics to motility regulation', *Current Opinion in Plant Biology*, 28: 120-6.
- Lei, L., S. D. Li, J. Du, L. Bashline, and Y. Gu. 2013. 'CELLULOSE SYNTHASE INTERACTIVE3 Regulates Cellulose Biosynthesis in Both a Microtubule-Dependent and Microtubule-Independent Manner in Arabidopsis', *Plant Cell*, 25: 4912-23.
- Levy, M., Q. Wang, R. Kaspi, M. P. Parrella, and S. Abel. 2005. 'Arabidopsis IQD1, a novel calmodulin-binding nuclear protein, stimulates glucosinolate accumulation and plant defense', *Plant J*, 43: 79-96.
- Li, W., T. Miki, T. Watanabe, M. Kakeno, I. Sugiyama, K. Kaibuchi, and G. Goshima. 2011. 'EB1 promotes microtubule dynamics by recruiting Sentin in Drosophila cells', *J Cell Biol*, 193: 973-83.
- Liang, W., B. Yang, B. J. Yu, Z. Zhou, C. Li, M. Jia, Y. Sun, Y. Zhang, F. Wu, H. Zhang, B. Wang, M. K. Deyholos, and Y. Q. Jiang. 2013. 'Identification and analysis of MKK and MPK gene families in canola (*Brassica napus* L.)', *Bmc Genomics*, 14: 392.
- Lin, D., L. Cao, Z. Zhou, L. Zhu, D. Ehrhardt, Z. Yang, and Y. Fu. 2013. 'Rho GTPase signaling activates microtubule severing to promote microtubule ordering in Arabidopsis', *Current Biology*, 23: 290-7.
- Liu, J., H. J. Whalley, and M. R. Knight. 2015. 'Combining modelling and experimental approaches to explain how calcium signatures are decoded by calmodulin-binding transcription activators (CAMTAs) to produce specific gene expression responses', *New Phytologist*, 208: 174-87.
- Liu, T., J. Tian, G. Wang, Y. Yu, C. Wang, Y. Ma, X. Zhang, G. Xia, B. Liu, and Z. Kong. 2014. 'Augmin triggers microtubule-dependent microtubule nucleation in interphase plant cells', *Current Biology*, 24: 2708-13.
- Liu, Z. 2016. 'Going off the rails? Guidance of the cellulose synthase complex by cortical microtubules in Arabidopsis', *PhD thesis*.
- Liu, Z., R. Schneider, C. Kesten, Y. Zhang, M. Somssich, Y. Zhang, A. R. Fernie, and S. Persson. 2016. 'Cellulose-Microtubule Uncoupling Proteins Prevent Lateral Displacement of Microtubules during Cellulose Synthesis in Arabidopsis', *Developmental Cell*, 38: 305-15.

- Lu, K. P., and X. Z. Zhou. 2007. 'The prolyl isomerase PIN1: a pivotal new twist in phosphorylation signalling and disease', *Nat Rev Mol Cell Biol*, 8: 904-16.
- Luan, S. 2009. 'The CBL-CIPK network in plant calcium signaling', *Trends Plant Sci*, 14: 37-42.
- Majovsky, P., C. Naumann, C. W. Lee, I. Lassowskat, M. Trujillo, N. Dissmeyer, and W. Hoehenwarter. 2014. 'Targeted proteomics analysis of protein degradation in plant signaling on an LTQ-Orbitrap mass spectrometer', *J Proteome Res*, 13: 4246-58.
- Martin, R. M., G. Ter-Avetisyan, H. D. Herce, A. K. Ludwig, G. Lattig-Tunnemann, and M. C. Cardoso. 2015. 'Principles of protein targeting to the nucleolus', *Nucleus*, 6: 314-25.
- Marx, A., A. Hoenger, and E. Mandelkow. 2009. 'Structures of kinesin motor proteins', *Cell Motil Cytoskeleton*, 66: 958-66.
- Matthies, H. J., R. J. Miller, and H. C. Palfrey. 1993. 'Calmodulin binding to and cAMP-dependent phosphorylation of kinesin light chains modulate kinesin ATPase activity', *Journal of Biological Chemistry*, 268: 11176-87.
- Mayer, U., and G. Jurgens. 2002. 'Microtubule cytoskeleton: a track record', *Current Opinion in Plant Biology*, 5: 494-501.
- Meng, X., and S. Zhang. 2013. 'MAPK cascades in plant disease resistance signaling', *Annu Rev Phytopathol*, 51: 245-66.
- Moller, B. K., C. A. Ten Hove, D. Xiang, N. Williams, L. G. Lopez, S. Yoshida, M. Smit, R. Datla, and D. Weijers. 2017. 'Auxin response cell-autonomously controls ground tissue initiation in the early Arabidopsis embryo', *Proc Natl Acad Sci U S A*, 114: E2533-E39.
- Mori, I. C., and J. I. Schroeder. 2004. 'Reactive oxygen species activation of plant Ca<sup>2+</sup> channels. A signaling mechanism in polar growth, hormone transduction, stress signaling, and hypothetically mechanotransduction', *Plant Physiology*, 135: 702-8.
- Moschou, P. N., E. Gutierrez-Beltran, P. V. Bozhkov, and A. Smertenko. 2016. 'Separase Promotes Microtubule Polymerization by Activating CENP-E-Related Kinesin Kin7', *Developmental Cell*, 37: 350-61.
- Moustafa, K., S. AbuQamar, M. Jarrar, A. J. Al-Rajab, and J. Tremouillaux-Guiller. 2014. 'MAPK cascades and major abiotic stresses', *Plant Cell Reports*, 33: 1217-25.
- Mukhtar, M. S., A. R. Carvunis, M. Dreze, P. Eppele, J. Steinbrenner, J. Moore, M. Tasan, M. Galli, T. Hao, M. T. Nishimura, S. J. Pevzner, S. E. Donovan, L. Ghamsari, B. Santhanam, V. Romero, M. M. Poulin, F. Gebreab, B. J. Gutierrez, S. Tam, D. Monachello, M. Boxem, C. J. Harbort, N. McDonald, L. T. Gai, H. M. Chen, Y. J. He, J. Vandenhoute, F. P. Roth, D. E. Hill, J. R. Ecker, M. Vidal, J. Beynon, P. Braun, J. L. Dangl, and Conso European Union Effectoromics. 2011. 'Independently Evolved Virulence Effectors Converge onto Hubs in a Plant Immune System Network', *Science*, 333: 596-601.
- Mylona, A., F. X. Theillet, C. Foster, T. M. Cheng, F. Miralles, P. A. Bates, P. Selenko, and R. Treisman. 2016. 'Opposing effects of Elk-1 multisite phosphorylation shape its response to ERK activation', *Science*, 354: 233-37.
- Nakagawa, T., T. Suzuki, S. Murata, S. Nakamura, T. Hino, K. Maeo, R. Tabata, T. Kawai, K. Tanaka, Y. Niwa, Y. Watanabe, K. Nakamura, T. Kimura, and S. Ishiguro. 2007. 'Improved Gateway binary vectors: high-performance vectors for creation of fusion constructs in transgenic analysis of plants', *Biosci Biotechnol Biochem*, 71: 2095-100.
- Oda, Y., and H. Fukuda. 2013. 'Rho of plant GTPase signaling regulates the behavior of Arabidopsis kinesin-13A to establish secondary cell wall patterns', *Plant Cell*, 25: 4439-50.
- Oppenheimer, D. G., M. A. Pollock, J. Vacik, D. B. Szymanski, B. Ericson, K. Feldmann, and M. D. Marks. 1997. 'Essential role of a kinesin-like protein in Arabidopsis trichome morphogenesis', *Proc Natl Acad Sci U S A*, 94: 6261-6.
- Pan, Y., X. Liang, M. Gao, H. Liu, H. Meng, Y. Weng, and Z. Cheng. 2017. 'Round fruit shape in WI7239 cucumber is controlled by two interacting quantitative trait loci with one putatively encoding a tomato SUN homolog', *Theor Appl Genet*, 130: 573-86.

- Pandey, N., A. Ranjan, P. Pant, R. K. Tripathi, F. Ateek, H. P. Pandey, U. V. Patre, and S. V. Sawant. 2013. 'CAMTA 1 regulates drought responses in *Arabidopsis thaliana*', *Bmc Genomics*, 14: 216.
- Park, C. Y., J. H. Lee, J. H. Yoo, B. C. Moon, M. S. Choi, Y. H. Kang, S. M. Lee, H. S. Kim, K. Y. Kang, W. S. Chung, C. O. Lim, and M. J. Cho. 2005. 'WRKY group IId transcription factors interact with calmodulin', *FEBS Lett*, 579: 1545-50.
- Pederson, T., and R. Y. Tsai. 2009. 'In search of nonribosomal nucleolar protein function and regulation', *J Cell Biol*, 184: 771-6.
- Perochon, A., D. Aldon, J. P. Galaud, and B. Ranty. 2011. 'Calmodulin and calmodulin-like proteins in plant calcium signaling', *Biochimie*, 93: 2048-53.
- Petzold, H. E., S. B. Rigoulot, C. Zhao, B. Chanda, X. Sheng, M. Zhao, X. Jia, A. W. Dickerman, E. P. Beers, and A. M. Brunner. 2017. 'Identification of new protein-protein and protein-DNA interactions linked with wood formation in *Populus trichocarpa*', *Tree Physiol*: 1-16.
- Prabakaran, S., G. Lippens, H. Steen, and J. Gunawardena. 2012. 'Post-translational modification: nature's escape from genetic imprisonment and the basis for dynamic information encoding', *Wiley Interdiscip Rev Syst Biol Med*, 4: 565-83.
- Pringle, J., A. Muthukumar, A. Tan, L. Crankshaw, L. Conway, and J. L. Ross. 2013. 'Microtubule organization by kinesin motors and microtubule crosslinking protein MAP65', *J Phys Condens Matter*, 25: 374103.
- R. A. Laskowski, M. W. MacArthur, D. S. Moss and J. M. Thornton. 1993. 'PROCHECK: a program to check the stereochemical quality of protein structures', *J. Appl. Cryst.*, 26: 283-91.
- Reddy, A. S., A. Ben-Hur, and I. S. Day. 2011. 'Experimental and computational approaches for the study of calmodulin interactions', *Phytochemistry*, 72: 1007-19.
- Reddy, A. S., and I. S. Day. 2001. 'Kinesins in the *Arabidopsis* genome: a comparative analysis among eukaryotes', *Bmc Genomics*, 2: 2.
- Reddy, A. S., S. B. Narasimhulu, F. Safadi, and M. Golovkin. 1996. 'A plant kinesin heavy chain-like protein is a calmodulin-binding protein', *Plant J*, 10: 9-21.
- Reddy, V. S., G. S. Ali, and A. S. Reddy. 2002. 'Genes encoding calmodulin-binding proteins in the *Arabidopsis* genome', *Journal of Biological Chemistry*, 277: 9840-52.
- Reddy, V. S., I. S. Day, T. Thomas, and A. S. Reddy. 2004. 'KIC, a novel Ca<sup>2+</sup> binding protein with one EF-hand motif, interacts with a microtubule motor protein and regulates trichome morphogenesis', *Plant Cell*, 16: 185-200.
- 'Retraction: "An enhanced transient expression system in plants based on suppression of gene silencing by the p19 protein of tomato bushy stunt virus"'. 2015. *Plant J*, 84: 846.
- Rigden, D. J., and M. Y. Galperin. 2004. 'The DxDxDG motif for calcium binding: multiple structural contexts and implications for evolution', *Journal of Molecular Biology*, 343: 971-84.
- Rodriguez, M. C., M. Petersen, and J. Mundy. 2010. 'Mitogen-activated protein kinase signaling in plants', *Annu Rev Plant Biol*, 61: 621-49.
- Rogers, G. C., C. L. Hart, K. P. Wedaman, and J. M. Scholey. 1999. 'Identification of kinesin-C, a calmodulin-binding carboxy-terminal kinesin in animal (*Strongylocentrotus purpuratus*) cells', *Journal of Molecular Biology*, 294: 1-8.
- Samajova, O., G. Komis, and J. Samaj. 2014. 'Immunofluorescent localization of MAPKs and colocalization with microtubules in *Arabidopsis* seedling whole-mount probes', *Methods Mol Biol*, 1171: 107-15.
- Schweighofer, A., V. Shubchynskyy, V. Kazanaviciute, A. Djamei, and I. Meskiene. 2014. 'Bimolecular fluorescent complementation (BiFC) by MAP kinases and MAPK phosphatases', *Methods Mol Biol*, 1171: 147-58.
- Scott, M. S., F. M. Boisvert, M. D. McDowall, A. I. Lamond, and G. J. Barton. 2010. 'Characterization and prediction of protein nucleolar localization sequences', *Nucleic Acids Res*, 38: 7388-99.

- Sippl, M. J. 1990. 'Calculation of conformational ensembles from potentials of mean force. An approach to the knowledge-based prediction of local structures in globular proteins', *Journal of Molecular Biology*, 213: 859-83.
- . 1993. 'Recognition of errors in three-dimensional structures of proteins', *Proteins*, 17: 355-62.
- Smedler, E., and P. Uhlen. 2014. 'Frequency decoding of calcium oscillations', *Biochimica Et Biophysica Acta-General Subjects*, 1840: 964-69.
- Smith, J. M., A. C. Hedman, and D. B. Sacks. 2015. 'IQGAPs choreograph cellular signaling from the membrane to the nucleus', *Trends Cell Biol*, 25: 171-84.
- Stepinski, D. 2014. 'Functional ultrastructure of the plant nucleolus', *Protoplasma*, 251: 1285-306.
- Stern, H., F. B. Johnston, and G. Setterfield. 1959. 'Some chemical properties of isolated pea nucleoli', *J Biophys Biochem Cytol*, 6: 57-60.
- Stewart, J. L., and J. L. Nemhauser. 2010. 'Do trees grow on money? Auxin as the currency of the cellular economy', *Cold Spring Harb Perspect Biol*, 2: a001420.
- Sugiyama, Y., M. Wakazaki, K. Toyooka, H. Fukuda, and Y. Oda. 2017. 'A Novel Plasma Membrane-Anchored Protein Regulates Xylem Cell-Wall Deposition through Microtubule-Dependent Lateral Inhibition of Rho GTPase Domains', *Current Biology*, 27: 2522-28 e4.
- Sui, H., and K. H. Downing. 2010. 'Structural basis of interprotofilament interaction and lateral deformation of microtubules', *Structure*, 18: 1022-31.
- Szymanski, D. B., and D. J. Cosgrove. 2009. 'Dynamic coordination of cytoskeletal and cell wall systems during plant cell morphogenesis', *Current Biology*, 19: R800-11.
- Takahashi, F., T. Mizoguchi, R. Yoshida, K. Ichimura, and K. Shinozaki. 2011. 'Calmodulin-dependent activation of MAP kinase for ROS homeostasis in Arabidopsis', *Mol Cell*, 41: 649-60.
- Thiry, M., and D. L. Lafontaine. 2005. 'Birth of a nucleolus: the evolution of nucleolar compartments', *Trends Cell Biol*, 15: 194-9.
- Tian, J., L. Han, Z. Feng, G. Wang, W. Liu, Y. Ma, Y. Yu, and Z. Kong. 2015. 'Orchestration of microtubules and the actin cytoskeleton in trichome cell shape determination by a plant-unique kinesin', *Elife*, 4.
- Tulin, A., S. McClerkin, Y. Huang, and R. Dixit. 2012. 'Single-molecule analysis of the microtubule cross-linking protein MAP65-1 reveals a molecular mechanism for contact-angle-dependent microtubule bundling', *Biophysical Journal*, 102: 802-9.
- Tuteja, N., and S. Mahajan. 2007. 'Calcium signaling network in plants: an overview', *Plant Signal Behav*, 2: 79-85.
- Vagnoni, A., L. Rodriguez, C. Manser, K. J. De Vos, and C. C. Miller. 2011. 'Phosphorylation of kinesin light chain 1 at serine 460 modulates binding and trafficking of calyculin-1', *Journal of Cell Science*, 124: 1032-42.
- Van Damme, D., K. Van Poucke, E. Boutant, C. Ritzenhaller, D. Inze, and D. Geelen. 2004. 'In vivo dynamics and differential microtubule-binding activities of MAP65 proteins', *Plant Physiology*, 136: 3956-67.
- Van Damme, D., M. Vanstraelen, and D. Geelen. 2007. 'Cortical division zone establishment in plant cells', *Trends Plant Sci*, 12: 458-64.
- Vinogradova, M. V., G. G. Malanina, J. S. Waitzman, S. E. Rice, and R. J. Fletcher. 2013. 'Plant Kinesin-Like Calmodulin Binding Protein Employs Its Regulatory Domain for Dimerization', *Plos One*, 8: e66669.
- Vos, J. W., F. Safadi, A. S. Reddy, and P. K. Hepler. 2000. 'The kinesin-like calmodulin binding protein is differentially involved in cell division', *Plant Cell*, 12: 979-90.
- Walia, A., J. S. Lee, G. Wasteneys, and B. Ellis. 2009. 'Arabidopsis mitogen-activated protein kinase MPK18 mediates cortical microtubule functions in plant cells', *Plant J*, 59: 565-75.
- Walia, A., M. Nakamura, D. Moss, V. Kirik, T. Hashimoto, and D. W. Ehrhardt. 2014. 'GCP-WD mediates gamma-TuRC recruitment and the geometry of microtubule nucleation in interphase arrays of Arabidopsis', *Current Biology*, 24: 2548-55.

- Walter, W. J., I. Machens, F. Rafieian, and S. Diez. 2015. 'The non-processive rice kinesin-14 OsKCH1 transports actin filaments along microtubules with two distinct velocities', *Nat Plants*, 1: 15111.
- Wang, J. P., J. P. Munyampundu, Y. P. Xu, and X. Z. Cai. 2015. 'Phylogeny of Plant Calcium and Calmodulin-Dependent Protein Kinases (CCaMKs) and Functional Analyses of Tomato CCaMK in Disease Resistance', *Front Plant Sci*, 6: 1075.
- Wang, X. T., D. S. Pei, J. Xu, Q. H. Guan, Y. F. Sun, X. M. Liu, and G. Y. Zhang. 2007. 'Opposing effects of Bad phosphorylation at two distinct sites by Akt1 and JNK1/2 on ischemic brain injury', *Cell Signal*, 19: 1844-56.
- Wang, X., L. Zhu, B. Liu, C. Wang, L. Jin, Q. Zhao, and M. Yuan. 2007. 'Arabidopsis MICROTUBULE-ASSOCIATED PROTEIN18 functions in directional cell growth by destabilizing cortical microtubules', *Plant Cell*, 19: 877-89.
- Wendrich, J.R., B. J. Yang, P. Mijnhout, H.W. Xue, B. De Rybel, and D. Weijers. 2018. 'IQD proteins integrate auxin and calcium signaling to regulate microtubule dynamics during Arabidopsis development', *bioRxiv*.
- Wendrich, Jos R. 2016. 'Stem cell organization in Arabidopsis: from embryos to roots', Thesis Wageningen University, 2016-06-03.
- Wu, S., H. Xiao, A. Cabrera, T. Meulia, and E. van der Knaap. 2011. 'SUN regulates vegetative and reproductive organ shape by changing cell division patterns', *Plant Physiology*, 157: 1175-86.
- Xie, K., J. Chen, Q. Wang, and Y. Yang. 2014. 'Direct phosphorylation and activation of a mitogen-activated protein kinase by a calcium-dependent protein kinase in rice', *Plant Cell*, 26: 3077-89.
- Xu, D., and Y. Zhang. 2012. 'Ab initio protein structure assembly using continuous structure fragments and optimized knowledge-based force field', *Proteins*, 80: 1715-35.
- . 2013. 'Toward optimal fragment generations for ab initio protein structure assembly', *Proteins*, 81: 229-39.
- Xu, J., and S. Zhang. 2015. 'Mitogen-activated protein kinase cascades in signaling plant growth and development', *Trends Plant Sci*, 20: 56-64.
- Yap, K. L., J. Kim, K. Truong, M. Sherman, T. Yuan, and M. Ikura. 2000. 'Calmodulin target database', *J Struct Funct Genomics*, 1: 8-14.
- Yoo, S. D., Y. H. Cho, and J. Sheen. 2007. 'Arabidopsis mesophyll protoplasts: a versatile cell system for transient gene expression analysis', *Nat Protoc*, 2: 1565-72.
- Zeytuni, N., and R. Zarivach. 2012. 'Structural and functional discussion of the tetra-trico-peptide repeat, a protein interaction module', *Structure*, 20: 397-405.
- Zhou, Y., S. Yang, T. Mao, and Z. Zhang. 2015. 'MAPanalyzer: a novel online tool for analyzing microtubule-associated proteins', *Database (Oxford)*, 2015.

## 6. Supplements

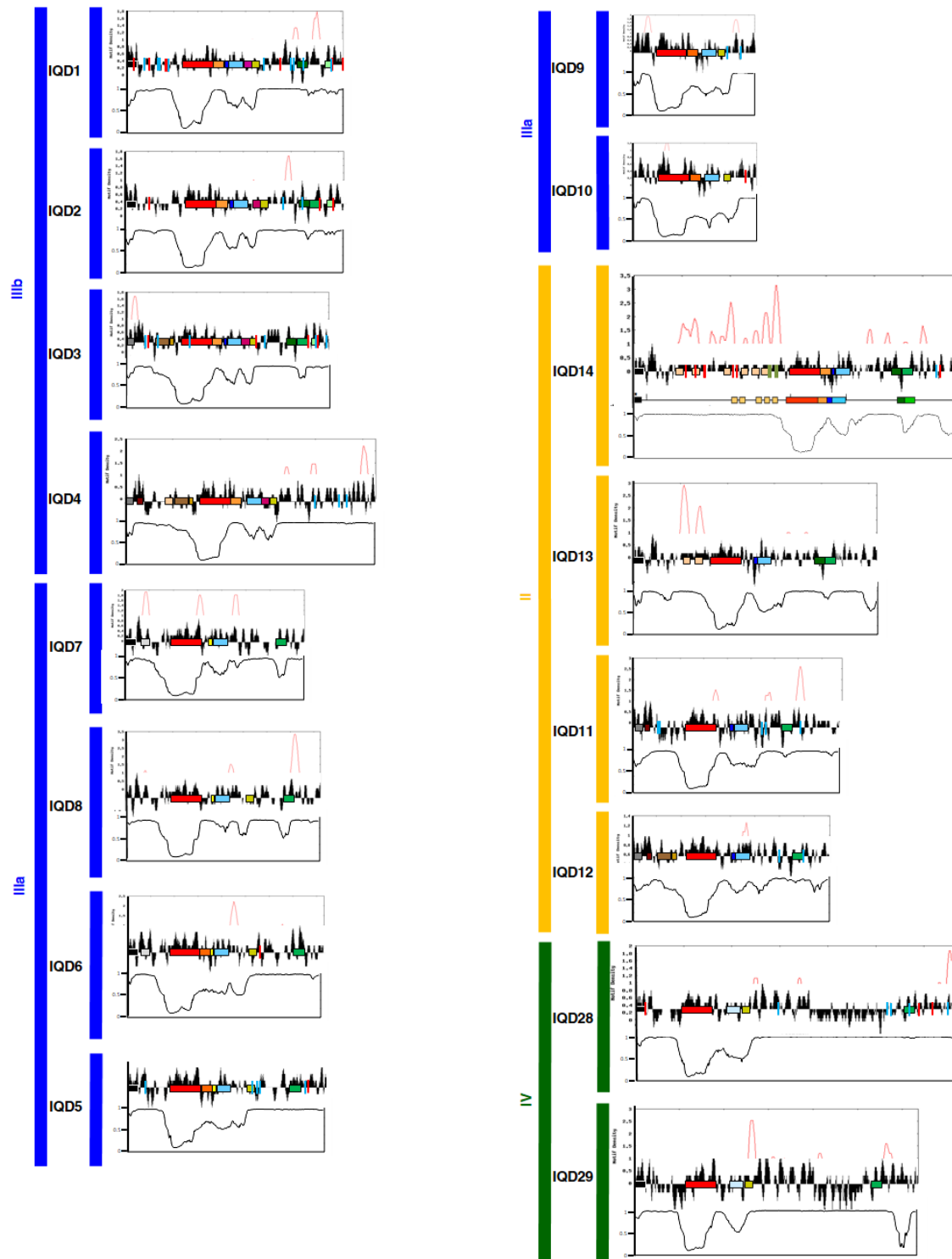


Figure S1: For description see following page.



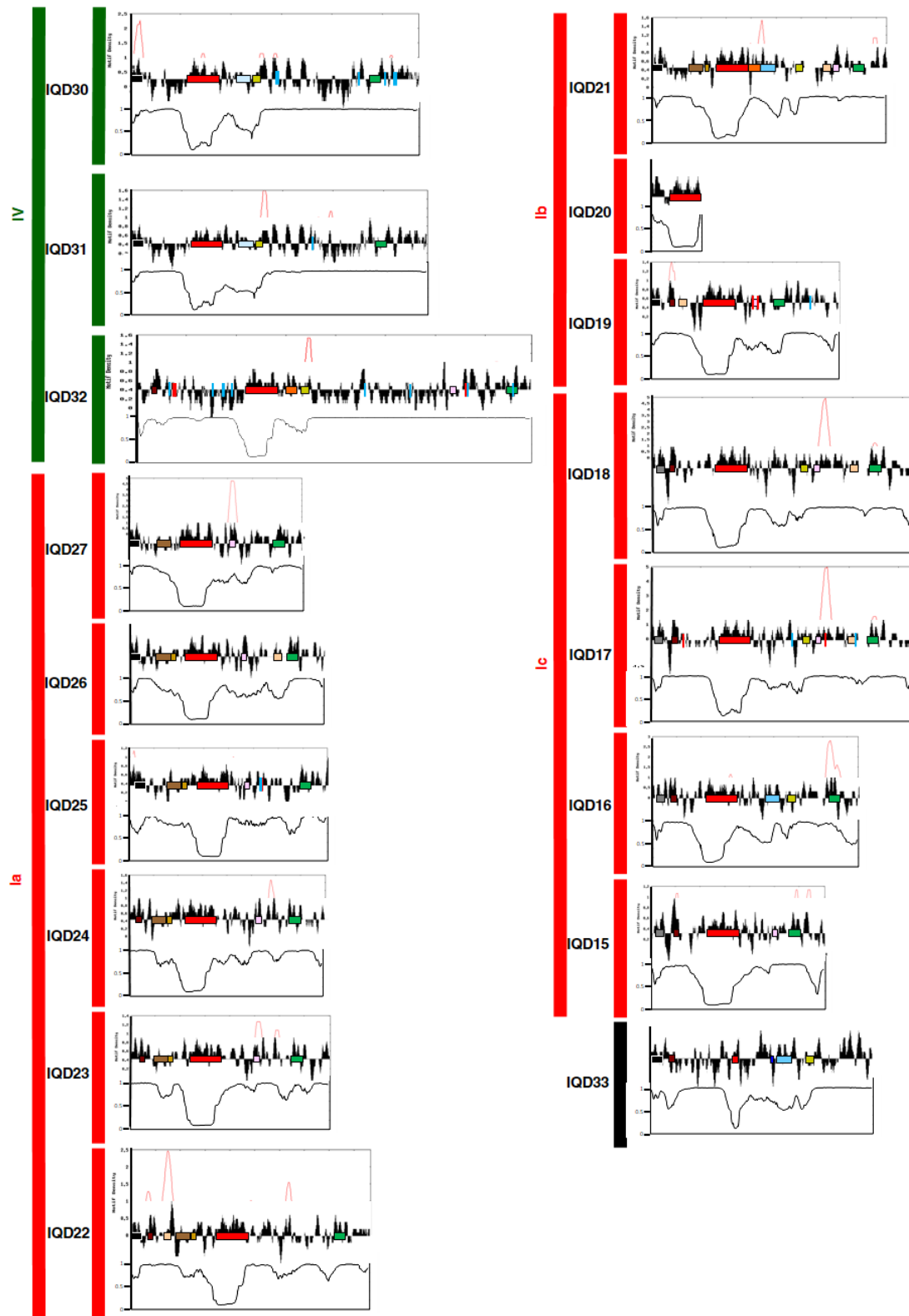
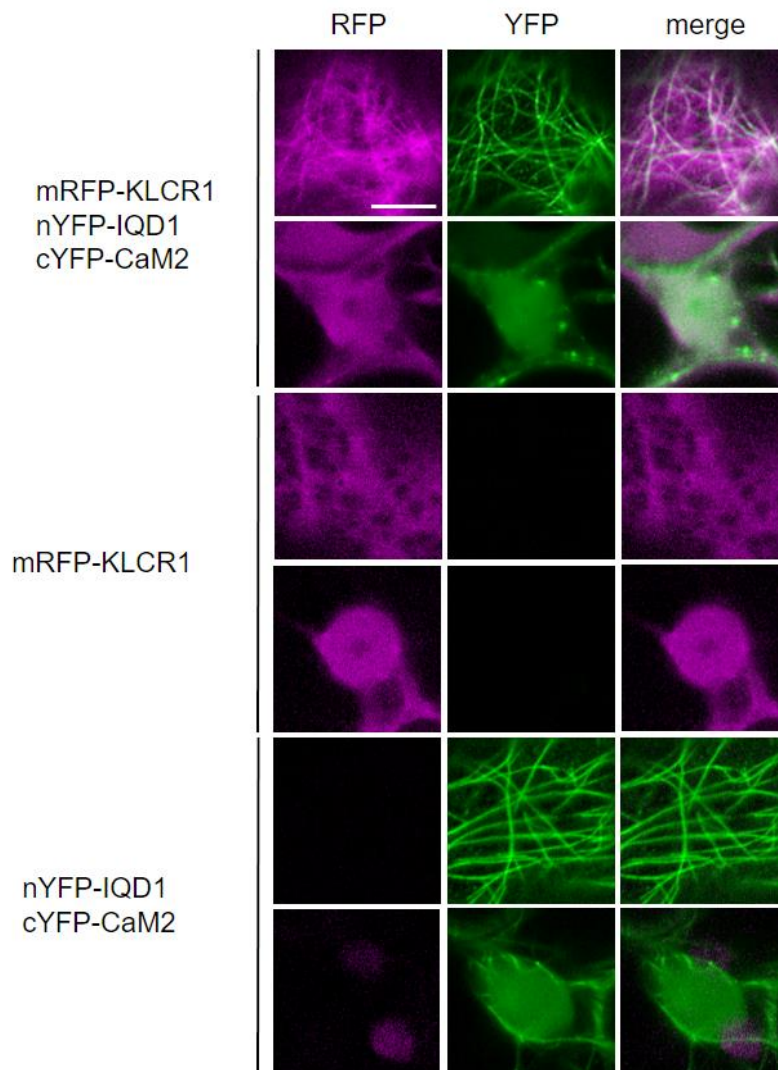


Figure S 1: **Structural features of IQD proteins**

IQD proteins are categorized into their clades. The MT-binding site motif density is shown in the upper red graph, only values over the threshold of 1.0 are shown (Motif density was calculated using MAPanalyzer (Zhou et al. 2015)). The middle graph (black) shows the charges of the protein stretches. The graph was calculated using <http://www.bioinformatics.nl/cgi-bin/emboss/charge> with a window length of 5 aa. In the middle the conserved motifs are shown as colored boxes (see (Abel, Savchenko, and Levy 2005b)), the IQ67 domain is depicted in red. The lower graph shows the probability of intrinsically disordered regions calculated using MetaDisorder (Kozłowski and Bujnicki 2012) and visualized using the “MetaDisorder” output. Values above 0.5 are considered disordered.



**Figure S 2: mRFP-KLCR1 is recruited to the MT by nYFP-IQD1:cYFP-CaM2 complex**

Single optical sections of YFP-signals after bimolecular fluorescent complementation and RFP signals after coexpression with RFP-tagged KLCR1 (upper panel shows the cytosol, the lower picture shows the nucleus). Agrobacterium mediated transient coexpression of IQD1 fused to the N-terminal part of Venus (nYFP) CaM2 fused to the C-terminal part of Venus (cYFP) and RFP-KLCR1 under the control of the 35S promotor in tobacco. Single expression of RFP-KLCR1 and the BiFC constructs are used as controls. Bars = 10µm. Experiment was performed once.

**Experiment was performed by Dr. Katharina Bürstenbinder**

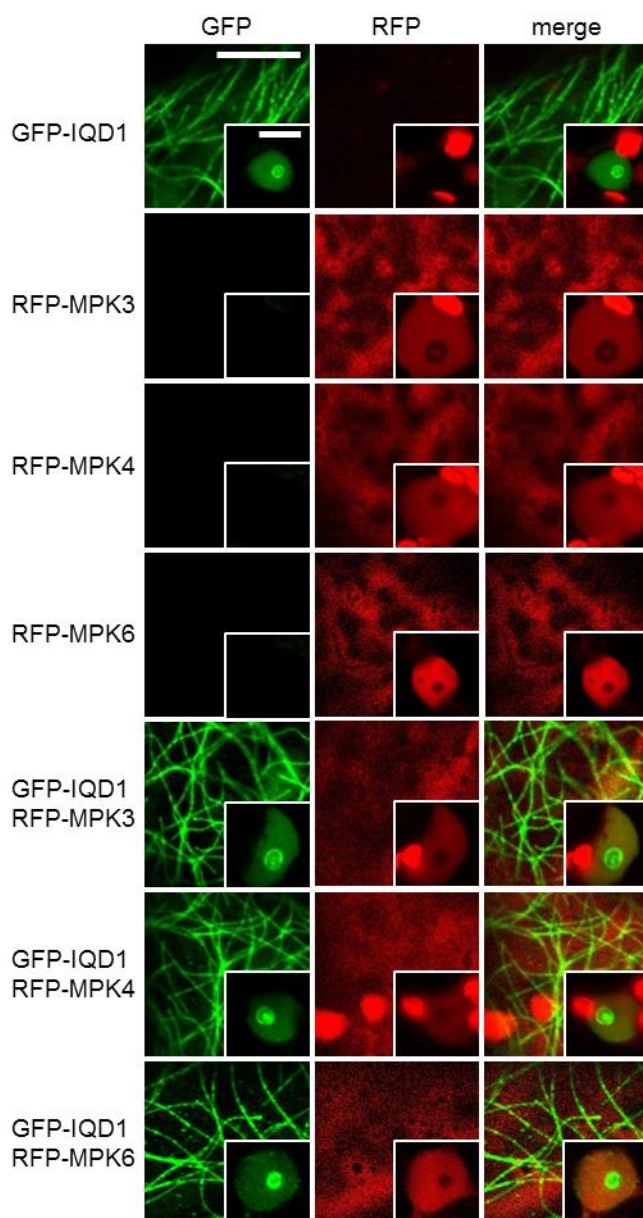


Figure S 3: **IQD1 does not recruit RFP-tagged MPKs to MT.**

Single optical sections of *N. benthamina* pavement cells transiently expressing GFP-IQD1 and RFP-MPKs under the control of the 35S promoter. Big pictures show the cytoplasm, insets show the nucleus. Recruitment of RFP-MPKs to the MT indicates interaction. Bars=10 $\mu$ m. Experiments was performed two times. At least three cells were analyzed per infiltration. Representative images are shown.

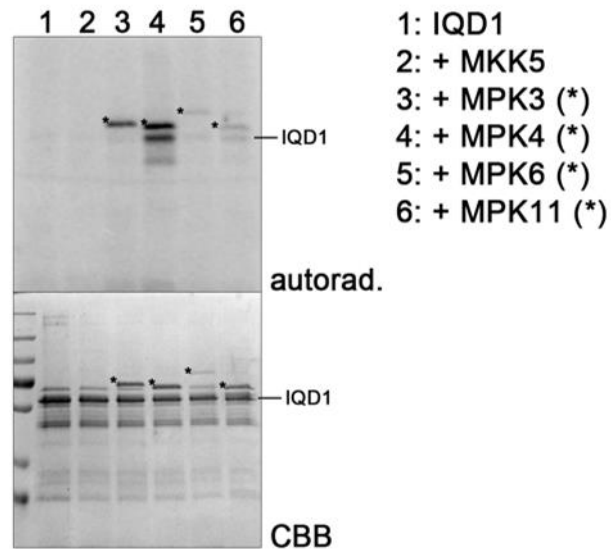


Figure S 4: **IQD1 is phosphorylated by MPKs *in vitro***

*In vitro* phosphorylation assays using recombinantly expressed and purified proteins (A). MPKs were activated using a constantly active MKK5. The active MPKs were incubated with the IQD proteins including  $^{32}\text{P}$ - $\alpha$ -ATP. After 30min proteins were applied to SDS-PAGE. Loading of gel was analyzed by CBB staining. Phosphorylation was visualized using a phosphoimager. Mapping of *in vitro* phosphorylation sites.

**Experiments were performed by Dr. Lennart Eschen-Lippold and Nicole Bauer.**

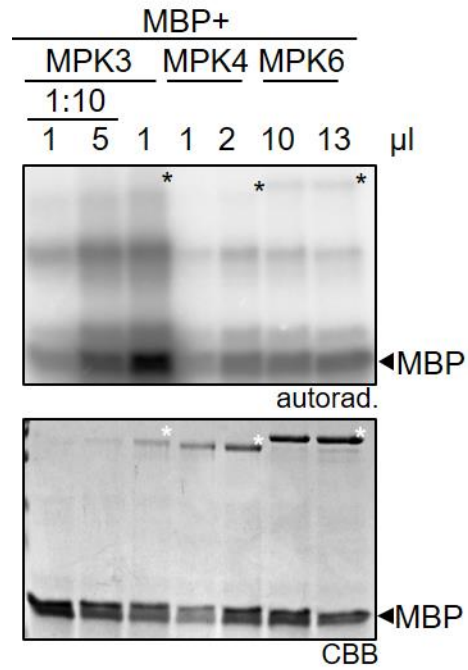


Figure S 5: **MPK activity *in vitro***

Controls for equal MPK activity for *in vitro* MPK phosphorylation assays were performed. The known substrate Myelin Basic Protein (MBP) was incubated with different amounts of activated MPKs. The phosphorylation activity was analyzed by comparing the autoradiography of the different MPKs. For later experiments four μl of 1:10 diluted MPK3, two μl of MPK4 and ten μl of MPK6 were used in the assays. Experiment was performed once.

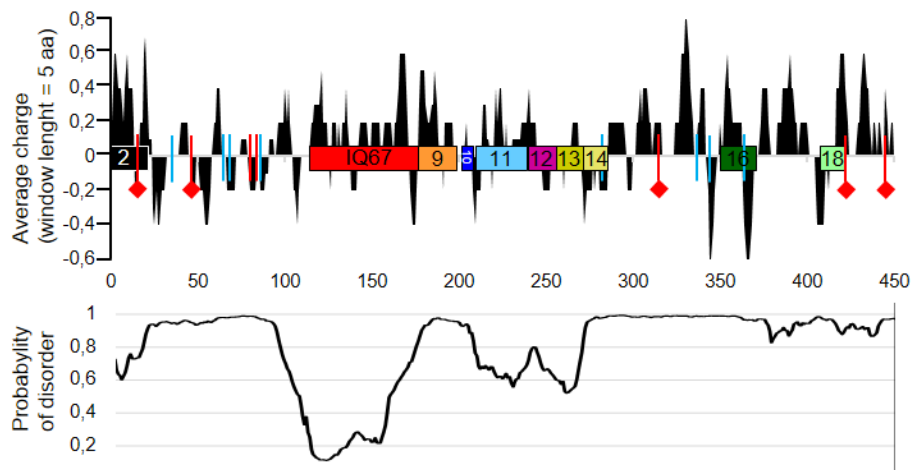


Figure S 6: **Overview of IQD1 features**

Colored boxes indicate position of conserved motifs (Abel, Savchenko, & Levy, 2005). Red lines show position of putative MPK phosphorylation sites (TP/SP). Blue lines show position of phosphorylated aa found in PhosPhAt database excluding MPK sites. Red lines with diamond show *in vitro* phosphorylated aa. Average charge plot indicates stretches of charged residues (<http://www.bioinformatics.nl/cgi-bin/emboss/charge>). Disorder plot shows stretches of ordered (probability < 0.5) and disordered (probability > 0.5) regions (<http://genesilico.pl/metadisorder/>).

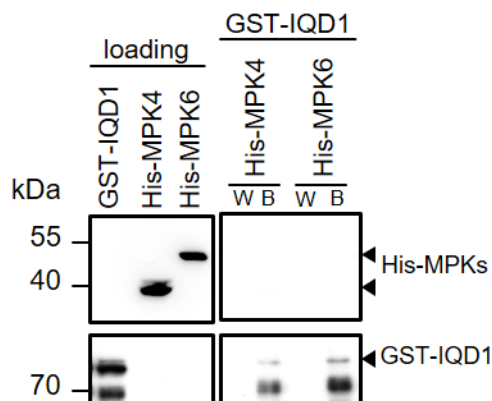


Figure S 7: **IQD1 does not interact with MPKs *in vitro***

To perform the GST-pulldown assay, cleared crude *E. coli* extracts containing GST-tagged IQD1 protein were applied to the glutathione beads. After washing, the crude cleared protein extracts containing His-tagged proteins were added. The beads were again washed three times. The last washing step was used as the washing control (W). Beads and last washing step were boiled in Laemmli buffer and proteins were separated by SDS-PAGE. Detection of proteins was conducted by western blotting using tag-specific antibodies. GST was used as a negative control. Experiment was performed two times showing similar results. A representative image is shown.

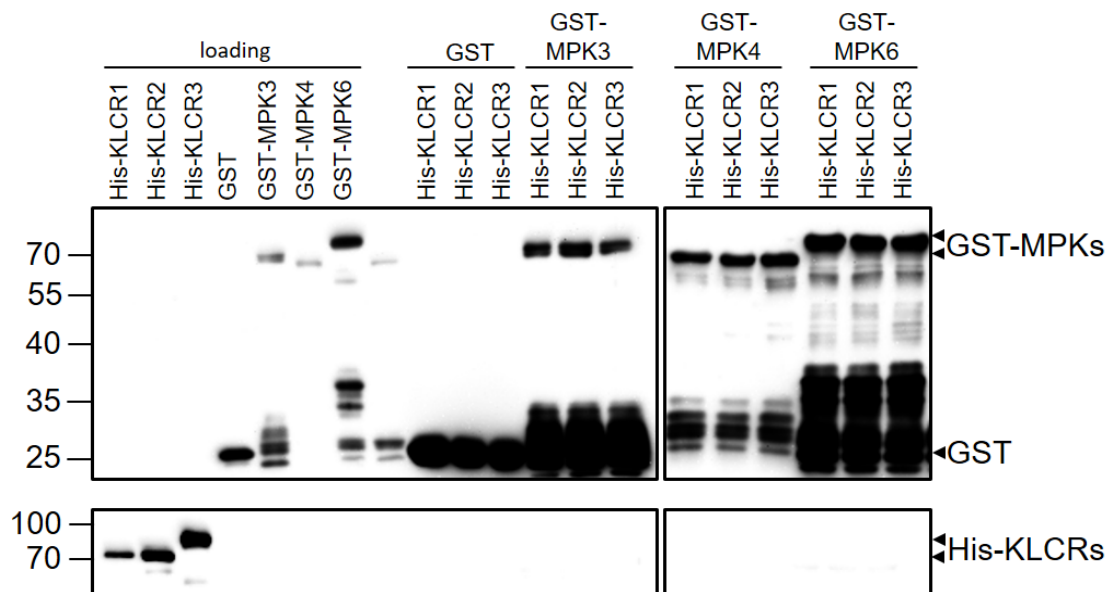


Figure S 8: **KLCRs do not interact with MPKs *in vitro***

GST-pulldown assay was done using containing extracts cleared crude *E. coli* extracts containing GST-tagged proteins that were applied to the glutathione beads. After washing cleared crude *E. coli* extracts containing His-tagged proteins were added. The beads were again washed three times. The beads were boiled in Laemmli buffer and proteins separated by SDS-PAGE. Detection of proteins was conducted by western blotting using tag-specific antibodies. GST was used as a negative control. Experiment was performed once.



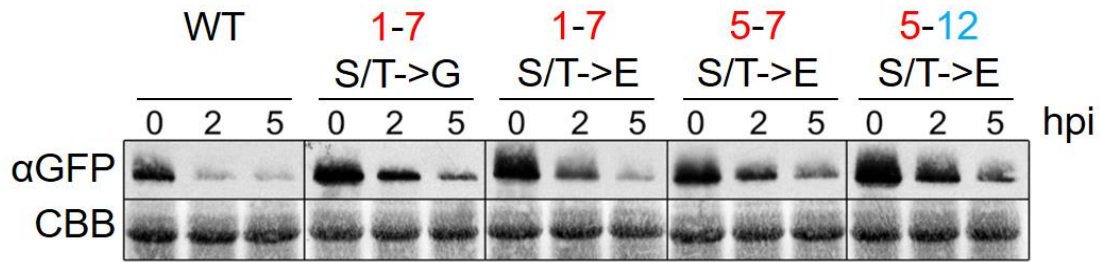


Figure S 9: **Phosphorylation of IQD1 might increase its stability**

Stability was measured in transiently transformed Arabidopsis protoplasts. Cells were treated with five  $\mu$ M cycloheximide. After 2 and 5 h cells were pelleted and boiled in Laemmli-buffer. Protein detection was done using western blotting and a GFP-specific antibody. hpi – hours post induction. For information about the position see table 2. Experiment was performed once.

**Experiments were performed by Dr. Lennart Eschen-Lippolt.**

## 6. Supplements

```

IQD1/1-454      1  . . MVKKAKWLNKVKKAFSPDSKLLKHESVECDSVISYPV . . . . . LIATSRSSSPQFE . . . . . 51
IQD13/1-517    1  . . MGKKGWFSAIKRVFTPHSKEKQLS . NNNQPEPIKSENKEKKGKGFQKGLRN - GETNSFLPIFRQPSSIE 68
IQD16/1-423    1  MAKKNGTSWFTAVKKILWVSPSKDSDKKTTHHKEETDIK . . . . . RKEKKGWIFRKTKLETTNSVLQ . . . . . 59

IQD1/1-454     52  VRVDEVNVEYEQKKNLYPPS . . . . . SDSVTATV . . . . . AHVLDVDSPP . . . . . 86
IQD13/1-517    69  KILSEAEEREHNLVFRPPTPTDRANSSSTSVASPLVRPASPKVPSQRYVSSPKPISPRVAYPQVHYPKPPSPK 140
IQD16/1-423    80  . . . . . HTVRT . . . . . VEAAE . . . . . KEKPPVIV 77

IQD1/1-454     87  . . SPESVHQAIV . . . . . VNRFAKKSKEEAAAII . IQSTFRGHLARRESQVMRGGQERLKLLEGGSVVQRQAAI 151
IQD13/1-517    141  PPSPRAVSPRIVQRREFVHRPEPSLLVKNAYAIKIQAAFQGYMARRSFALKGLVRLQGVVRGHSSVKRQTMN 212
IQD16/1-423    78  S . . . . . SVEEGVT . . . . . EIVKLTATPGFIRRHWAALIIQTAFRGYLSRRALRALKGIVKLGALVRGNMVRNDAKL 143

IQD1/1-454     152  TLKCMQTL . SRVQSQIRSRRIIRMSEEN . . . . . QARHKQLLQKHAKELGGLKNGGNWNYNS . . . . . 205
IQD13/1-517    213  AMKYMQLLVVRVQTQVQSRRIQM . . . . . LENRARNDK . . . . . DDTKLVSRMSDDWDDSV . . . . . 261
IQD16/1-423    144  TLRICIKALVVRVQDQVLNHHQQQRRSRVLLSPPSRNYNIE . . . . . ARNSMFAESNGFWDTKTYLQDIRSRRLSRD 213

IQD1/1-454     206  . . . . . QSKEQVEAGMLHKYEATMRRERALAYAFTHQQNLKSF . SKTANPMFMDPSNPTWGWSWLERWMAGR 270
IQD13/1-517    262  . . . . . LTKEEKDVRLHRKIDAMIKRERSMAYAYSHQLWKNRPKS . . . . . AQDIRTSGFPLWNNWVDRQKNQN 323
IQD16/1-423    214  MNRRCNNEFYSEETELIQKLEIAIKREKAQALALSNGIRSRSRN . . . . . QSAGDRELLERTQWLDLRWMAK 282

IQD1/1-454     271  PWESSEKEQNTT . NNDNSSVKNSTNRNSQGGETAKSSNRNKLNS . . . . . STKPNTPSASSTATRNP . . . . . RPIPS 338
IQD13/1-517    324  Q . . . . . PFRLLTPTRP . SLSLSPQPSSNQ . . . . . HFRLLNSFDTSTFNSSKSTFVTPSRPIHTPQPYSS 380
IQD16/1-423    283  QWDDTITNSTNVRDPIKLTLEAVTTHH . . . . . H . . . . . QRYPATP . . . . . SC . . . . . 320

IQD1/1-454     339  SIKSKSSDDEAKSSERNR . . . . . PS . . . . . IAR . . . . . SVSDETLSSSTARRSSNLIP . . . . . TKSARGKPKSQTSSRVAVTT . . . . . 405
IQD13/1-517    381  SVSRY . . . . . RGGGRATQDSPFKDDD . . . . . SLTSCPPFSAPSYMAPTVSAKAKLRANSNPKERMDRTPVS . . . . . 442
IQD16/1-423    321  . . . . . RASRSVMVRSASPRIPC . . . . . SPS . . . . . SSMQPNYMSATE . . . . . SAKAKARTQSTPRRRPMTAKKRL 374

IQD1/1-454     406  STTEESSI . . . . . LPEKA . . . . . PAKKRLSTSASPAPKRRSSAPPKVEKQVLKAERTP . . . . . 454
IQD13/1-517    443  . . . . . TNEKRRSS . . . . . SFLG . . . . . SFKWNK . . . . . GSLFMS . . . . . NNS . . . . . NNK . . . . . GPGSSSSGAVVLEKHKTLKSVG . . . . . NLSIDSTV . . . . . SMPAT 507
IQD16/1-423    375  CYAEELSLRSPSFKSCLWGDHESDY . . . . . CCYGDGF . . . . . AGKISPCSTTEL . . . . . RWLK . . . . . 423

IQD1/1-454     . . . . .
IQD13/1-517    508  I . . . . . GRRAFNRFA . . . . .
IQD16/1-423    . . . . .

```

Figure S 10: **Alignment of amino acid sequences of IQD1, IQD13 and IQD16**

The red boxes highlight the MT binding sites. For IQD13 data has been retrieved from Sogiyama Y. *et al.*, 2017, for IQD1 the MT binding IQD1-C<sub>327-454</sub>-fragment is highlighted. The blue boxes mark conserved aa. The alignment was performed using clustal omega (<https://www.ebi.ac.uk/Tools/msa/clustalo/>), data was visualized using jalview (<http://www.jalview.org/>)

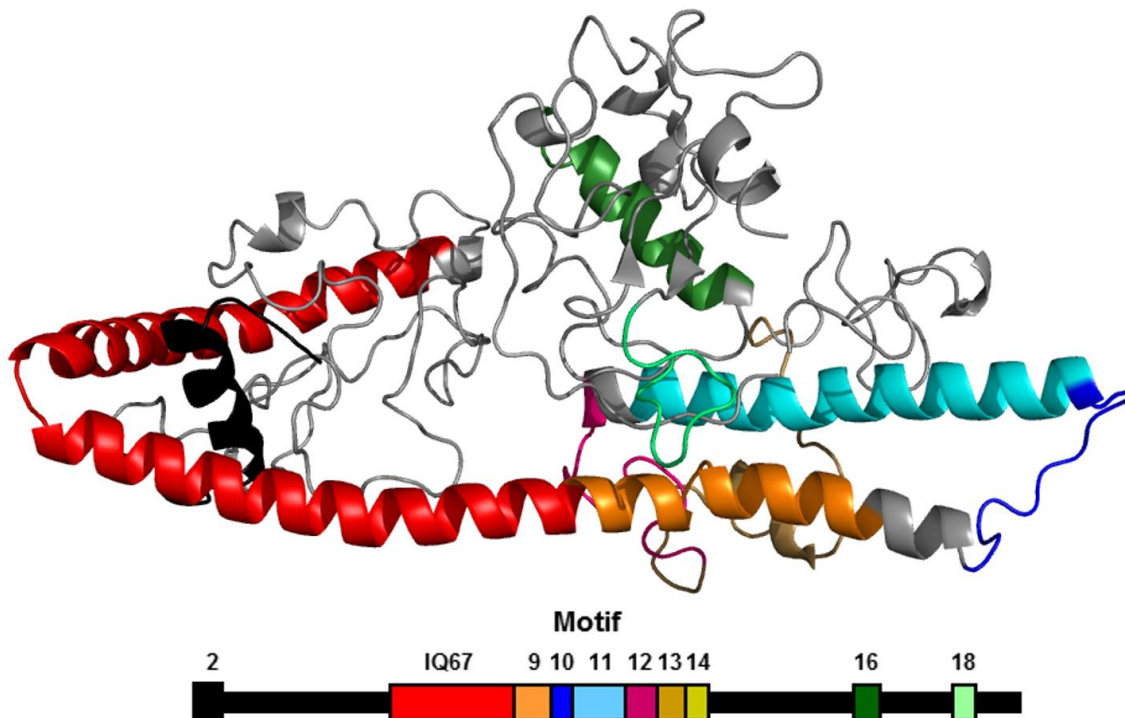


Figure S 11: **Predicted structure of IQD1**

IQD1 contains mostly unstructured regions. The IQ67 domain and some adjacent motifs are predicted to form helical structures. The structured regions are motifs with protein-protein binding capacity as CaM interacts with the IQ67 domain and KLCR1 with the C-terminally adjacent motifs.

**Modelling was performed by Dr. Wolfgang Brandt.**

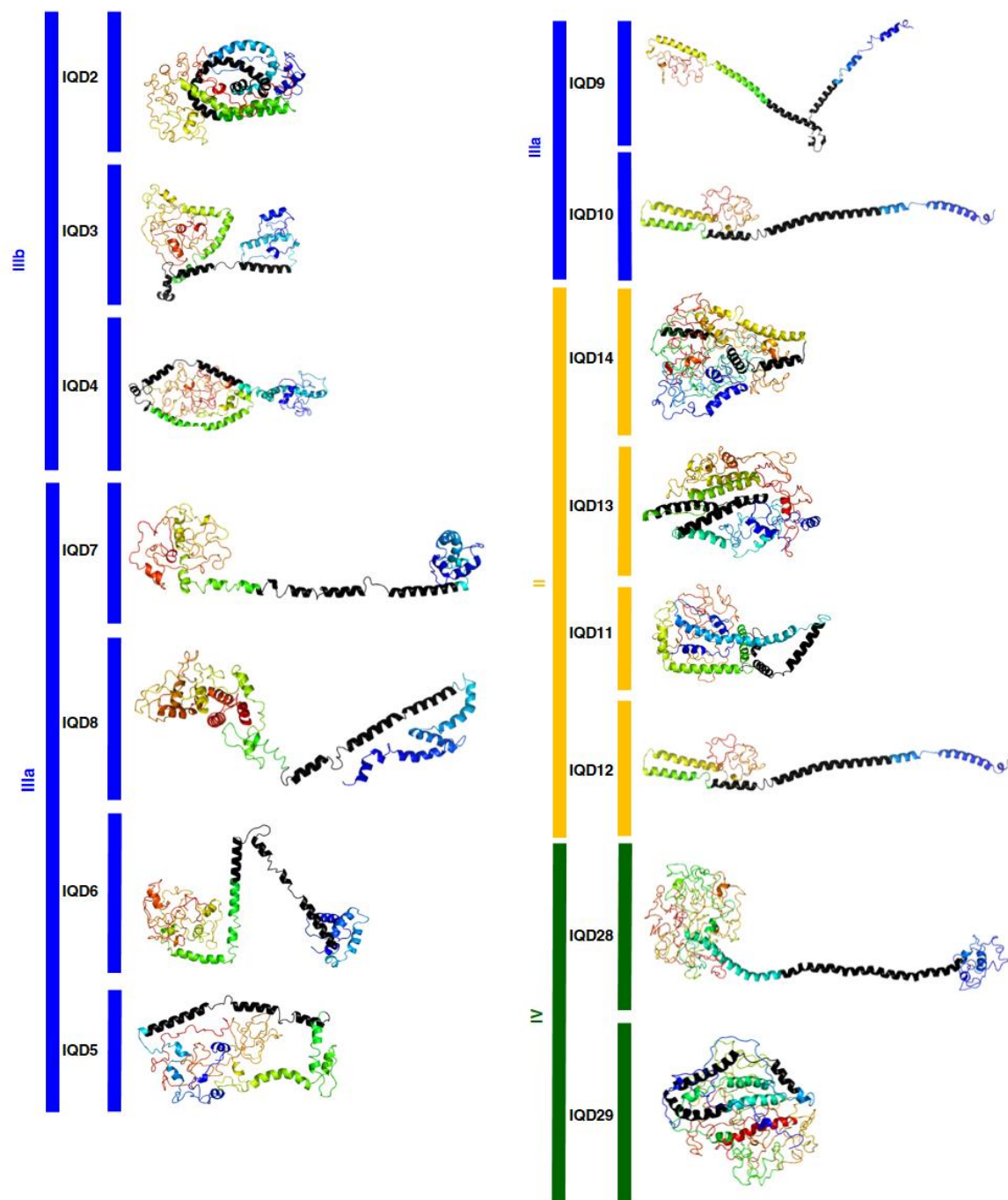


Figure S12: For description see following page.

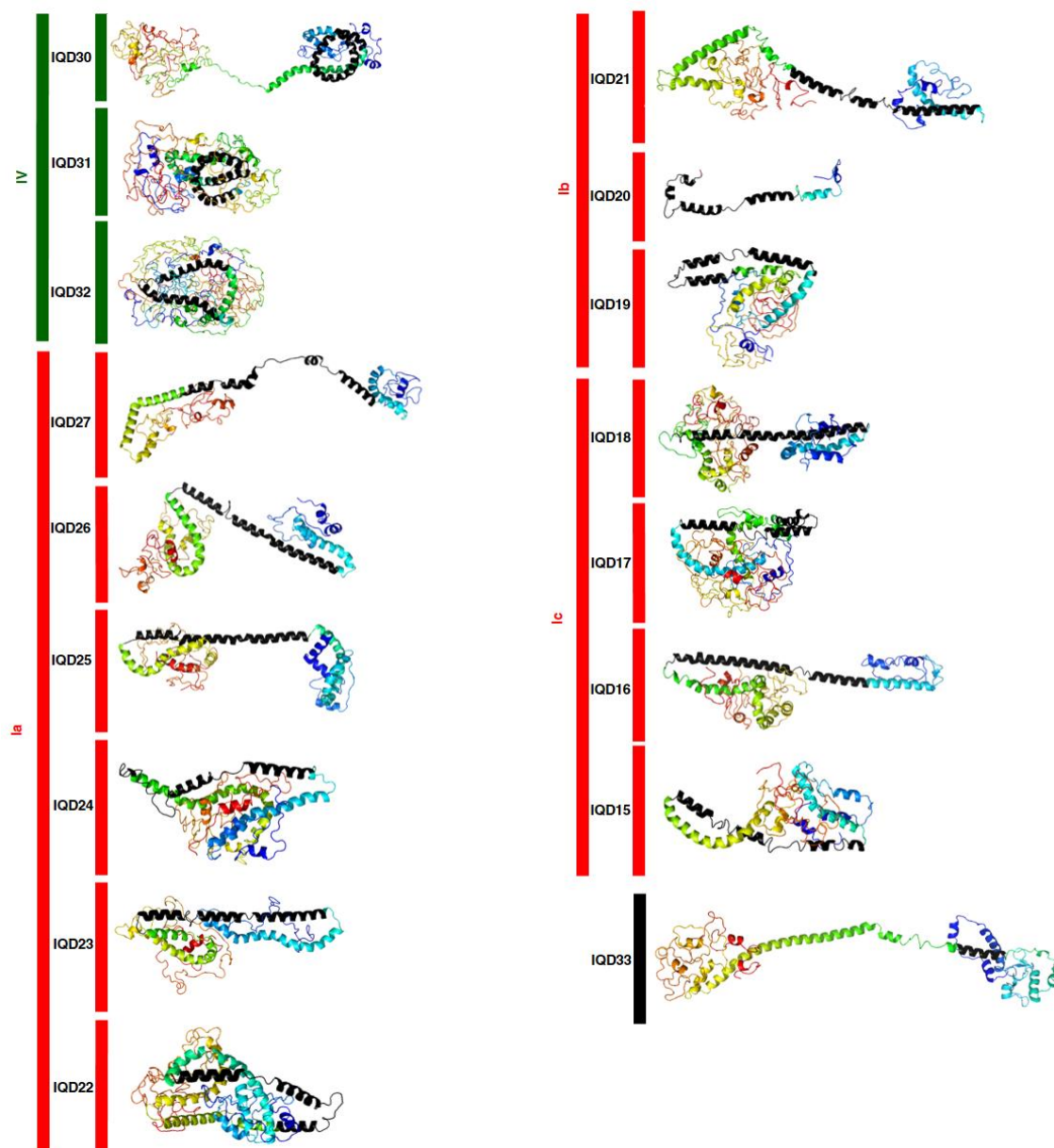


Figure S 12: **Structural prediction of IQD proteins**

Structures of IQD proteins were predicted using the phyre2 database. The resulting structures were colored in “rainbow” depicting the c-terminus in red and the n-terminus in blue using pymol. The IQD67-domain is shown in black.

Table S 1: **Examples of MAP and their proposed function.**

<b>Function</b>	<b>Gene</b>	<b>Publication</b>
rescue	<i>AtKin7</i>	(Moschou et al. 2016)
catastrophe	<i>AtMAP18</i>	(Wang, Zhu, et al. 2007)
transport	<i>AtPAKRP2</i>	(Lee, Giang, and Liu 2001)
recruiting	<i>AtTRM</i>	(Drevensek S. 2012)
bundling	<i>AtMAP65-1</i>	(Pringle et al. 2013)
crosslinking	<i>OsKCH1</i>	(Walter et al. 2015)
branching	<i>Augmin complex</i>	(Liu et al. 2014)
nucleation	<i><math>\gamma</math>-tubulin (<math>\gamma</math>-TuRC)</i>	(Binarova et al. 2006)
sliding	<i>NbTKRP125</i>	(Asada, Kuriyama, and Shibaoka 1997)
membrane tethering	<i>AtROP11/AtMIDD1</i>	(Oda and Fukuda 2013)

Table S 2: Mass spectrometric analysis of *in vitro* MPK-phosphorylated KLCCR1

GST-KLCCR1 was phosphorylated *in vitro* by MPKs. Proteins were separated by SDS-PAGE. After in-gel tryptic digestion peptides were separated via reverse-phase chromatography. Peptides were injected using a Nanospray flex ion source into an Orbitrap Velos Pro mass spectrometer. A phosphoRS module was used to localize the phosphorylation site in the peptide's primary structure. MH+ = Molecular mass after protonation; RT = Retention Time; #PSM = Protein Spectrum Matches. GST alone was used as a negative control.

**MS/MS analysis was performed by Dr. Wolfgang Höhenwarter (KLCCR1) and Dr. Kai Naumann (IQD1).IQD1 protein expression and *in vitro* phosphorylation was performed by Dr. Lennart Eschen-Lippolt and Nicole Bauer.**

(A) Accession Number  
Protein Name

Sequence	Charge	MH+ [Da]	Modifications	MPK3				MPK4				MPK6						
				# PSMs	IonScore	Exp. Value	RT [min]	# PSMs	IonScore	Exp. Value	RT [min]	# PSMs	IonScore	Exp. Value	RT [min]			
AFAPDSK (1)	n.d.	n.d.	n.d.	n.d.	n.d.	n.d.	n.d.	n.d.	n.d.	n.d.	n.d.	n.d.	n.d.	n.d.	n.d.	n.d.	n.d.	
KAFPOSK (1)	2	959.42304	(P)phospho	11	31	9.10E-03	8.8	2	959.42348	(P)phospho	2	25	3.64E-02	8.8	n.d.	n.d.	n.d.	n.d.
GVKAERP (7)	2	1050.53329	(P)phospho	5	28	2.02E-02	11.6	2	1050.53318	(P)phospho	15	35	3.25E-03	9.2	n.d.	n.d.	n.d.	n.d.
SSSQEVR (2)	2	1116.47283	(P)phospho	306	63	4.30E-06	15.1	2	1116.47253	(P)phospho	296	57	1.49E-05	11.7	n.d.	n.d.	n.d.	n.d.
RTSKADAPRR (6)	3	1291.63796	(P)phospho	17	54	7.32E-05	9.9	2	1291.63666	(P)phospho	46	47	3.49E-04	10.1	n.d.	n.d.	n.d.	15.3
RISTKADAPRR (6)	3	1447.73995	(P)phospho	2	31	1.60E-02	9.1	2	1447.73883	(P)phospho	49	34	7.80E-03	9.2	n.d.	n.d.	n.d.	n.d.
LNSTRVPEASSTATT (5)	3	1899.87921	(P)phospho	183	47	1.48E-02	9.7	3	1899.86881	(P)phospho	254	50	1.94E-04	10.4	n.d.	n.d.	178	43
LNSTRVPEASSTATT (5)	3	1979.84431	(P)phospho, S11(P)phospho	14	28	2.33E-02	10.4	3	1979.84431	(P)phospho, S11(P)phospho	14	28	2.33E-02	10.4	n.d.	n.d.	43	1.10E-03
LNSTRVPEASSTATT (5)	3	2142.01391	(P)phospho	191	59	2.70E-05	9.5	3	2142.01211	(P)phospho	309	55	7.89E-05	9.5	n.d.	n.d.	542	58
NKLNSTRVPEASSTATT (5)	3	2221.98191	(P)phospho, S13(P)phospho	12	33	8.93E-05	9.6	3	2221.98191	(P)phospho, S13(P)phospho	32	43	1.32E-03	9.9	n.d.	n.d.	97	33
NKLNSTRVPEASSTATT (5)	3	2267.07805	(P)phospho	20	27	4.66E-02	9.7	3	2267.07513	(P)phospho	3	43	1.32E-03	9.9	n.d.	n.d.	97	33
LNSTRVPEASSTATT (5)	3	2347.03845	(P)phospho, S13(P)phospho	17	31	1.69E-02	10.0	3	2347.03845	(P)phospho, S13(P)phospho	17	31	1.69E-02	10.0	n.d.	n.d.	211	50
NKLNSTRVPEASSTATT (5)	3	2509.21035	(P)phospho	64	46	6.30E-04	9.4	3	2509.21035	(P)phospho	37	46	5.86E-04	9.5	n.d.	n.d.	211	50
NKLNSTRVPEASSTATT (5)	3	2589.17891	(P)phospho, S13(P)phospho	16	33	1.17E-02	9.5	4	2589.17891	(P)phospho, S13(P)phospho	16	33	1.17E-02	9.5	n.d.	n.d.	211	50
KNLVPSDSVTLVAHVLDSPSPSEVYHQAQVWNR (9)/(14)	n.d.	n.d.	n.d.	n.d.	n.d.	n.d.	n.d.	4	4078.02315	(S28)(P)phospho	11	62	9.38E-06	22.1	n.d.	n.d.	n.d.	n.d.

(B) Accession Number  
Protein Name

Sequence	Charge	MH+ [Da]	Modifications	MPK3				MPK4				MPK6						
				# PSMs	IonScore	Exp. Value	RT [min]	# PSMs	IonScore	Exp. Value	RT [min]	# PSMs	IonScore	Exp. Value	RT [min]			
VAVPDTQPSINPPTPMKK	3	2172.08401	T15(P)phospho, M17(Oxidation)	133	50	2.06E-04	22.2	3	2172.08373	T15(P)phospho, M17(Oxidation)	169	60	2.18E-05	22.8	25	55	6.63E-05	21.9
VAVPDTQPSINPPTPMKK	3	2156.09391	T15(P)phospho	57	50	2.08E-04	24.9	3	2156.09401	T15(P)phospho	89	42	1.17E-03	25.4	2	27	3.99E-02	23.5
VAVPDTQPSINPPTPMKK	3	2043.99121	T15(P)phospho, M17(Oxidation)	16	43	9.60E-04	24.4	3	2043.99201	T15(P)phospho, M17(Oxidation)	20	42	1.49E-03	24.5	n.d.	n.d.	n.d.	n.d.
VAVPDTQPSINPPTPMKK	n.d.	n.d.	n.d.	n.d.	n.d.	n.d.	n.d.	3	2027.99891	T15(P)phospho	13	65	6.16E-06	26.4	n.d.	n.d.	n.d.	n.d.

## 7. Publications

Mitra, D.; Klemm, S.; Kumari, P.; Quegwer, J.; Möller, B.; Poeschl, Y.; **Pflug, P.**; Stamm, G.; Abel, S.; Bürstenbinder, K. "Microtubule-associated protein IQ67 DOMAIN5 regulates morphogenesis of leaf pavement cells in *Arabidopsis thaliana*" J Exp Bot 70, 529-543, (2019) DOI: 10.1093/jxb/ery395

### 7.1 Oral Presentations

2nd SFB-workshop of 2013: „*Biochemical characterization of IQD1 and related proteins in Arabidopsis thaliana*“, IPB Halle

1st SFB-workshop of 2014: „*Biochemical characterization of IQD1*“ IPB Halle  
*and related proteins in Arabidopsis thaliana*“ IPB Halle

3rd SFB-workshop of 2014: „*Biochemical characterization of IQD1 and related proteins in Arabidopsis thaliana*“ Wittenberg

2nd SFB-workshop of 2015: „*Towards an understanding of calmodulin-mediated regulation of IQD protein function*“ IPB Halle

1st SFB workshop of 2016: „*Structural and functional analysis of IQD1 and related proteins*“ IPB Halle

10th Plant Science Student Conference (2014): „*Biochemical function of IQD1 and related proteins in Arabidopsis thaliana*“ IPK Gatersleben

11th Plant Science Student Conference (2015): „*Towards an understanding of calmodulin-mediated regulation of IQD protein function*“ IPB Halle

12th Plant Science Student Conference (2016): „*IQD proteins: part of a calcium decoding machinery?*“ IPK Gatersleben

13th Plant Science Student Conference (2017): „*IQD proteins: part of a calcium decoding machinery?*“ IPB Halle

### 7.2 Poster Presentations

9th Plant Science Student Conference (2013): „*Biochemical characterization of Arabidopsis IQD1, a novel calmodulin target involved in protein recruitment to microtubules*“ IPB Halle



26th „Molekularbiologie der Pflanzen“ (2015): “*Biochemical characterization of Arabidopsis IQD1, a novel calmodulin target involved in protein recruitment to microtubules*”  
Dabringhausen

3rd SFB Meeting “Communication in Plants and their Responses to the Environment“ (2015):  
„*The role of IQD1 in plant defense*“ MLU Halle

## 8. Curriculum Vitae

- Juli 2018 – heute**                      Wissenschaftlicher Mitarbeiter „Stability Studies“  
IDT-Biologika, Dessau-Rosslau
- Jan. 2013 – Juni 2018**                Doktorand am Leibniz-Institut für Pflanzenbiochemie,  
Abteilung „Molekulare Signalverarbeitung“,  
Forschungsgruppe „Zelluläre Koordination“
- Okt. 2006 – Nov. 2012**            Diplomstudium „Biochemie“ an der Martin-Luther-Universität  
Halle-Wittenberg  
Diplomarbeit angefertigt am Leibniz-Institut für  
Pflanzenbiochemie,  
Abteilung „Stress- und Entwicklungsbiologie“,  
Forschungsgruppe „Induzierte Pathogenabwehr“,  
Titel: “Analysen des StCERK1-Gens in Solanum tuberosum“
- 1997 – 2004**                            Abitur am Gymnasium Dresden-Plauen

## 9. Danksagung

Mein erster Dank richtet sich an Katharina, die während meiner Arbeit meine Ergebnisse kritisch aber immer mit dem nötigen Positivismus evaluiert hat und den Anstoß für die meisten der hier vorgestellten Experimente gegeben hat. Des Weiteren möchte ich Prof. Steffen Abel danken, mir die Möglichkeit gegeben zu haben, diese Arbeit in der kollegialen aber fordernden Atmosphäre der MSV-Abteilung erstellt zu haben.

Diese Arbeit wäre auch nicht ohne die Hilfe meiner vielen Kollegen möglich gewesen. Besonderer Dank gilt hierbei Lennart, der mir trotz seines immer vollen Kalenders stets unter die Arme gegriffen hat und mir die Arbeit mit MPKs erst ermöglicht hat. Auch Justin möchte ich für seinen Einsatz als Mentor danken, der immer kritisch war aber nie eine Diskussion ohne guten Vorschlag beendet hat.

Schlussendlich geht mein größter Dank an Juliane, die mich immer begleitet und unterstützt hat. Sei es schwere Lebenslagen zu überstehen oder monatelange schlechte Laborergebnisse zu ertragen.

## 10. Eidesstattliche Erklärung

Hiermit erkläre ich an Eides statt, dass ich mich mit der vorliegenden wissenschaftlichen Arbeit erstmals um die Erlangung des Doktorgrades bewerbe, die Arbeit selbständig und ohne fremde Hilfe verfasst, nur die angegebenen Quellen und Hilfsmittel genutzt und die den benutzten Werken wörtlich oder inhaltlich entnommenen Stellen als solche kenntlich gemacht habe.

Halle (Saale), den \_\_\_\_\_

\_\_\_\_\_  
Friedrich Paul Pflug